EPRI | ELECTRIC POWER RESEARCH INSTITUTE

Benchmarks for Quantifying Fuel Reactivity Depletion Uncertainty

2011 TECHNICAL REPORT

Benchmarks for Quantifying Fuel Reactivity Depletion Uncertainty

This document does NOT meet the requirements of 10CFR50 Appendix B, 10CFR Part 21, ANSI N45.2-1977 and/or the intent of ISO-9001 (1994)

EPRI Project Manager
A. Machiels

EPRI | ELECTRIC POWER RESEARCH INSTITUTE

3420 Hillview Avenue
Palo Alto, CA 94304-1338
USA

PO Box 10412
Palo Alto, CA 94303-0813
USA

800.313.3774
650.855.2121

askepri@epri.com

www.epri.com

1022909
Final Report, August 2011

DISCLAIMER OF WARRANTIES AND LIMITATION OF LIABILITIES

THE FOLLOWING ORGANIZATION, UNDER CONTRACT TO EPRI, PREPARED THIS REPORT:

Studsvik Scandpower, Inc.

THE TECHNICAL CONTENTS OF THIS DOCUMENT WERE **NOT** PREPARED IN ACCORDANCE WITH THE EPRI NUCLEAR QUALITY ASSURANCE PROGRAM MANUAL THAT FULFILLS THE REQUIREMENTS OF 10 CFR 50, APPENDIX B AND 10 CFR PART 21, ANSI N45.2-1977 AND/OR THE INTENT OF ISO-9001 (1994). USE OF THE CONTENTS OF THIS DOCUMENT IN NUCLEAR SAFETY OR NUCLEAR QUALITY APPLICATIONS REQUIRES ADDITIONAL ACTIONS BY USER PURSUANT TO THEIR INTERNAL PROCEDURES.

NOTE

For further information about EPRI, call the EPRI Customer Assistance Center at 800.313.3774 or e-mail askepri@epri.com.

Acknowledgment

The following organization, under contract to the Electric Power Research Institute (EPRI), prepared this report:

Studsvik Scandpower, Inc.
1087 Beacon Street, Suite 301
Newton, MA 02459

Principal Investigators:

K. S. Smith
S. Tarves
T. Bahadir
R. Ferrer

This report describes research sponsored by EPRI.

This publication is a corporate document that should be cited in the literature in the following manner:

Benchmarks for Quantifying Fuel Reactivity Depletion Uncertainty. EPRI, Palo Alto, CA: 2011. 1022909.

Abstract

Analytical methods, described in this report, are used to systematically determine experimental fuel sub-batch reactivities as a function of burnup. Fuel sub-batch reactivities are inferred using more than 600 in-core pressurized water reactor (PWR) flux maps taken during 44 cycles of operation at the Catawba and McGuire nuclear power plants. The analytical methods systematically search for fuel sub-batch reactivities that minimize differences between measured and computed reaction rates, using Studsvik Scandpower's CASMO and SIMULATE-3 reactor analysis tools. More than eight million SIMULATE-3 core calculations are used to reduce one million measured reaction rate signals to a set of 2500 experimental fuel sub-batch reactivities over the range of 0 to 55 gigawatt-days per metric ton (GWd/T) burnup.

Experimental biases derived for the CASMO lattice physics code were used to develop a series of experimental benchmarks that can be used to quantify reactivity decrement biases and uncertainties of other code systems used in spent-fuel pool (SFP) and cask criticality analyses. Specification of 11 experimental lattice benchmarks, covering a range of enrichments, burnable absorber loading, boron concentration, and lattice types are documented in this report. Numerous tests are used to demonstrate that experimental reactivity burnup decrements are insensitive to the specific lattice physics codes and neutron cross-section libraries used to analyze the flux map data.

Experimental results also demonstrate that CASMO hot full power (HFP) reactivity burnup decrement biases are less than 250 pcm over the burnup range from 0 to 55 GWd/T, and corresponding 2σ uncertainties are less than 250 pcm. The TSUNAMI tools of Oak Ridge National Laboratory's SCALE 6 package were used to extend HFP results to cold conditions, and cold reactivity burnup decrement uncertainties increased to approximately 600 pcm.

This report provides a basis for quantification of combined nuclide inventory and cross-section uncertainties in computed reactivity burnup decrements. Results support the Kopp Memo 5% reactivity decrement uncertainty assumption, often applied in SFP criticality analysis, which is shown to be both valid and conservative for CASMO-based fuel depletion analyses.

Keywords
Cask criticality
Depletion uncertainty
Experimental benchmarks
Nuclear criticality
Reactivity depletion
Spent fuel pool criticality

Table of Contents

List of Figures

List of Tables

Section 1: Executive Summary

Current methods for treating burnup credit in spent fuel pool criticality analysis commonly make use of the NRC 1998 "Kopp Memo[1]," which instruct analysts to use 5% of the computed fuel depletion delta-k to compensate for reactivity decrement uncertainties (see Figure 1-1) which might arise from uncertainties in computed nuclide number densities and neutron cross sections.

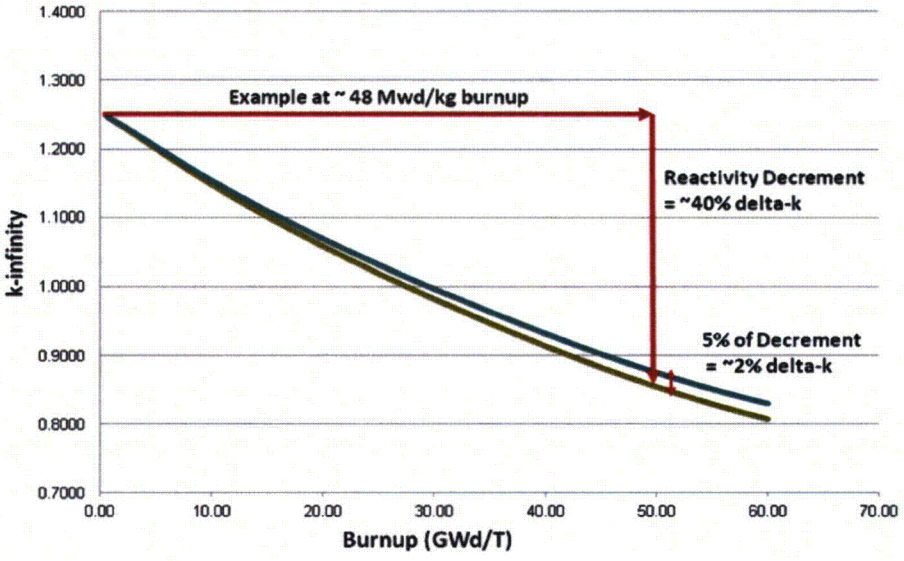

Figure 1-1
Reactivity Decrement

Recently, the NRC has requested that applicants supply quantification and/or justification for this 5% reactivity decrement uncertainty assumption.

This report provides experimental quantification of PWR fuel reactivity burnup decrement biases and uncertainties obtained through extensive analysis of in-core flux map data from operating power reactors. Analytical methods, described in this report, are used to systematically determine experimental fuel sub-batch reactivities that best match measured reaction rate distributions and to evaluate biases and uncertainties of computed lattice physics fuel reactivities.

1.1 Analytical Methods

Forty-four cycles of flux map data from Duke Energy's Catawba (Units 1 and 2) and McGuire (Units 1 and 2) plants[2] have been analyzed with Studsvik Scandpower's CASMO and SIMULATE-3 reactor analysis codes. By systematically searching for fuel sub-batch reactivities that best match measured reaction rate distributions, biases and uncertainties of computed CASMO reactivity decrements are experimentally determined. These analyses employ more than 8 million SIMULATE-3 nodal core calculations to extract approximately 2500 measured sub-batch reactivities from flux map data. The individual estimates of reactivity decrement errors form a large data set plotted here as a function of sub-batch burnup in Figure 1-2. (Comment: numbers present in upper right corner of all plots of this report are QA-trail data, and they can be ignored by the readers of this report.)

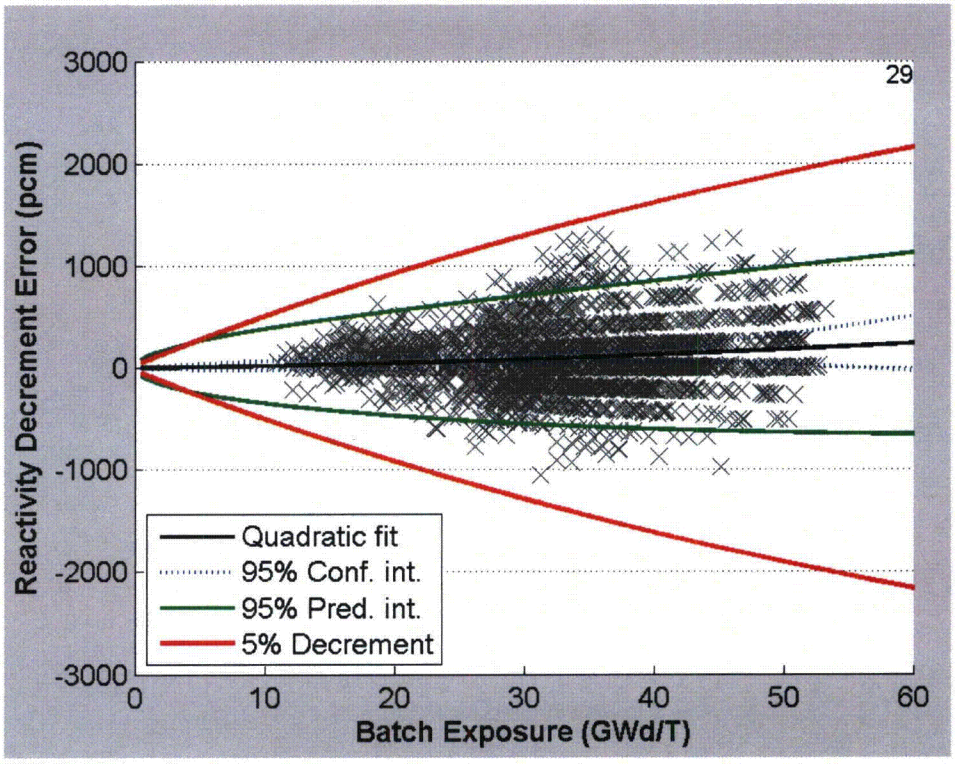

Figure 1-2
CASMO-5 HFP Reactivity Decrement Error vs. Batch Burnup

1.2 Summary of Results

Differences between predicted and measured assembly reactivities (illustrated in the preceding figure) are caused by a number of factors – reaction rate measurement uncertainties, modeling approximations in the nodal core simulator, uncertainties in fuel burnups, and uncertainties in assembly reactitivities as a function of burnup. The objective of this report is to quantify the latter compo-

nent of uncertainty – even though scatter in the data is dominated by other components. Regression analysis is used to determine best-estimate biases and uncertainties of CASMO reactivity decrements, and it is shown that biases are less than 250 pcm and uncertainties are approximately 250 pcm over the burnup range from 10 to 55 GWd/T, as summarized in Table 1-1.

Table 1-1
Measured HFP Reactivity Decrement Bias and Uncertainty

Burnup (GWd/T)	10.0	20.0	30.0	40.0	50.0	60.0
CASMO-4 Bias (pcm)	81	140	178	196	192	167
CASMO-5 Bias (pcm)	19	46	81	125	177	238
95% Uncertainty (pcm)	250	250	250	250	250	250

Analysis demonstrates that the bias and uncertainty are independent (within experimental uncertainties) of fuel assembly design, core boron concentration, and cycle burnup.

Analysis with ORNL's TSUNAMI (SCALE 6) code system is used to extend HFP results to cold conditions. It is shown that extremely high correlation of reactivities between hot and cold conditions results in additional uncertainties from HFP to cold conditions, and final biases and uncertainties are summarized in Table 1-2.

Table 1-2
Measured Cold Reactivity Decrement Bias and Uncertainty

Burnup (GWd/T)	10.0	20.0	30.0	40.0	50.0	60.0
CASMO-4 Bias (pcm)	81	140	178	196	192	167
CASMO-5 Bias (pcm)	19	46	81	125	177	238
95% Uncertainty (pcm)	521	576	571	560	544	534

1.3 Experimental Benchmarks

The experimental biases derived for the CASMO lattice reactivities are used to develop a series of experimental benchmarks that can be used to quantify reactivity decrement biases and uncertainties for other code systems used in lattice depletion and criticality analysis. Specification of eleven experimental lattice benchmarks, covering a range of enrichments, burnable absorber loading, boron concentration, and lattice types are documented in this report.

Results demonstrate that experimental benchmarks are not sensitive to the cross-section library or code version used to reduce the experimental data.

Interested parties can use these experimental benchmarks and their analysis tools to generate reactivity decrement biases and uncertainties which are specific to those tools.

1.4 Summary of Conclusions

Results presented in this report provide quantification of combined nuclide inventory and cross-section uncertainties in reactivity burnup decrements which support a smaller reactivity decrement uncertainty than the 5% criteria suggested in the Kopp Memo.

Experimental reactivity decrement biases derived from flux map data are shown to be similar to those derived from changes in biases of reactor soluble boron concentration from beginning of cycle (BOC) to end of cycle (EOC).

Section 2: Introduction

2.1 Background

The application of burnup credit in spent fuel pool and cask criticality analysis involves defining a large sequence of conservative calculations that cover all anticipated loadings and uncertainties in those analyses. Conservative assumptions and/or uncertainties are applied to compensate for lack of complete knowledge, for quantities such as: maximum fuel temperature, maximum moderator temperature, maximum soluble boron concentration, maximum burnable absorber usage, most limiting axial burnup distribution, maximum error in the declared burnup. This report provides additional data that can be used for conservative validation (in both bias and uncertainty) of burnup/criticality codes.

Criticality analysis of spent fuel pools and casks is performed using large-scale Monte Carlo or multi-group transport eigenvalue calculations for various loadings of spent fuel racks. These calculations have two fundamental sources of uncertainty: the nuclide inventory of the fuel assemblies, and neutron cross-section data. For racks loaded with fresh fuel, these uncertainties can be quantified directly by making extensive comparisons of calculations with the many cold critical measurements that have been performed in rack geometries. Such analyses provide quantification of calculational uncertainties as a function of fuel assembly design, fuel pin enrichments, rack geometries, coolant temperature, coolant boron concentration, etc. Such uncertainties include contributions from: the nuclide inventory of the fuel assemblies, basic neutron cross-section data, and analytical methods.

Since experimental criticals do not exist for depleted fuel assemblies, rack criticals provide no quantification of uncertainties arising from changes in nuclide concentrations and/or uncertainties in cross-section data for nuclides produced by depletion (e.g., production of transuranic nuclides and fission products). The difficulty and expense of performing depleted fuel criticals makes it clear that such data will not be available in the near future – so direct quantification of depletion uncertainties is not easily achieved.

2.2 Historical Approaches

In order to compensate for the lack of depleted criticals, current methods for treating burnup credit in spent fuel pool criticality analysis often make use of the NRC 1998 "Kopp Memo[1]," which instructs analysts to use 5% of the fuel depletion delta-k (computed using criticality tools) to compensate for reactivity

decrement uncertainties which might arise from uncertainties in computed nuclide number densities and/or neutron cross sections. Recently, the NRC has requested applicants to supply quantification and/or justification for this 5% uncertainty assumption.

Figure 2-1 displays a CASMO-4 k-infinity curve versus burnup computed for a typical 17x17 fuel assembly without burnable absorbers. By comparing the computed k-infinity at any burnup with k-infinity at zero burnup, the computed reactivity decrement can be evaluated. In this figure, at a burnup of about 48 GWd/T, the reactivity decrement is about 40% delta-k. The Kopp Memo instructs one to assume that the reactivity decrement is only 95% of the computed reactivity decrement, which in this example, is equivalent to assuming that the fuel is approximately 2% delta-k more reactive than computed.

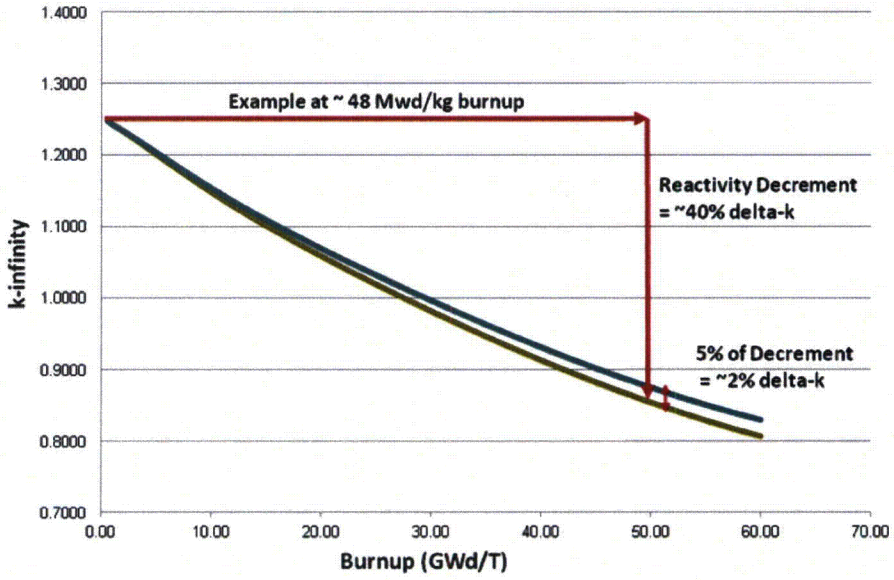

Figure 2-1
CASMO-4 Reactivity Decrement

For cask criticality analysis, chemical assays have been used to validate the isotopic content, and MOX and UO_2 critical experiments have been used to validate actinide worths. Various approaches have been used for validating fission product worths. The approach presented in this report simplifies the current approach for cask burnup credit by simultaneously addressing nuclide inventory and nuclide reactivity biases.

2.3 Project Outline

The remainder of this document details a direct approach to quantifying fuel depletion uncertainties by using operational reactor data and corresponding reactor analysis tools. Comparisons of computed fuel depletion effects and

measured core depletion effects are available from every operating reactor on a near continuous basis. One way of viewing reactor data is that they provide a great many instances of the "depleted fuel criticals" that we desire. These power reactor configurations include:

- many assembly lattice types
- many burnable absorber types
- a spectrum of assembly burnups
- impacts of numerous minor fuel depletion effects, including:
- fuel stack elongation
- fuel pellet cracking
- fuel pellet swelling
- cladding corrosion/crud buildup
- fuel rod bowing

Challenges in using measured reactor data and computed reactor models to quantify the uncertainty in reactivity decrements arise because of the need to:

- extract uncertainties for each fuel assembly enrichment/absorber type in cores containing many different fuel types.
- determine the burnup dependence of assembly reactivity decrement biases and uncertainties.
- account for differences in assembly reactivity uncertainties at hot operating conditions (~900K fuel temperature, ~550K coolant temperature) and the cold conditions that exist in spent fuel pools and casks.

The next section of this report provides an overview of the procedure used to experimentally quantify fuel reactivity decrement uncertainties. Subsequent sections provide:

- specific details of the implementation of this procedure.
- an application of this analysis procedure to 44 cycles of measured reactor data from four Duke Energy PWRs.
- documentation of derived biases and uncertainties in CASMO-4 and CASMO-5 reactivity burnup decrements.
- a set of experimental benchmarks that can be used to quantify reactivity burnup decrement biases and uncertainties for any lattice physics code/criticality analysis tool.

Section 3: Summary of Analysis Approach

3.1 Overview

In-core flux maps taken as a routine part of PWR operation (usually every 30 days) provide measured data that can be used to quantify the accuracy of computed bundle "power distributions." This data is routinely used to determine 95/95 confidence intervals on predicted assembly and pin power distributions needed for NRC licensing of core designs.

The analytical methods employed in this project use the same measured flux map data and core analysis tools to deduce errors in assembly reactivities at each flux map and to determine the assembly depletion decrement bias and uncertainty. In order to use power reactor data to develop depletion decrement biases and uncertainties for each type of fuel assembly (e.g., lattice pitch, fuel enrichment, burnable absorber type), one needs to separate the reactivity contributions of each fuel type in the core. Section 3 of this report outlines the analytical procedures used to determine depletion decrement biases and uncertainties, and Section 5 provides in-depth details of the procedure - as it has been implemented.

3.2 Flux Map Measurements

At each flux map measurement, several (usually 5 or 6) traversing ^{235}U fission chambers are passed axially through instrumentation tubes at the center of approximately 50 instrumented fuel assemblies. By collecting detector signals from all fission chambers as they are passed through a common instrument tube, an inter-calibration of the detector signals is performed and all 50 measured signals are re-normalized to provide a measured 3D spatial distribution of fission rates throughout the reactor core. The reaction rates are typically integrated axially into 61 discrete intervals (~6 cm), which are later collapsed to correspond to the 24 axial nodes (~15 cm) that are typically used in reactor analysis models. This type of measurement is performed routinely, and measured reaction rate distributions are used to monitor technical specification compliance of core power distributions.

3.3 Relationship of Flux Map Errors to Fuel Reactivity

The concept of using flux maps to deduce errors in sub-batch fuel reactivities is motivated by the fact that the distribution of reaction rates errors is sensitive to errors in the burnup dependence of computed fuel reactivity. If analysis models have errors in fuel reactivity that are independent of the fuel depletion, the spatial

shape of flux map errors would not be sensitive to errors in fuel reactivity. Such space-independent errors would be similar to those observed when the boron concentration is altered in a computational model – the reactivity change is nearly the same at all core locations, and differences between computed and measured reaction rates are very insensitive to errors in boron concentration.

However, errors in fuel reactivity arising from imperfect predictions of nuclide concentrations or errors in neutron cross-section data will necessarily change (usually increase) with assembly burnup. Since reactors are loaded with fuel having a large range of burnups, any depletion-induced errors in fuel reactivity will necessarily have a spatial dependence across the reactor core. Consequently, the accuracy of computed reaction rate distributions is sensitive to the spatial distribution of these reactivity errors. This core characteristic makes it possible to deduce the magnitude of errors in reactivity of each fuel sub-batch by determining the spatial distribution of fuel reactivities that produces the best agreement with measured reaction rate distributions.

3.4 Flux Map Perturbation Calculations

The analysis technique employed here uses the SIMULATE-3 reactor analysis nodal code to perform a series of exact perturbation calculations to minimize the global root-mean-square deviation between measured and computed detector signals for each fuel sub-batch (assembly type, enrichment, and burnable absorber configuration, and burnup batch) in the reactor core. In this approach, sub-batch reactivity is altered by re-evaluating all nuclear lattice parameters (cross sections, discontinuity factors, detector response functions, etc.) at a new sub-batch nodal burnup. The computed sub-batch nodal burnup, which is used as the interpolant in the nuclear data library, is systematically altered by a factor, M_B. The spatial distribution of reaction rates is very sensitive to the fuel sub-batch reactivity, as is depicted in Figure 3-1 for three values of the sub-batch burnup multiplier (0.90, 1.0 and 1.10) applied to the highlighted assemblies. From this figure, it can be seen that the root mean square (r.m.s.) difference between calculated and measured radial reaction rates (at the instrumented locations) are 4.2, 1.2, and 3.3%, for these cases. Individual assembly reaction rates are more sensitive, with differences as large as 8.4% being observed for M_B =0.9.

The reason for choosing a sub-batch burnup multiplier is that if there are errors in reactivity predictions of the lattice depletion code, the errors would be seen by all assemblies in the sub-batch. For example, if reaction rates predicted in all assemblies of a sub-batch were either consistently low or consistently high, this would be a strong indication of lattice code depletion errors (e.g., nuclide concentration errors, cross-section data errors, resonance modeling approximations, approximations in solving neutron transport equations, approximations in solving the nuclide depletion equations, approximations in modeling of boron history, etc.) The data often shows, however, that reaction rate differences vary in both sign and magnitude within a sub-batch. This indicates that most of the differences in reaction rates are due to factors not directly related to errors in reactivity predictions with burnup.

3.5 Measured Sub-batch Reactivity Errors

If the sub-batch burnup multiplier M_B is driven through a range of values, one can determine the value of M_B that minimizes the r.m.s. deviation between measured and computed detector signals, as depicted in Figure 3-2. One can see that the set of M_B values creates a smooth function, the minimum of which is the burnup multiplier (M_{min}) that leads to the most accurate prediction of radial reaction rates for this flux map. In this example, the M_B value of ~1.01 produces the most accurate prediction of reaction rates. SIMULATE-3 edits of batch k-infinities for each value of M_B are then used to construct an **estimate of the reactivity error [defined as k-infinity (M_B=M_{min}) minus k-infinity (M_B=1.0)]** for this fuel sub-batch at its sub-batch burnup.

By applying this procedure to many cycles of flux maps, one can estimate the reactivity error for each sub-batch as a function of burnup. Figure 3-3 displays plots of the r.m.s. differences between measured and computed reaction rates (on the left axis) vs. computed batch burnup x M_B, for one sub-batch of fuel as it progresses through three successive cycles of reactor operation. The values of M_{min} are also plotted as symbols (on the right axis). By measuring sub-batch reactivity errors for every flux map in every reactor cycle, one can construct estimates of the error in sub-batch reactivity and the corresponding shapes of sub-batch reactivity error vs. sub-batch burnup.

	R	P	N	M	L	K	J	H	G	F	E	D	C	B	A
1							-0.005 0.008 0.020			-0.023 0.000 0.022					
2			-0.046 -0.020 0.006			-0.045 -0.006 0.032		0.012 0.004 -0.003							
3								0.032 0.020 0.007		-0.017 0.012 0.039		-0.042 0.012 0.064		-0.039 -0.012 0.013	
4		-0.056 -0.017 0.020	-0.051 0.003 0.055					0.061 -0.008 -0.062							
5					0.032 0.010 -0.010				0.069 -0.001 -0.066		0.027 0.005 -0.015		-0.042 0.007 0.055		
6	-0.013 0.004 0.026		-0.018 0.011 0.038			0.038 -0.001 -0.040									
7				0.039 0.011 -0.014			0.031 -0.011 -0.053			0.064 0.011 -0.039			-0.011 -0.004 0.002		
8	-0.008 -0.003 0.001		0.025 0.013 0.001		0.080 0.008 -0.059		0.042 0.002 -0.037					0.057 -0.002 -0.056	0.029 0.017 0.005	0.009 0.001 -0.007	
9		-0.009 0.007 0.022							0.048 0.006 -0.036		0.084 0.014 -0.051				-0.017 -0.004 0.009
10												-0.005 -0.002 0.001			
11	-0.039 -0.018 0.003				0.005 -0.017 -0.037			0.092 0.020 -0.047			0.026 0.004 -0.016				-0.036 -0.015 0.005
12						-0.015 -0.012 -0.009			0.037 0.009 -0.016			-0.048 -0.003 0.040			
13			-0.057 0.000 0.054		-0.068 -0.018 0.029			0.025 0.013 0.001						-0.041 -0.014 0.011	
14			-0.052 -0.026 0.000				0.002 0.018 0.033			-0.036 0.003 0.041		-0.070 -0.031 0.006			
15					-0.033 -0.012 0.008			-0.005 -0.001 0.003						r.m.s. diff M_B=0.9 4.2% M_B=1.0 1.2% M_B=1.1 3.3%	

Figure 3-1
Computed Reaction Rate Errors for One Fuel Sub-batch

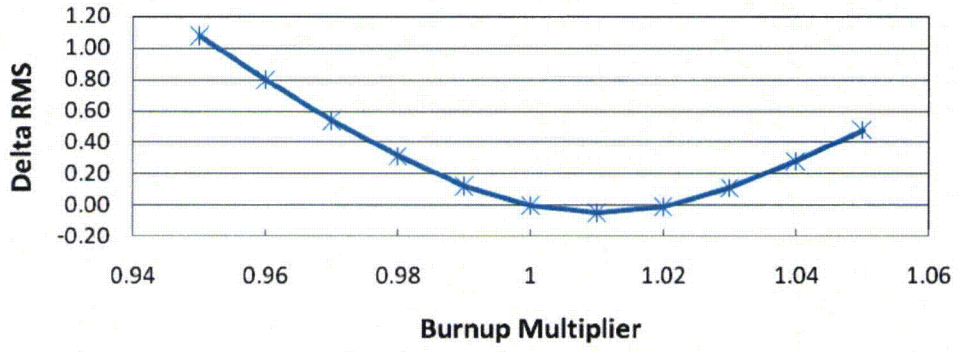

Figure 3-2
Change in r.ms. Reaction Rate Error vs. Sub-batch Multiplier

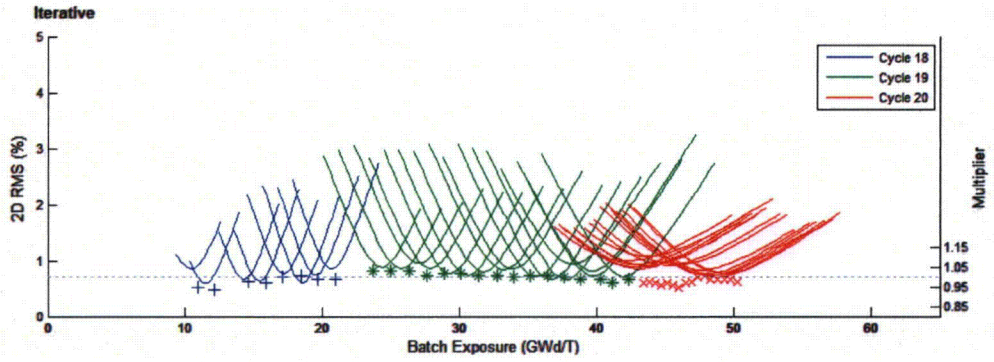

Figure 3-3
Determination of Sub-batch Burnup Multiplier as a Function of Burnup

3.6 Simultaneous Determination of All Sub-batches Reactivities

At any one time, the reactor core contains many sub-batches of fuel (typically 10 to 15), and it is important that M_{min} be determined simultaneously for all sub-batches such that the global r.m.s. differences between computed and measured reaction rates are minimized. This is achieved by performing a local search in a succession of passes over all sub-batches to determine the local minimum. The plots in Figure 3-4 show the minimized r.m.s reaction rate differences and optimal values of M_{min} for one sub-batch between the zero pass (upper plot) and final iterative pass (lower plot). Several things can be observed from these plots: 1) for high sensitivity cases (e.g., end of cycle 16 and all of cycle 17), the iterative results are not very sensitive to the iteration, 2) for cases with low sensitivities to the sub-batch burnup multiplier, the zero pass results (independent perturbations of each sub-batch in the core) can be far from the converged results, and 3) the iteratively converged results display more consistent burnup trends than zero pass results. Thus, the iterative approach is preferable to the non-iterative approach.

Note that if sub-batch multipliers could reduce the r.m.s. to zero, then it could be argued that each sub-batch assembly is experiencing the same discrepancy, which would be indicative of depletion errors. The data, however, shows that although r.m.s. differences are reduced with sub-batch multipliers, the reduction is a small fraction of the total deviation, and therefore, residual deviations must be caused by factors other than sub-batch reactivity (and hence are not indicative of depletion errors).

One normally considers the core radial power distribution to be more sensitive to batch reactivities than the axial shape, which would lead one to conclude it might be preferable to minimize the radial (2D) r.m.s deviations rather than the nodal (3D) r.m.s deviation. Figure 3-5 displays plots of the radial r.m.s. deviations (both searches were performed to minimize the 3D differences), and one can observe that there is little difference between the minimum points of the 2D r.m.s. values and the 3D r.m.s. values of Figure 3-4. However, 2D r.m.s

differences are more sensitive (i.e., display bigger changes) to the burnup multipliers.

Section 5 provides a detailed description of the final algorithm implemented to solve the many sub-batch minimizations. It should be noted that this method of determining errors in computed assembly reactivities from flux map data has one unique characteristic – **this analytical method is completely independent of errors in core-wide reactivity predictions (e.g., k-eff, critical boron, etc.).** Thus, the proposed analysis method is completely complementary to reactivity-based methods normally used for quantifying errors in computational models (e.g., critical assembly analysis, reactor startup criticals, shutdown margin measurements, and boron letdown comparisons).

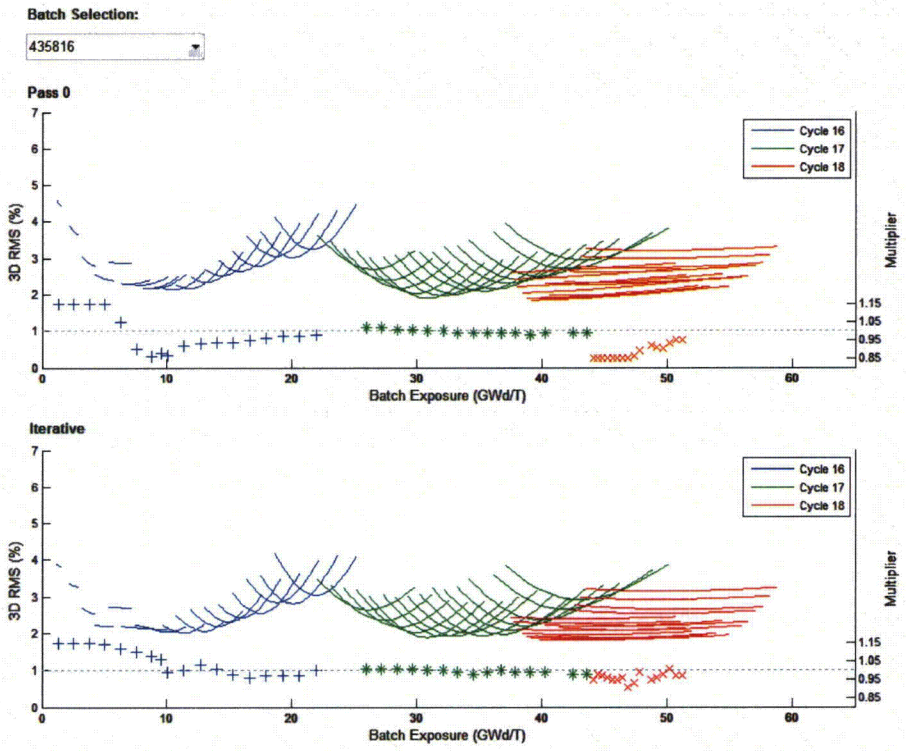

Figure 3-4
Nodal (3D) r.m.s. Differences for One Sub-batch

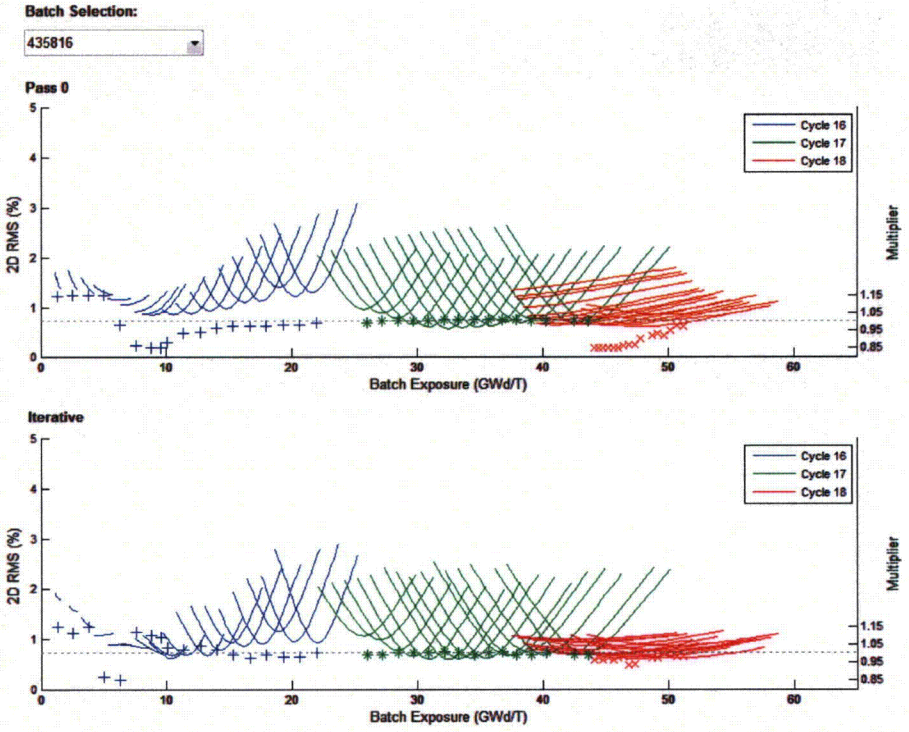

Figure 3-5
Radial (2D) r.m.s. Differences for One Sub-batch

Section 4: Analysis Codes: Studsvik CMS

The Studsvik Core Management System (CMS) is routinely used to perform the neutronic and thermal-hydraulic analysis needed for design, optimization, and safety analysis of nuclear reactor cores. While the CMS suite of codes is capable of performing steady-state and transient (dynamic) analysis of reactor cores, the methods described in this document are restricted to the CMS codes needed to perform steady-state and pseudo steady-state core analysis.

4.1 Code System Overview

The CMS code system consists of five separate codes which are used as a package to perform reactor core analysis. The five codes are:

- **INTERPIN-4**[3] for analyzing the 1-D fuel temperatures for an individual fuel pin, as a function of:
- Fuel pin design (e.g., enrichment, gas pressurization, etc.)
- Linear heat loading
- Fuel burnup
- **CASMO-4**[4] **or CASMO-5**[5] for analyzing the 2-D neutronic behavior of an individual fuel assembly, as a function of:
- Lattice design (e.g., pin enrichment layout, burnable absorber design, etc.)
- Local conditions (e.g., fuel temperature, coolant density, boron content, etc.)
- Fuel burnup
- Control rod insertion
- **CMSLINK**[6] for generating a library of tabularized CASMO-4 data for a collection of fuel assemblies and reflector types, as a function of:
- Fuel burnup
- Thermal hydraulic conditions
- Control rod insertion
- Fuel history effects
- **SIMULATE-3**[7-18] for analyzing the detailed 3-D reactor core neutronic and thermal hydraulic behavior over the reactor core lifetime, as a function of:
- Reactor power

- Coolant flow rate and inlet temperature
- Fuel burnup
- Control bank insertion

INTERPIN-4 and CMSLINK are often considered as auxiliary codes in the CMS suite. On the other hand, CASMO and SIMULATE-3 are very large (many hundreds of thousands of lines of FORTRAN) codes which perform the bulk of the physics modeling in CMS. Appendix A details the physics models and methods of these codes - which are important for understanding how CASMO and SIMULATE-3 are used for this project.

Section 5: Duke Energy's Reactor Models

5.1 Overview

Data from four of Duke Energy's PWR units[2] have been used to determine measured fuel burnup reactivity decrement biases and uncertainties. All units are 4-loop Westinghouse reactors containing 17x17 fuel assemblies. Duke Energy provided complete specifications for the reactor, the fuel, and operational data so that CASMO/SIMULATE models could be independently constructed for this project. Detailed flux map data for all cycles of operation were included in the data package, thus enabling application of the previously-outlined reactivity decrement methodology. Reactor cycle parameters are summarized in Table 5-1.

Table 5-1
Reactor and Fuel Data

Unit	Cycles	Cycle Length (EFPD)	Enrichment Range (%)	HZP Boron (ppm)	Maximum LBP #	Maximum IFBA #	Maximum WABA+IFBA #
McGuire-1	10 to 21	363–514	3.40–4.95	1576–2000	24	128	24 + 128
McGuire-2	10 to 20	429–518	3.64–4.90	1690–2037	24	128	24 + 128
Catawba-1	9 to 19	407–522	3.45–4.75	1501–2104	24	128	16 + 128
Catawba-2	8 to 17	451–527	3.50–4.90	1819–2109	24	128	20 + 128

5.2 Fuel Types

The fuel assemblies loaded into the Duke reactors for these cycles were of two distinct mechanical types: Areva's MarkBW with LBPs (lumped burnable poisons) and Westinghouse's RFA fuel with WABAs (wet annular burnable absorbers) and/or IFBA (integral fuel burnable absorbers). The MarkBW fuels used a range of LPB enrichment spanning from 1% to 4% by weight B_4C. As the reactors moved to 18-month cycles, the core loadings became more complex with the introduction of split enrichment feeds and many different burnable poison combinations. As one observes from the fuel descriptions in Table 5-2, each cycle contains feed fuel divided into 5 to 12 sub-batches (e.g., different combinations of enrichment and/or burnable absorbers). The number of fuel assembly types exceeds 100 for the analyzed cycles of each of the four units.

CASMO lattice calculations were performed for each unique axial layer (e.g., b.p. zone, cutback b.p. zone, axial blanket, etc.) of each fuel type. Complete CASMO PWR case matrices of data were generated spanning the full range of hot to cold

reactor conditions with burnups up to 80 GWd/T. Depletion histories were performed for boron, moderator temperature, and fuel temperature – so that the effects from variable reactor boron concentrations and local power density could be modeled directly in SIMULATE-3.

CASMO reflector cases (for lower, upper, radial with baffle, and radial with both baffle and barrel) were executed to generate equivalent reflector data as a function of moderator temperature and boron concentration for use in SIMULATE-3 reflector nodes.

Table 5-2
Feed Fuel Characteristics

Cycle	Enrichment (%)	# of sub batches	Cycle	Enrichment (%)	# of sub batches
McGuire-1			**McGuire-2**		
10	3.40	4	10	3.85 / 3.95	7
11	3.40 / 3.55	9	11	3.90 / 4.15	7
12	3.67	9	12	3.78	6
13	3.92	8	13	4.09 / 4.39	11
14	4.14 / 4.50	7	14	3.77 / 4.33	7
15	4.40 / 4.75	6	15	4.16 / 4.56	12
16	3.92 / 4.35	7	16	4.37 / 4.67	8
17	4.45 / 4.74	9	17	4.35 / 4.75	8
18	4.01 / 4.64	5	18	4.05 / 4.70	6
19	4.00 / 4.68	7	19	3.90 / 4.80	8
20	4.00 / 4.85	9	20	3.65 / 4.90	9
21	3.60 / 4.95	10			
Catawba-1			**Catawba-2**		
9	3.86	8	8	3.98	6
10	3.65 – 3.92	6	9	4.32 / 4.42	9
11	4.02	6	10	4.54	5
12	4.50	6	11	3.90 / 4.20	6
13	3.81 / 4.31	6	12	4.35 / 4.66	8
14	4.19 / 4.46	9	13	4.00 / 4.75	8
15	4.18 / 4.53	10	14	4.45 /4.75	8
16	4.42 / 4.67	10	15	3.80 / 4.73	11
17	3.88 / 4.51	9	16	4.38 / 4.90	8
18	4.05 / 4.51	8	17	3.80 / 4.82	9
19	3.96 / 4.75	7			

5.3 CMS Code Versions

The analysis in this project used the following QA production code versions for all cycle depletion analysis:

- INTERPIN-4Version 4.01
- CASMO-4EVersion 2.10.22P
- CASMO-5 Version 2.00.00
- CMSLINKVersion 1.27.00
- SIMULATE-3Version 6.09.22_PWR_1

A special branch version of SIMULATE-3 was created to perform the automated perturbation cases described in Section 6. That version is designated:

- SIMULATE-3Version 6.09.22_EPRI

5.4 Core Follow Summary Results

SIMULATE-3 core follow calculations were performed for each reactor cycle, using the core loading patterns and the operational reactor history. The as-measured core power, core coolant flow, coolant inlet temperature, and control rod positions were used as boundary conditions for the SIMULATE-3 calculations, and a boron search to critical was performed at each depletion step. The SIMULATE-3 model used a four-node-per-assembly radial nodalization, 24 axial nodes over the active fuel height (356.76 cm), and one homogenized reflector node at the top and at the bottom of the fuel stack. Each cycle was divided into fine depletion steps (30-100 depletion points per cycle) so fluctuations in reactor conditions faithfully followed the history of reactor operations.

The accuracy of SIMULATE-3 depletion calculations was checked by comparing computed and measured boron concentrations at points where measured plant chemistry boron data and measured ^{10}B isotopic data were available. A typical comparison between plant boron data (corrected to natural ^{10}B /^{11}B ratio) and computed SIMULATE-3 critical boron concentrations are displayed in Figure 5-1. From the data in this figure, it can be observed that the gross core reactivity is well-predicted, including the early-cycle burnout of the strongly self-shielded burnable poisons.

Comparisons of calculated and measured hot zero power (HZP) critical boron concentrations, as well as beginning of cycle (BOC ~25 EPFD) and end of cycle (EOC, extrapolated to zero ppm) boron concentrations, are summarized for all four units in Tables 5-3 to 5-6. Of particular interest are any trends from BOC to EOC in the mean differences of calculated and measured borons, which can be seen to be less that 26 ppm for all four units.

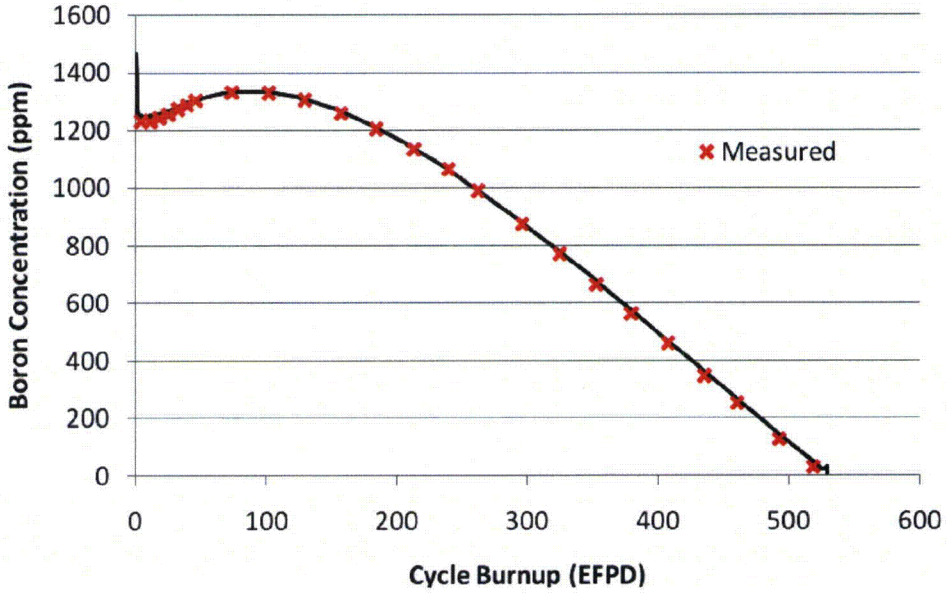

Figure 5-1
Comparison of SIMULATE and Measured Boron

Table 5-3
McGuire Unit-1 Boron Comparisons

Cycle	Cycle Length at end of HFP, 0 ppm = EOC	Measured Boron (ppm)			Calculated – Measured Boron (ppm)		
		HZP BOC	HFP		HZP BOC	HFP	
			BOC	EOFP		BOC	EOC
10	383.4	---	1142	86	---	12	-28
11	363.2	1746	1107	45	27	8	-22
12	380.0	1803	1150	154	28	5	-24
13	442.5	2000	1328	50	19	-6	-26
14	465.5	1955	1252	59	5	4	-36
15	492.7	1576	906	49	9	-9	-24
16	501.9	1920	1299	91	10	-4	-22
17	514.0	1975	1337	135	-3	-10	-37
18	505.0	1973	1331	109	-4	-7	-28
19	487.5	1899	1279	149	-2	-25	-35
20	478.2	1942	1267	93	8	-6	-52
21	---	1840	1161	---	12	-7	---
				Average	10	-4	-30

Table 5-4
McGuire Unit-2 Boron Comparisons

Cycle	Cycle Length at end of HFP, 0 ppm = EOC	Measured Boron (ppm)			Calculated – Measured Boron (ppm)		
		HZP BOC	HFP		HZP BOC	HFP	
			BOC	EOFP		BOC	EOC
10	431.8	1839	1177	13	20	-2	-41
11	429.0	1906	1248	106	13	-17	-17
12	423.9	2037	1359	41	26	3	-11
13	446.2	1896	1189	15	-10	-30	-35
14	486.4	1691	1090	141	18	-13	-35
15	517.8	1919	1301	25	13	-1	-38
16	502.6	1887	1241	26	-13	-19	-33
17	511.9	1908	1238	114	2	-14	-34
18	494.8	1818	1146	158	26	6	-44
19	475.8	1817	1117	4	23	2	-30
20	---	1713	1035	---	5	-23	---
				Average	11	-10	-32

Table 5-5
Catawba Unit-1 Boron Comparisons

Cycle	Cycle Length at end of HFP, 0 ppm = EOC	Measured Boron (ppm)			Calculated – Measured Boron (ppm)		
		HZP BOC	HFP		HZP BOC	HFP	
			BOC	EOFP		BOC	EOC
9	421.1	1876	1214	43	27	-1	2
10	407.6	1840	1173	82	37	14	-8
11	445.4	1983	1267	116	44	18	0
12	486.8	2012	1275	28	32	3	-3
13	491.2	1501	871	17	35	7	8
14	515.7	1899	1285	82	44	17	15
15	500.9	1888	1246	157	18	12	9
16	521.8	2104	1371	112	21	9	4
17	505.7	2097	1402	131	51	34	12
18	482.6	2011	1341	10	45	25	8
19	---	1920	1241	---	24	2	---
				Average	34	13	5

Table 5-6
Catawba Unit-2 Boron Comparisons

Cycle	Cycle Length at end of HFP, 0 ppm = EOC	Measured Boron (ppm)			Calculated – Measured Boron (ppm)		
		HZP BOC	HFP		HZP BOC	HFP	
			BOC	EOFP		BOC	EOC
8	451.5	1869	1186	69	46	35	12
9	472.0	2082	1352	49	38	30	9
10	490.9	1906	1164	222	64	37	4
11	495.6	1797	1153	15	44	32	20
12	483.1	1781	1153	49	51	27	16
13	527.3	1889	1256	30	32	18	22
14	501.2	1871	1195	103	30	20	16
15	498.5	1967	1253	58	52	43	16
16	464.4	1828	1106	42	37	27	15
17	499.0	1750	1054	---	35	25	9
				Average	43	30	14

5.5 Flux Map Summary Results

Measured flux map data for each unit was taken at intervals of about 30 EFPD throughout the cycles. Each flux map has been analyzed with SIMULATE-3, and a summary of comparisons with measured data are displayed in Table 5-7. It can be seen that the SIMULATE-3 radial reaction rate distributions (axial integrals over each of the detector positions) are predicted with a mean difference slightly above 1 percent. 3D node-by-node (24 axial nodes) reaction rates are predicted with a mean difference of less than 3 percent.

Accurate predictions of reaction rate distributions are very important as a starting point for subsequent application of the burnup reactivity decrement methodology because the analytical tools must be capable of accurately predicting reaction rate distributions when provided accurate fuel assembly reactivities.

Table 5-7
Comparison of SIMULATE-3 and Measured Reaction Rates

Reactor	# of Flux Maps	Mean Radial (2D) r.m.s. Difference (%)	Mean Axial r.m.s. Difference (%)	Mean Nodal (3D) r.m.s. Difference (%)
McGuire-1	161	1.15	1.64	2.64
McGuire-2	171	1.20	1.70	2.67
Catawba-1	179	1.22	1.46	2.50
Catawba-2	169	1.24	1.82	2.82
Un-weighted Average		1.20	1.66	2.66

5.6 Reactor Model Summary

The CMS models for the Duke reactors have been developed by applying a production model to all reactor and fuel data supplied by Duke Energy. All four units employ consistent modeling techniques, which is important for combining cross-units results needed for the cumulative statistics in this project.

The agreement of the SIMULATE-3 core follow model with plant measured data demonstrates that both core reactivity and spatial distributions of reaction rates are well-predicted throughout the cycles and across all units. Consequently, these models and measured reactor data form a well-qualified basis for the analysis presented in this report.

Section 6: Details of Analysis Implementation

For every reactor condition at which a flux map is available, a sequence of SIMULATE-3 calculations is performed to evaluate the error in sub-batch reactivity for all the sub-batches in the reactor core. Section 3 provided a brief overview of the analysis procedure used to quantify the computed reactivity decrement bias and uncertainty. However, in the overall iterative sequence described in Section 3, there are a number of details that are needed for practical implementation.

6.1 Super-batch Definitions

Since there are many sub-batches (e.g., 10-15) introduced in each cycle (as displayed in Table 5-2), it is important that there be enough assemblies in the core to make a search for the sub-batch reactivity meaningful. For instance, when there are eight or fewer assemblies in a sub-batch, the sub-batch would only occupy a single core location in an octant-symmetrically-loaded core. In such a case, the sensitivity of the r.m.s. differences in computed and measured reaction rates would be very sensitive to measurement errors at that core location. In order to alleviate such sensitivities, we have chosen to lump any sub-batches having fewer than 12 assemblies into a super-batch with all corresponding enrichment sub-batches also having fewer than 12 assemblies. Consequently, this super-batch actually represents a number of different burnable poison configurations. All sub-batches with more than 12 assemblies are treated explicitly as their own sub-batch, since the sub-batch will occupy at least 2 different locations in an octant of the reactor core.

6.2 3-D Versus 2-D Searches

As was pointed out in Section 3, it is not obvious if the search to minimize differences between computed and measured reaction rates should be performed with the radial (2D) or nodal (3D) reaction rates. We have examined a large number of searches using both the radial and nodal differences to drive the search. In general, little difference has been observed between the results of either type of search, but individual cases can be found in which one or the other seems more effective. Since the nodal search is intuitively more general, we have chosen to base the searches in this report on minimizing the r.m.s. differences in the nodal (3D) reaction rates.

In all cases, this search for optimal sub-batch burnup multipliers is guaranteed to reduce the deviation between computed and measured reaction rates. Typical reductions in nodal r.m.s. values and corresponding radial r.m.s. values are displayed in Figures 6-1 and 6-2. In such cases, one observes that even though the search minimizes the nodal r.m.s. differences, the radial r.m.s. differences are also all reduced. In fact, it is not uncommon for the magnitude of the reduction in radial r.m.s. differences to exceed that of the nodal r.m.s. differences.

However, there is nothing inherent in the search process to guarantee that the radial r.m.s. differences will actually be reduced. By examining a great number of cycles of data, some instances have been found in which iterative reduction of the nodal r.m.s differences actually increases the radial r.m.s differences, as displayed in Figures 6-3 (consistent improvement in core-wide 3D r.m.s.) and 6-4 (inconsistent improvement in core-wide 2D r.m.s.). This behavior has only been observed when initial radial r.m.s. differences are very small (less than 1%), and the increases in the iterative r.m.s. differences are also very small.

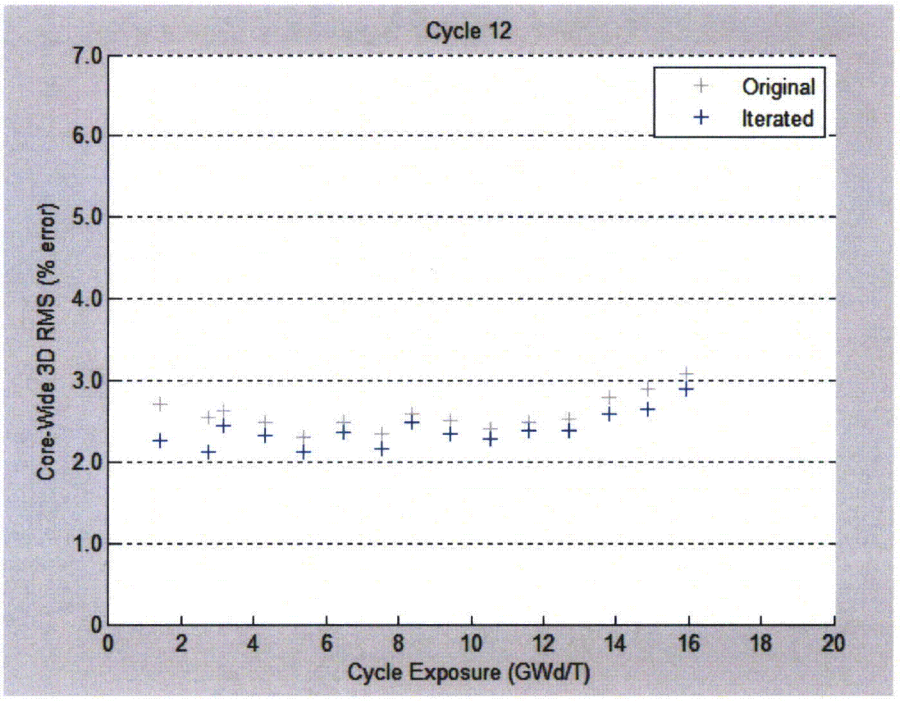

Figure 6-1
Cycle 12 – Nodal r.m.s. Reaction Rates

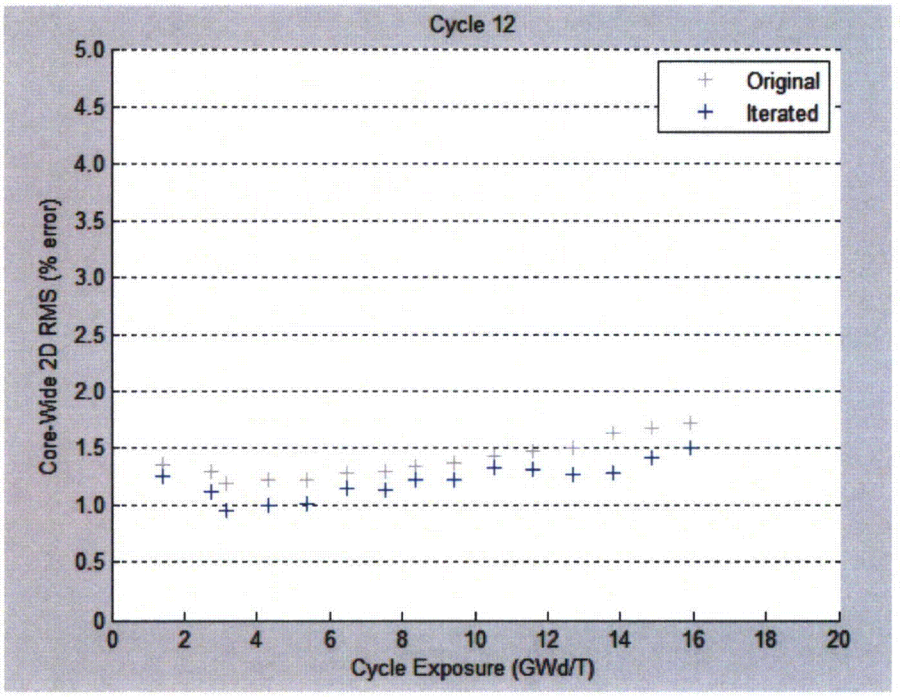

Figure 6-2
Cycle 12 – Radial r.m.s. Reaction Rates

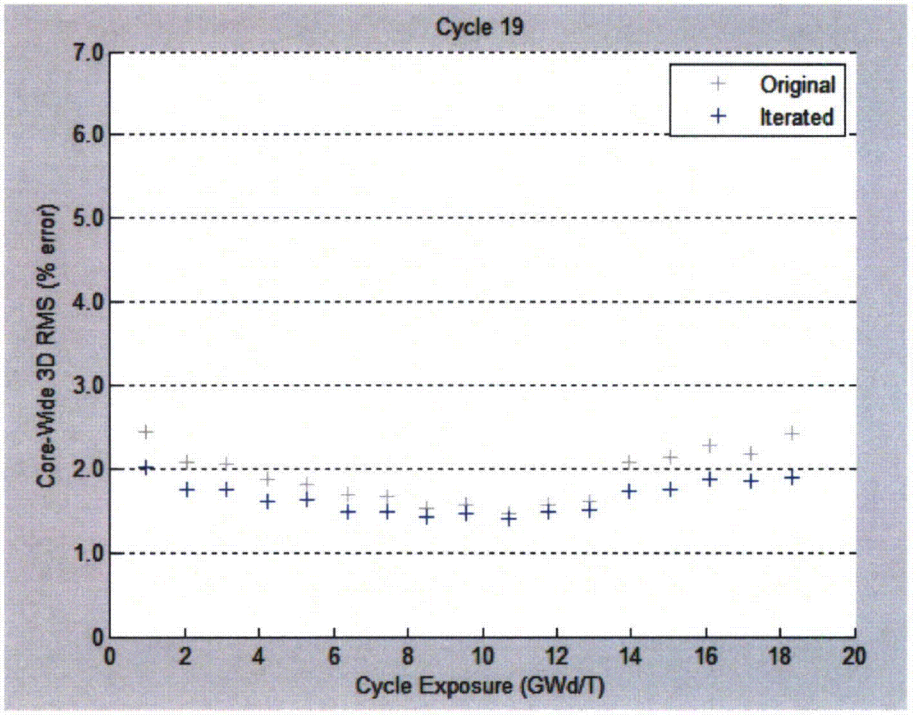

Figure 6-3
Cycle 19 – Nodal r.m.s. Reaction Rates

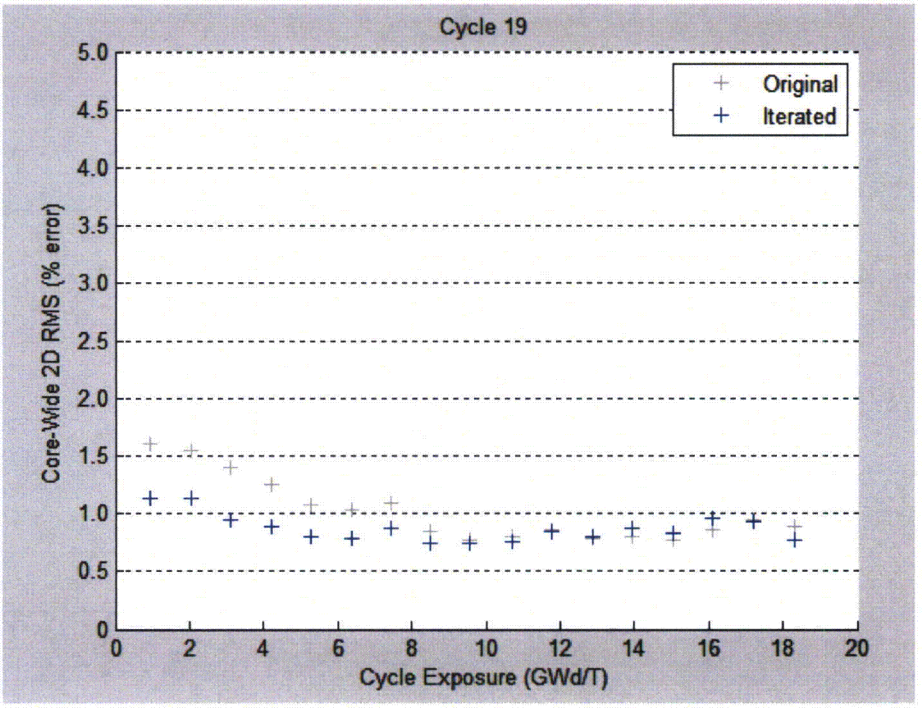

Figure 6-4
Cycle 19 – Radial r.m.s. Reaction Rates

6.3 Sub-batch Sensitivities

In order for the search to determine the sub-batch burnup multipliers that minimize r.m.s. differences between the calculation and the measurement, it is important that the sub-batch actually display a significant sensitivity to the sub-batch reactivity multiplier. There are several instances in which this sensitivity does not exist. One such case occurs when a sub-batch is located in core positions of little reactivity worth relative to the locations of in-core detectors – such as when it is placed in extreme peripheral core locations for the sub-batch's last cycle in the core (e.g., very low-leakage core loading patterns). When a search for the sub-batch multiplier is performed, one observes a very flat r.m.s. difference as the sub-batch multiplier is changed – as depicted in Figure 6-5 for the Cycle 18 cases. In such cases, the sub-batch multipliers are very sensitive to the iteration, and converged sub-batch multipliers often display large fluctuations at successive flux maps – which is clearly unphysical.

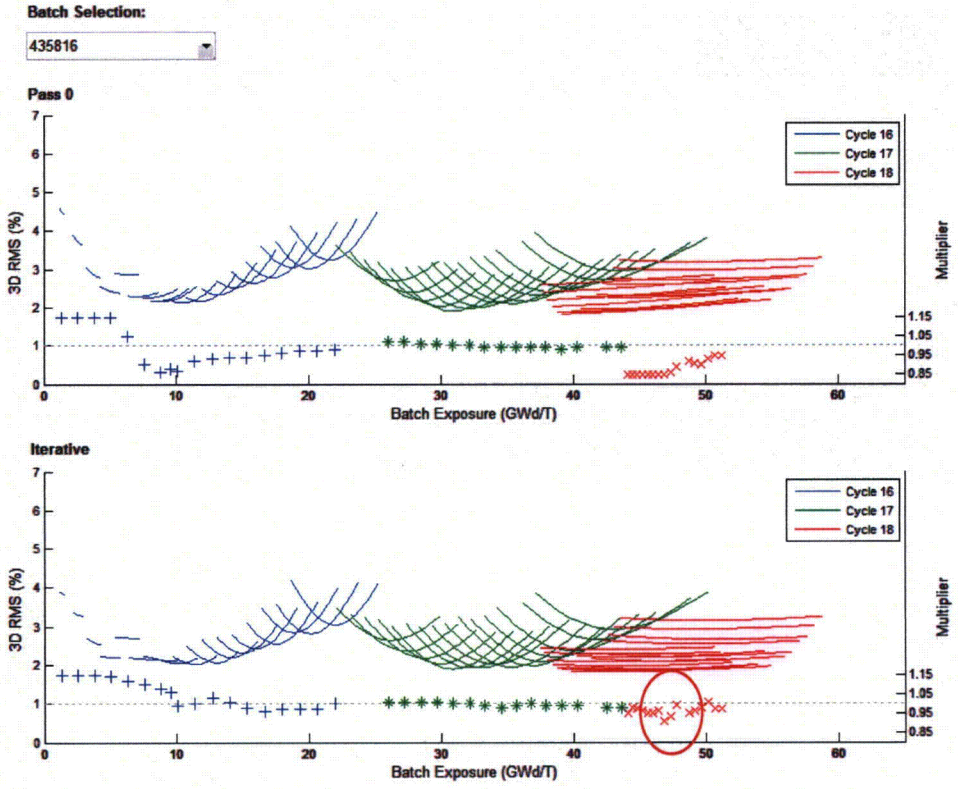

Figure 6-5
Multi-cycle Sub-batch Minimization

Another instance of very low sensitivity can be observed in Figure 6-6 for the data from the first half of cycle 18. In these cases, the large amount of burnable absorbers makes the k-infinity curve versus burnup almost flat. As a result, there is little sensitivity to the sub-batch burnup - until the burnable absorber is significantly depleted (e.g., 10-15 GWd/T).

Another situation which can lead to small sensitivities occurs when only a few assemblies from a sub-batch are used in a cycle. This often occurs when fuel is inserted into the core for its fourth cycle, as depicted in Figure 6-6. Here for cycle 21, only a few assemblies of the sub-batch are re-used and there is very little sensitivity to this sub-batch – as evidenced by the flat r.m.s. differences, as the sub-batch multiplier is changed. Note also that the initial and iterative results for this case (the large blue dots) are dramatically different and very uncertain for such low sensitivity cases.

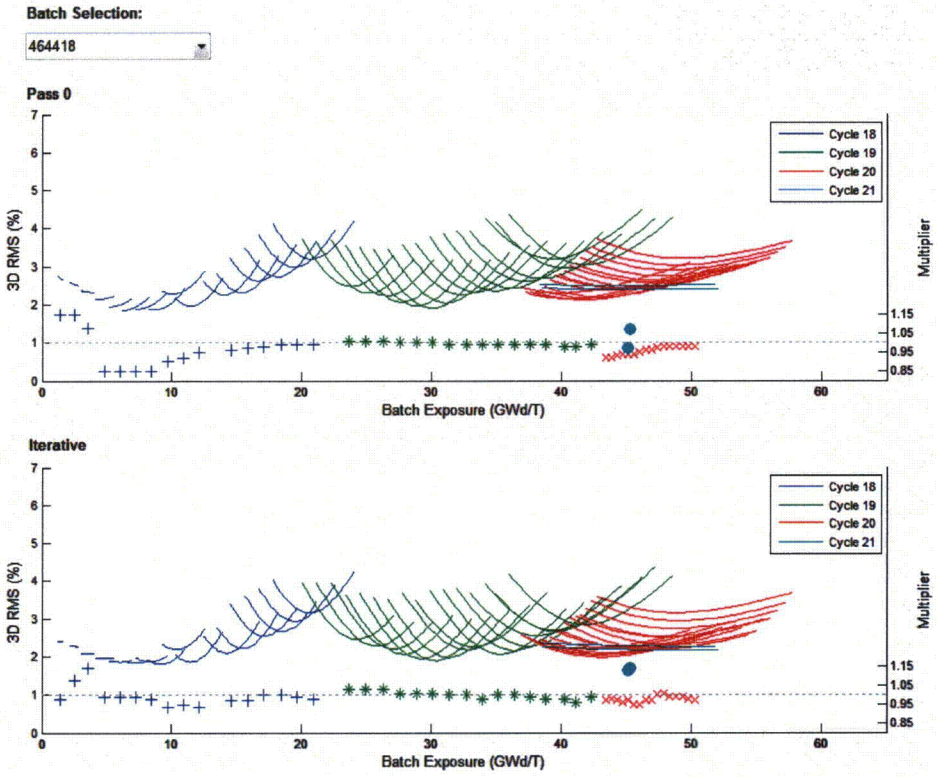

Figure 6-6
Multi-cycle Sub-batch Minimization, Split Batch

Cases that have such low sensitivities are easy to eliminate from the overall search space by simply performing the calculation and monitoring the sensitivity. All such low sensitivity cases are eliminated from the search space – as is explained in the following sub-section of this report.

6.4 Iteration Implementation

The final computational sequence implemented for the analysis in this report can be broken down into a number of discrete steps. For each reactor state at which flux map data is available, the following sequence of steps is performed:

1. Perform standard flux map analysis and compute the initial r.m.s deviation between computed and measured 3D reaction rates
2. Start loop over all sub-batches in the core and over all values of the sub-batch burnup multipliers, M_b, from 0.85 to 1.15
    a. For each sub-batch, determine the sub-batch sensitivity, defined as the minimum of the 2D r.m.s with 0.85 and 1.15 multipliers minus the minimum 2D r.m.s.
3. End loop over sub-batches
4. Set all active sub-batch burnup multipliers, $M_b^{use}=1.0$

5. Start iterative loop for 8 sequential passes
6. Start loop over all sub-batches in the core from maximum to minimum sub-batch sensitivity and over all values of sub-batch burnup multipliers from 0.85 to 1.15
   a. update the active value of M_b^{use} with the value of M_b corresponding to the minimum 3D r.m.s. (subject to the constraint that M_b^{use} not change by more than +/- an input value (0.02) in any single pass.)
   b. If the current sub-batch sensitivity is less than an input value (0.3%) or if the number of assemblies in the sub-batch is less that an input value (12) set the active value of the sub-batch multiplier M_b^{use} to 1.0
7. End loop over sub-batches
8. End iterative loop over sequential passes
9. For all sub-batches (not subject to the constraint of step 6b), compute the SIMULATE-3 reactivity error as the difference of sub-batch reactivities for $M_b = M_b^{use}$ and $M_b = 1.0$

This iterative procedure constrains the change in sub-batch multipliers to be less than 0.02 at each pass so that small changes in sub-batch multipliers are made for all sub-batches before any sub-batch multiplier is changed by a large amount. The rationale for this choice is that the r.m.s differences are often sensitive to all sub-batch multipliers, and it is undesirable to complete a search for one sub-batch before examining the impacts of the other sub-batches in the core. In any case, it should be recognized that this search solves a local minimization problem and is not guaranteed to find the global minimum (which is nearly impossible to determine).

This analytical procedure is also performed for a fixed number of iterations rather than monitoring directly the convergence of results. The reason for this choice is that since sub-batch multipliers are changed in finite steps of 0.01, there are rare cases in which some sub-batches produce multipliers that oscillate by 0.01 in successive passes. This level of oscillation is certainly not important for determining the error in sub-batch reactivity (as explained in the following section), and it far more straightforward to accept such oscillations as an additional uncertainty – rather than switching to a continuous variable search to find the true local minimum.

Figure 6-7 displays sub-batch multipliers for one sub-batch in cycles 16 to 18, and it can be seen that the iteration produces values that are more consistent from cycle to cycle than the pass zero results. This is not only more physical (i.e., reactivity discrepancies should be smooth functions of sub-batch burnup across cycles), but also provides indirect indication that the simultaneous search across all sub-batches is effectively implemented in SIMULATE-3.

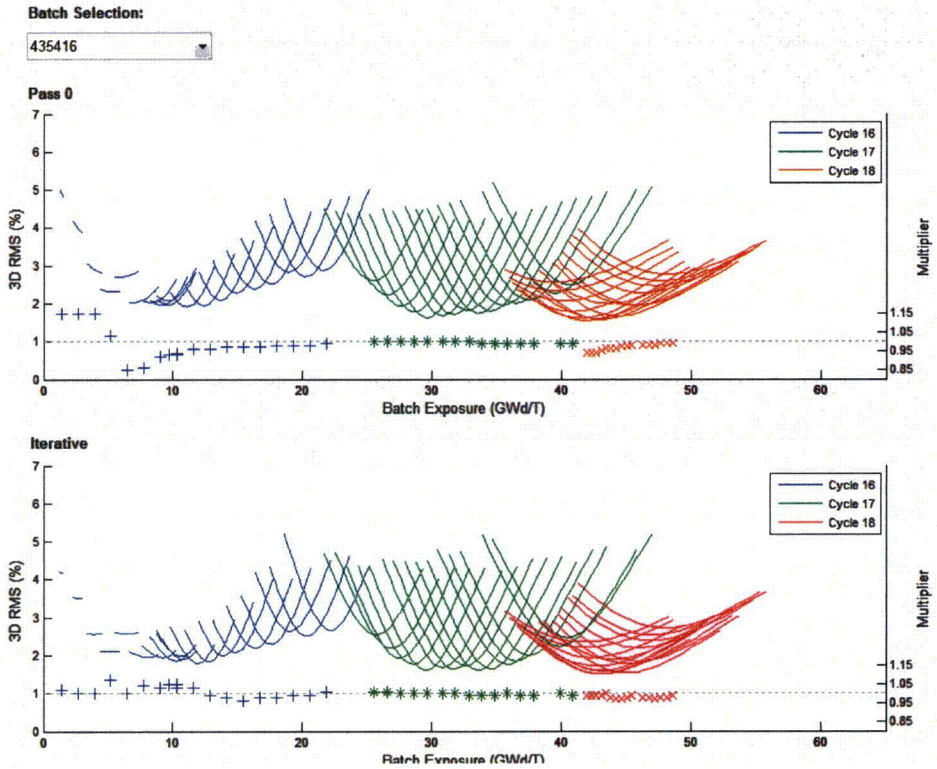

Figure 6-7
Effective Multi-cycle Sub-batch Minimization

For each flux map, this analytical procedure requires approximately 4000 SIMULATE-3 calculations (11 total passes x 31 sub-batch multipliers/sub-batch x ~12 sub-batches in the core). Consequently, analysis of the 44 Duke reactor cycles (680 flux maps) requires a total of approximately 2.7 million SIMULATE-3 cases to be executed. Coding changes have been made in SIMULATE-3 (Version 6.09.22_EPRI) so that this procedure is automatically invoked without need for human intervention, and search results are recorded in a special file that is post-processed to make plots and spreadsheets of results.

Section 7: Measured HFP Reactivity Bias and Uncertainty

The SIMULATE-3 flux map analysis procedure described in Section 6 was performed for all flux maps in the 44 cycles of Catawba Units 1 and 2 and McGuire Units 1 and 2 for which reactor power was above 95%. This analysis produces HFP measured reactivity errors for each sub-batch at each flux map. This section describes how the data from this analysis is used to infer biases in CASMO sub-batch reactivities, and how these biases are translated into measured reactivity decrements and corresponding uncertainties.

7.1 Interpretation of Data

If one plots the estimated sub-batch reactivity errors (delta-k in pcm) versus sub-batch burnup, the data appears as displayed in Figure 7-1. These 2822 measured sub-batch reactivities represent those points from the complete set of approximately 8000 data points (680 maps x ~12 sub-batches per map) that satisfied the two screening criteria of having 12 or more assemblies in a sub-batch and having a detector r.m.s. difference sensitivity greater than 0.3% – as reaction rate differences were iteratively minimized.

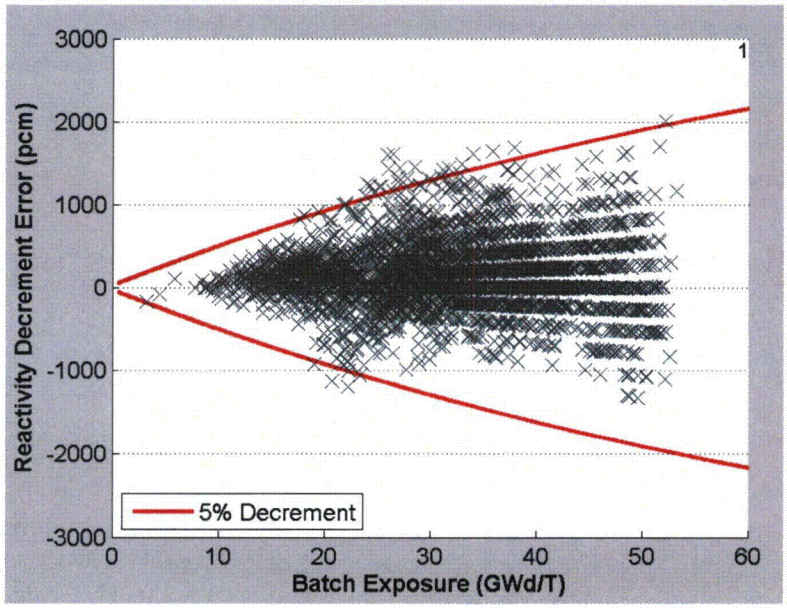

Figure 7-1
Error in Reactivity – No Filters

For comparison purposes, the +/-5% reactivity decrement curves (as computed for a 4.75% enriched, no burnable poison Westinghouse RFA fuel lattice at 900 ppm boron) is plotted in this figure with the two red lines. These curves do not correspond directly to the Kopp Memo's 5% reactivity decrement since reactivities in this plot are computed at HFP conditions with CASMO – not at cold conditions with SFP criticality tools. Nonetheless, the curves provide useful insight to help interpret the scatter in individual data points.

There are a number of things which can be observed from this data. First, there are very few data points at less than 10 GWd/T burnup. This is a result of the fact that almost all sub-batches have large amounts of burnable absorber – which makes the k-infinity curve very flat in burnup, as observed from the boron letdown curve in Figure 5-1. Consequently, **no attempt will be made to quantify the reactivity decrement biases or uncertainties for burnups less than 10 GWd/T.** One should note that since reactivity decrement biases and uncertainties at zero burnup are by definition zero, it should be easy to estimate reactivity decrement biases and uncertainties in this range. Normally, interest focuses on much higher burnups for spent fuel criticality analyses.

One also observes that the data form distinct "lines," particularly at high burnup. This is a direct result of two facts: 1) the slopes of fuel reactivity vs. burnup are very similar for all fuel types (after burnable absorbers are depleted), and 2) the search for sub-batch burnup multipliers was performed with a discrete 0.01 multiplier resolution. Consequently, the data behavior is expected, and one should simply interpret each data point as each having an intrinsic added "measurement" uncertainty proportional to burnup and having a magnitude of approximately +/-100 pcm at 50 GWd/T. Because there are so many data points in the com-

posite set of data, this uncertainty has almost no impact on results deduced from the data.

At first glance, the data appears to be nearly equally distributed around 0 pcm decrement error, with a large spread in individual points. It is important to understand what influences this spread in data. Items known to contribute to the spread in the individual data points of Figure 7-1 include:

- Reaction rate measurement errors or uncertainties
- Differences in sub-batch spectra vs. CASMO lattice assumption (zero leakage)
- Differences in intra-assembly spatial flux distributions vs. lattice assumption
- Influences from super-batch lumping of multiple burnable poison loadings
- Imperfect knowledge of core configuration (fuel bowing, fuel elongation, crud)
- Errors in computed sub-batch burnups (used as the plot ordinate)
- Errors in SIMULATE-3 nodal and detector physics models
- Errors in SIMULATE-3 cross-section data fitting models
- Imprecision in iterative analysis method, particularly for low sensitivity sub-batches
- Errors in CASMO computed nuclide inventory vs. fuel burnup
- Errors in fundamental neutron cross-section data
- Imperfect knowledge of reactor operating power level

The items in this list have been divided into three sets, indicated by text color. The first terms have two distinct characteristics: 1) because both measured and computed reaction rates are normalized distributions, these effects are expected to be randomly distributed with little bias, and 2) these effects either do not enter into SFP/cask criticality analysis or are treated with their own uncertainties. For instance, errors in SIMULATE-3 models or lattice spectral assumptions are not relevant for SFP analysis because such analysis is performed directly by Monte Carlo in rack geometry.

The second sub-list item can be addressed directly by refining our treatment of sub-batch sensitivities and will be treated directly in the following sections of this report.

The first two items in the third sub-list are the two terms we seek to measure in this project, and it is clear that the effects in this third sub-list will not be random in nature – as one expects these errors to change systematically (in an as yet unknown manner) as fuel assemblies are burned.

In the iterative analysis method, all three categories of errors are treated as if they are errors in CASMO sub-batch reactivities – which is the reason we expect the spread in individual data points to be much larger than the actual CASMO sub-

batch reactivity errors. What remains to be shown is that one can use this set of data, with its inherent spread, to correctly deduce the errors in CASMO lattice reactivities.

7.2 Sub-batch Sensitivities

It is important that reaction rate sensitivities to sub-batch burnups be sufficiently large to overcome measurement uncertainties – or the signals used to deduce sub-batch reactivity errors will not be meaningful. We have already outlined how sub-batch sensitivity has been used in the iterative process. However, it is also appropriate to examine analysis results to determine the sensitivities to screening parameters, which can be done by further post-screening of results.

If one increases the sensitivity screening parameter from 0.3% to 0.5%, 0.7%, 0.9%, and 1.1%, the changes in retained data are displayed in Figures 7-2 to 7-5. One observes that increasing the sensitivity screening parameter eliminates points at burnups less than 10 GWd/T and tightens the spread of data. This is a clear indication that it is important to choose the screening criteria large enough that our "measurement signal" is larger than the basic reaction rate measurement errors. As one increases the screening parameter, the number of remaining data points are reduced, from 2822 to 2417, 2122, and 1845, respectively, but the data shape is largely unchanged. Consequently, the remainder of this report uses sensitivity screening criteria of 0.9% as a compromise between reducing scatter and retaining large numbers of data points.

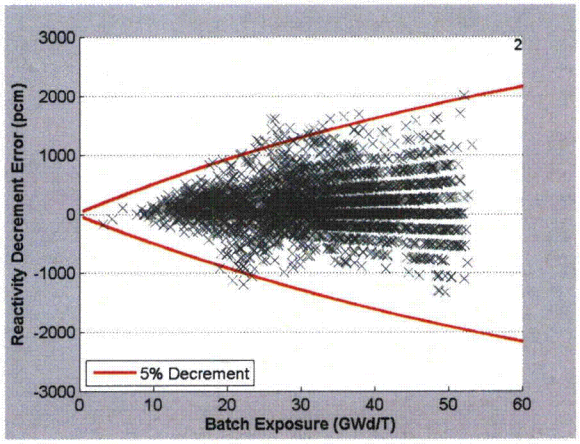

Figure 7-2
Error in Reactivity – 0.5% Sensitivity Filter

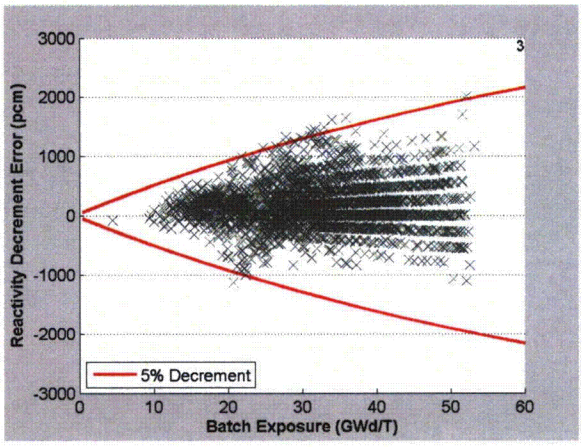

Figure 7-3
Error in Reactivity – 0.7% Sensitivity Filter

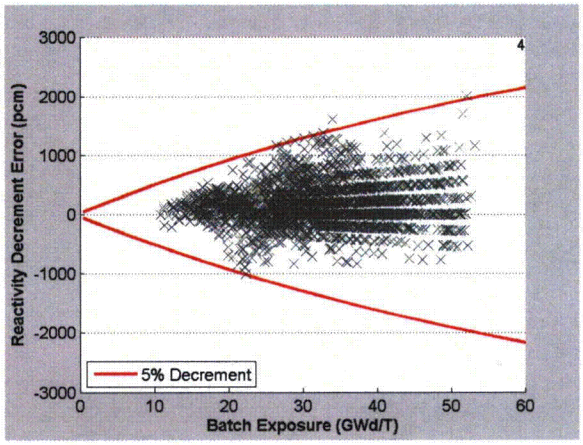

Figure 7-4
Error in Reactivity – 0.9% Sensitivity Filter

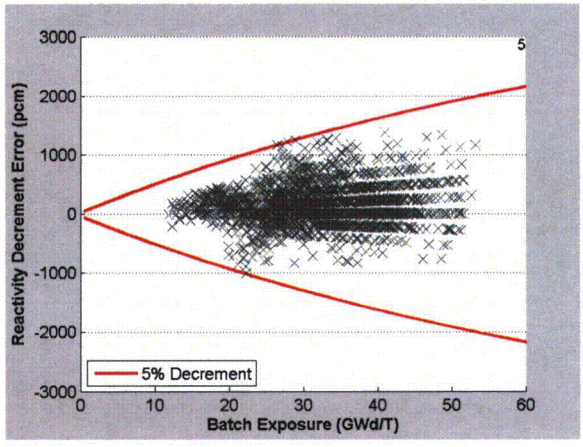

Figure 7-5
Error in Reactivity – 1.1% Sensitivity Filter

We have already outlined how the minimum of 12 assemblies in a sub-batch has been used as a screening parameter in the iterative process. This criterion can also be examined by performing further post-screening of data. If the number of assemblies required in a sub-batch is increased from 12 to 16, 20, 24, and 28, the retained data are displayed in Figures 7-6 to 7-9. The data shows very little change in spread as smaller batches are screened out, and the number of remaining sub-batches is dramatically reduced from 2122 to 1981, 1265, 1120, and 819, respectively. Consequently, there is no advantage for a screening criterion larger than 12, and the remainder of this report uses the screening of 12, as directly applied in the iterative analysis.

In the early part of a cycle, there are many changes in the fuel that are unique to depleting fuel after a shutdown interval: 1) short-lived fission product chains (e.g., I, Xe, Pm, Sm, etc.) are re-equilibrated, 2) some short half-life transuranic nuclides chains (e.g., ^{239}Np, ^{239}Pu) are re-equilibrated, and 3) operating fuel temperatures are re-established. These things are unique to early cycle operations and not important for fuel in SFP and cask analyses. Consequently, early cycle data can be examined for larger fluctuations in data than later-cycle points. By screening out the first 1.0, 2.0, and 3.0 GWd/T flux maps in each cycle, one obtains data displayed in Figures 7-10 to 7-12. It is clear that the early-cycle points introduce larger spread in the data, and eliminating maps below 3.0 GWd/T removes many of these points. The number of data points is reduced from 2122 to 1933, which is not very significant, and the remaining points span the complete range of burnup needed. Screening of flux maps at less than 3.0 GWd/T cycle burnup is used in the remainder of this report.

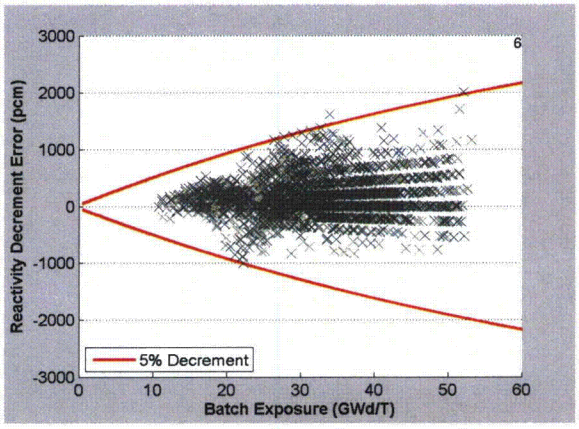

Figure 7-6
Error in Reactivity – Batch Size >= 16

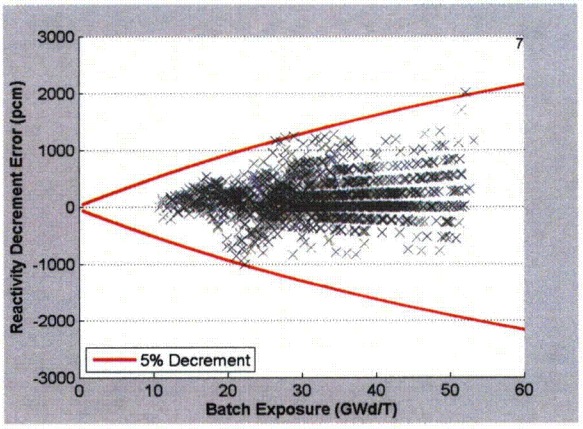

Figure 7-7
Error in Reactivity – Batch Size >= 20

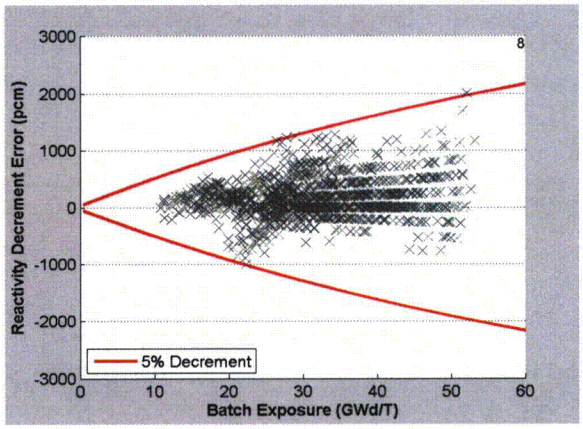

Figure 7-8
Error in Reactivity – Batch Size >= 24

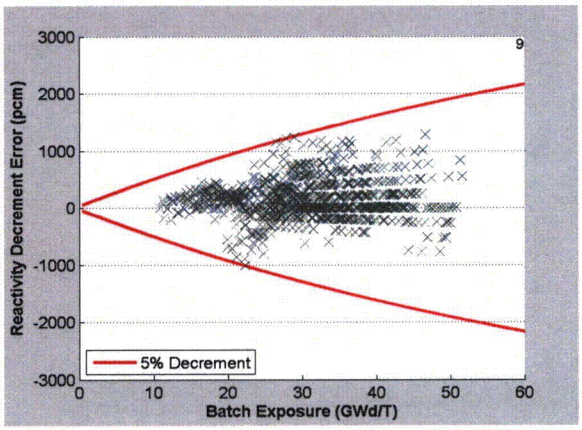

Figure 7-9
Error in Reactivity – Batch Size >= 28

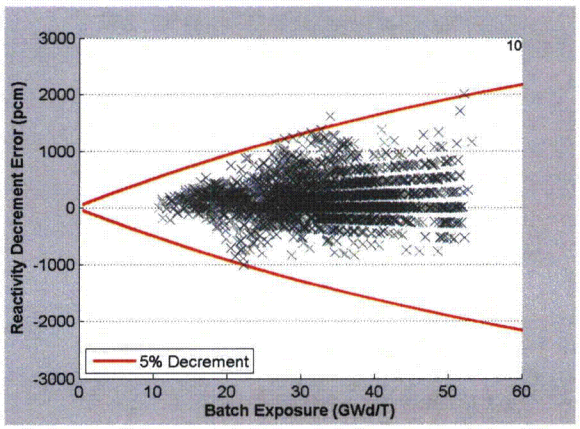

Figure 7-10
Error in Reactivity – Cycle Burnup >= 1.0

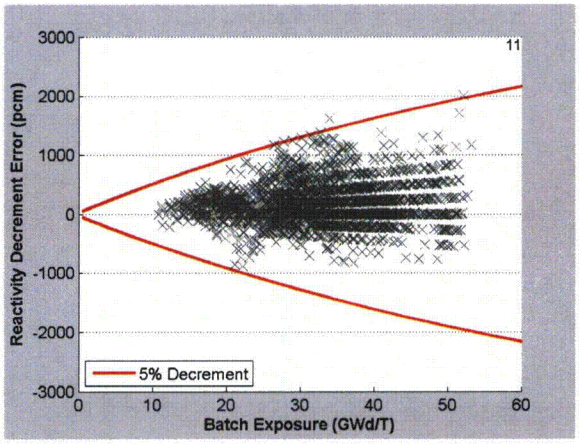

Figure 7-11
Error in Reactivity – Cycle Burnup >= 2.0

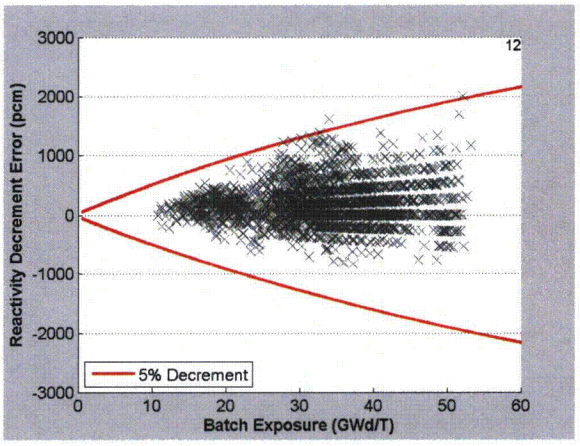

Figure 7-12
Error in Reactivity – Cycle Burnup >= 3.0

7.3 Sensitivities to Reactor Model

The data of Figure 7-12 is plotted here again, now with a MATLAB[19]-generated quadratic polynomial regression fit (constrained to 0.0 at 0 GWd/T) of the data points. This allows one to see the magnitude of the mean bias of computed CASMO-4 sub-batch reactivity decrements.

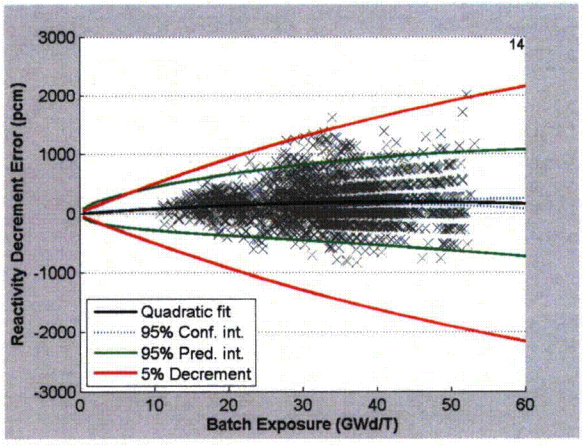

Figure 7-12A
Error in Reactivity – Point-wise Confidence Intervals

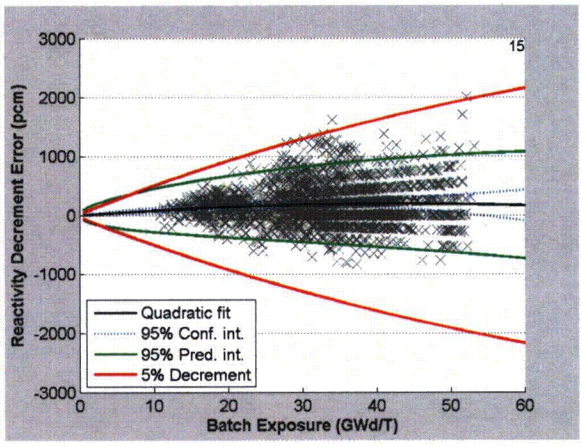

Figure 7-12B
Error in Reactivity – Batch-wise Confidence Intervals

To make upcoming comparisons easier to visualize, Figure 7-12A includes the classic 95% prediction interval and the 95% confidence intervals around the quadratic fit. Recognizing that there are significant correlations within the measured data of each cycle (each flux map changes slowly from the preceding flux map), Figure 7-12B includes a plot of the confidence interval in which complete correlation of the points within each batch is assumed. This assumption results in a statistical treatment with the number of points being equal to the number of unique sub-batch/cycle combinations, rather than the traditional total

number of data points. The resulting confidence band is approximately four times as wide as that displayed in Figure 7-12A. The quality of the data fits will be addressed in the following sections, so the prediction and confidence intervals should simply be considered here as "eye-guides," and the wider confidence interval will be used in all subsequent plots.

If the data is examined separately for each of the four reactor units, the plots displayed in Figures 7-13 to 7-16 are obtained. The regression fits in each plot show that CASMO reactivity decrements are over-predicted (i.e., CASMO k-infinity needs to be increased with burnup to match measurements), and there is little difference between one unit and another. Since all four units have fuels of similar range of enrichments and burnable absorbers, the latter is not surprising.

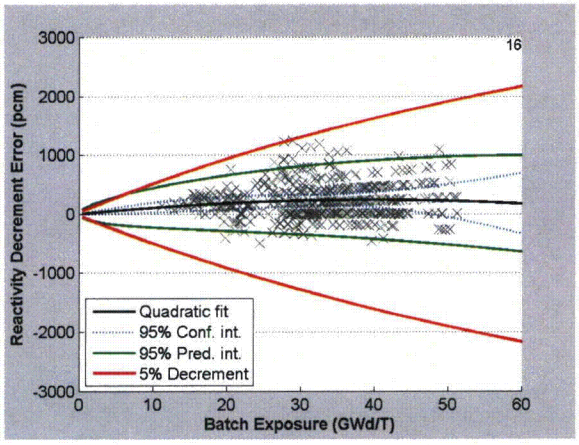

Figure 7-13
Error in Reactivity – McGuire-1

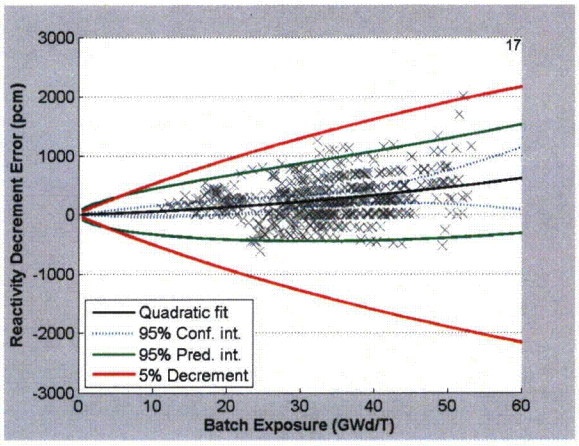

Figure 7-14
Error in Reactivity – McGuire-2

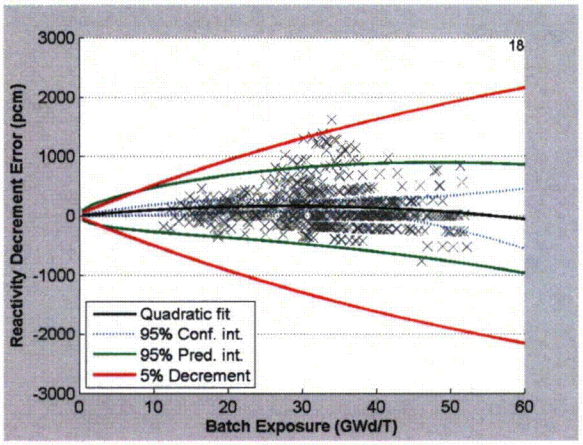

Figure 7-15
Error in Reactivity – Catawba-1

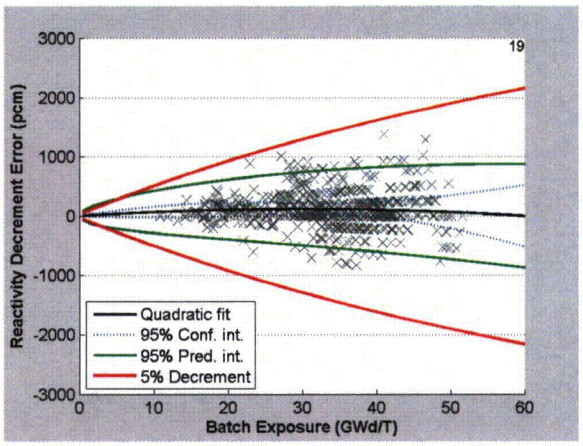

Figure 7-16
Error in Reactivity – Catawba-2

Because the data for each of the four units are so similar, all data will be lumped together for the remainder of this report so that more data points are available to improve the statistics of measured reactivity decrements biases.

7.4 Sub-batch Enrichment Sensitivities

If all of the units are lumped into one large data set, we can examine trends with fuel enrichment. By splitting the data into intervals of 0.25% ^{235}U enrichment, the enrichment-dependent plots of reactivity decrement errors are displayed in Figures 7-17 to 7-21. The data in these plots show, that at the 200 pcm level of discrimination, there is no significant difference in CASMO-4 reactivity decrement errors with enrichment (in the range of 3.75% to 5.0%).

Given that there are no significant differences in reactivity decrement with enrichment, we can treat all of the data as a single set and look closer at the burnup dependence of the data.

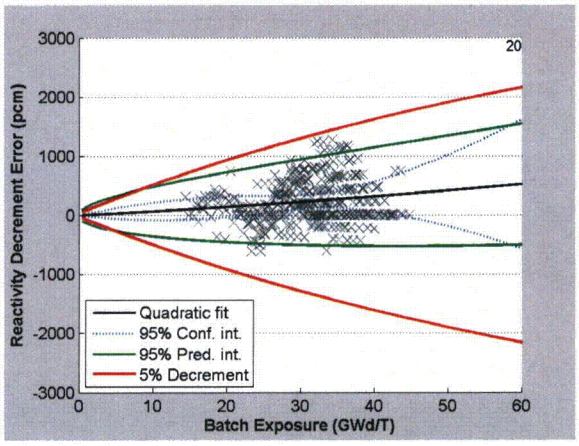

Figure 7-17
Error in Reactivity – Enrichment 3.75 - 4.0%

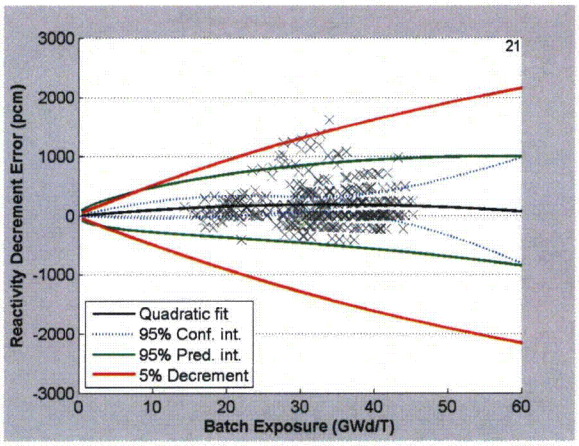

Figure 7-18
Error in Reactivity – Enrichment 4.00 - 4.25%

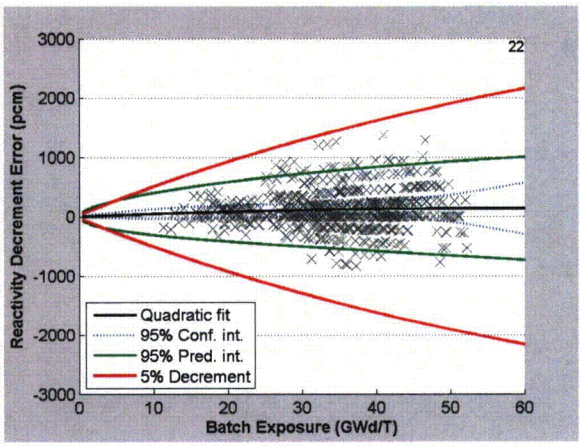

Figure 7-19
Error in Reactivity – Enrichment 4.25 - 4.50%

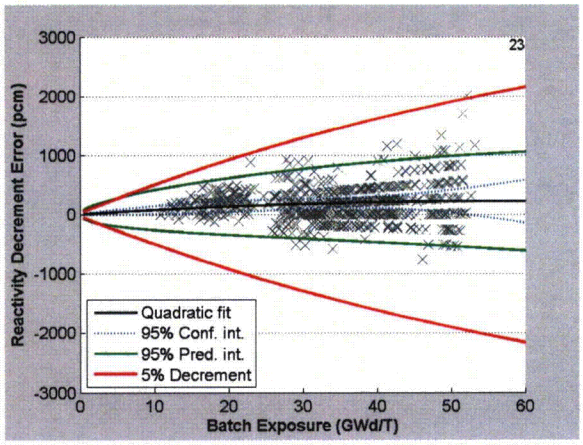

Figure 7-20
Error in Reactivity – Enrichment 4.50 - 4.75%

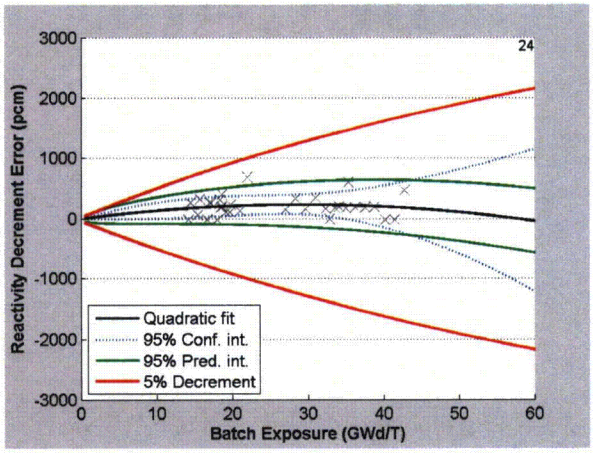

Figure 7-21
Error in Reactivity – Enrichment 4.75 - 5.00%

7.5 Burnup Reactivity Decrement Biases and Confidence Intervals

With all units lumped into one data set we can examine in detail the statistical implications of the regression analysis and make some statements about the CASMO-4 bias and uncertainty in burnup reactivity decrement. Figures 7-22 and 7-23 display results of linear and quadratic regressions assuming all units, enrichments, and sub-batches constitute a single set of data.

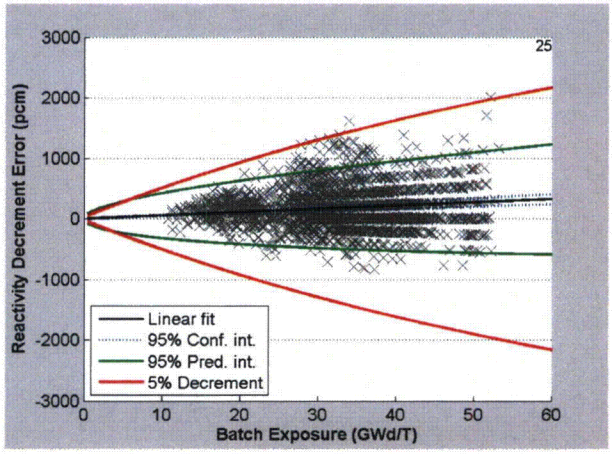

Figure 7-22
CASMO-4 Decrement Error – Linear Regression

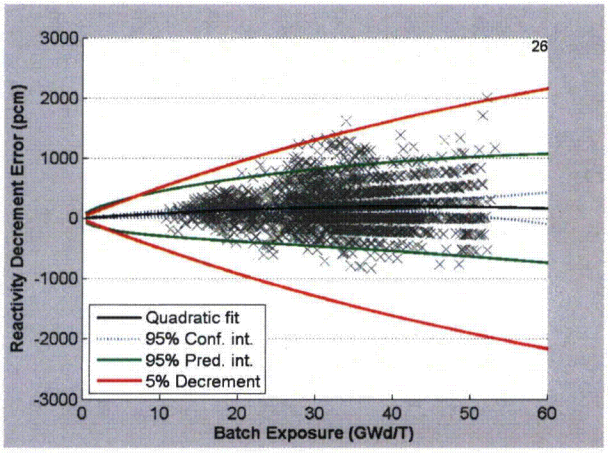

Figure 7-23
CASMO-4 Decrement Error – Quadratic Regression

What conclusions can be drawn from the data and the regressions? **First, almost none of the individual estimated CASMO HFP reactivity decrement errors points are outside the Kopp recommended bounds.** However, the line displayed as the 5% Decrement was computed for 4.75% enriched Westinghouse RFA assemblies with no burnable absorbers at core average conditions and 900 ppm

boron. Calculations show that the sensitivity of reactivity decrement curve versus enrichment, burnable absorber, and boron concentration is small – on the order of 200 pcm. Since it is difficult to compute reactivity decrements separately for each sub-batch (as each sub-batch has different boron histories), one should consider the 5% Decrement curves to be +/- 200 pcm at a burnup of 50 GWd/T. This does not change our basic interpretation, other than one should alter the preceding statement to say that **more than 99% of the individual estimated CASMO-4 HFP reactivity decrement error points lie within the Kopp recommended bounds.**

The plotted 95% prediction intervals of both the linear and quadratic regressions are much narrower than the Kopp bounds. At 20 GWd/T the prediction interval widths are 523 pcm for the linear fit and 522 pcm for the quadratic fit, while the Kopp bound widths are 922 pcm. At 40 GWd/T, the prediction interval widths are 740 pcm for the linear fit and 738 pcm for the quadratic fit, while the Kopp bound widths are 1615 pcm. Consequently, one can conclude that the **95% prediction bounds of estimated CASMO HFP reactivity decrement errors are narrower than the Kopp bounds by about a factor of two.**

However, one must temper the last statement with the knowledge that formal statistics require very stringent limitations on the data in order for the bound to be strictly applicable, such as:

- The ordinate values must be known exactly (the sub-batch burnups)
- Every data point must be independent from every other point
- The residuals (differences between the individual points and the fit at that ordinate) must have normal distributions for all ordinates
- The variance of data must have a constant (or known) variation with the ordinate

Unfortunately, none of these points are satisfied by this data: 1) the ordinates are not known exactly - since they are computed or measured burnups, 2) the data at successive flux maps are correlated - since core power distributions evolve slowly, results from one flux map and the next are highly correlated, 3) residuals are not normal at all burnups, and 4) the data is heteroscedastic, as the variance grows with burnup (we have assumed linear change of variance with burnup in these regression fits), and this variation cannot be known precisely.

None of this is surprising, since each reactor measurement is not an independent measurement of a fixed parameter. Prediction and confidence interval computations necessarily make the assumption that one is repeatedly sampling from a fixed, but unknown, distribution. The impact of this assumption on computed confidence intervals is very clear in the case of the linear regression – which has a classic confidence interval width of only 30 pcm. This is very narrow - only because there are ~1900 data points, and one should note that the confidence interval goes to zero as the number of measurements approaches infinity. Hence, the confidence interval from a regression to the data cannot be used directly as the uncertainty of the regression fit. The prediction interval, however, will not

change as the number of data points approach infinity. As a result, one should simply state that **more than 95% of the estimated CASMO-4 HFP reactivity decrement errors lie inside the arbitrary band computed as regression prediction intervals, and that band is narrower than the Kopp band by approximately a factor of two** – by simply counting points that lie within the band – regardless of the source of that prediction band. However, the true uncertainty of the regression fit lies between the confidence and prediction intervals, and one method of evaluating that uncertainty is presented in the following section.

7.6 Burnup Reactivity Decrement Biases and Uncertainties

A direct method by which one can measure the error of the regression fit to CASMO-4 reactivity decrement errors is to introduce a known deficiency into the CASMO-4 cross-section library, apply the analytical methods using the deficient library, and then compare the measured reactivity decrements errors with the known decrement change. This direct approach has been performed for a CASMO-4 cross-section library in which the lumped fission product (LFP) cross sections have been set to zero. This choice of deficiency was motivated by two considerations: 1) the deficiency introduces no change at zero burnup, and 2) the magnitude of the deficiency is similar in magnitude to the Kopp 5% reactivity decrement.

A small modification was made to the iterative procedure such that the iterative search for individual sub-batch multiplies would always start from the best estimate of the "core averaged" value of sub-batch multipliers:

1. Perform standard flux map analysis and compute the initial r.m.s deviation between computed and measured 3D reaction rates
2. Start loop over all sub-batches in the core and over all values of the sub-batch burnup multipliers, M_b, from 0.85 to 1.15
3. For each sub-batch, determine the sub-batch sensitivity, defined as the minimum of the 2D r.m.s with 0.85 and 1.15 multipliers minus the minimum 2D r.m.s.
4. End loop over sub-batches
5. **Start loop over values of the sub-batch burnup multipliers, M_b, from 0.85 to 1.15**
6. **Set all sub-batch burnup multipliers, M_b**
7. **End loop over sub-batch burnup multipliers**
8. **Save value of M_b ($=M^{use}_{core}$) that produced minimum 3D r.ms. in reaction rates**
9. Set all active sub-batch burnup multipliers, M^{use}_{core}
10. Start iterative loop for 8 sequential passes
11. Start loop over all sub-batches in the core from maximum to minimum sub-batch sensitivity and over all values of sub-batch burnup multipliers from 0.85 to 1.15

a. Update the active value of M_b^{use} with the value of M_b corresponding to the minimum 3D r.m.s. (subject to the constraint that M_b^{use} not change by more than +/- an input value (0.02) in any single pass.)

b. If the current sub-batch sensitivity is less than an input value (0.3%) or if the number of assemblies in the sub-batch is less that an input value (12) set the active value of the sub-batch multiplier M_b^{use} to M^{use}_{core}

12. End loop over sub-batches

13. End iterative loop over sequential passes

14. For all sub-batches (not subject to the constraint of step 11b), compute the SIMULATE-3 reactivity error as the difference of sub-batch reactivities for $M_b = M_b^{use}$ and $M_b = 1.0$

All 44 cycles flux maps (2.7 million SIMULATE-3 calculations) were re-evaluated with the deficient library and plots of the reactivity decrement errors are display in Figures 7-24 and 7-25. These results show that there is little difference between the linear and quadratic regressions, but the lack of data points below 10 GWd/T seems to affect the quadratic shape more adversely. The linear regression fit is close to the known CASMO decrement change (the difference between calculations with CASMO-4 and CASMO-4 with no-LFP for a 4.75% enriched Westinghouse RFA assembly at 900 ppm boron). However, since the normal CASMO-4 library has some error relative to measured, the correct comparison is the difference between the measured decrement errors with the normal CASMO-4 library (Figure 7-23) and with the no-LFP library (Figure 7-24). Figure 7-26 displays the difference of these measured decrement error fits and the known deficient library decrement change – over the range of burnups from 5 to 55 GWd/T. It can be seen that the maximum difference at any burnup is ~125 pcm. This indicates that the analytical method (with a regression fit to the resulting data) has measured errors in reactivity decrement of the CASMO-4 no-LFP library with a precision better than 125 pcm, even where the library deficiency is as large as 2000 pcm.

This direct test provides one concrete evaluation of the uncertainty in the regression fit of the estimated CASMO-4 sub-batch reactivity decrements. While any such test is not unique, this provides evidence that the uncertainty of the regression curve is far less than the prediction interval. This is not surprising because as was pointed out in Section 6, most of the terms that contribute to spread in the individual estimates of error are from random sources, not from the systematic deficiencies that we are attempting to measure. Since the regression fit is not sensitive to random errors, the fit provides a quite accurate measure of the underlying error of the CASMO-4 reactivity decrements.

Because the same flux map data and identical data analysis techniques are used in the regression fits of Figure 7-23 and in the no-LFP library test, the uncertainty of the regressions will be similar in both cases. If we take the largest observed deviation in Figure 7-26 (125 pcm) and assume it to be a conservative estimate of one-sigma uncertainty in the regression fits, we can then use (250 pcm) as the 2-sigma uncertainty of the regression fit for all sub-batch burnups.

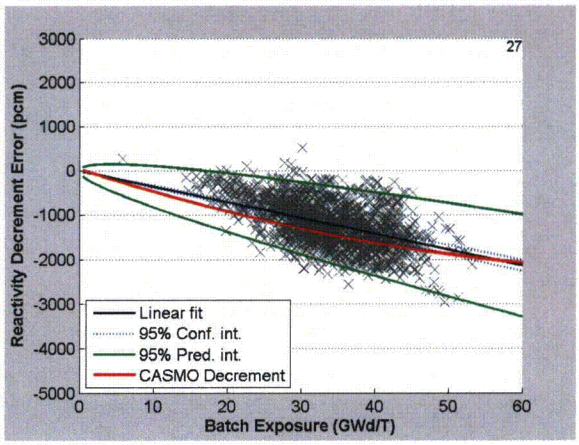

Figure 7-24
Error in Decrement – No-LFP - Linear

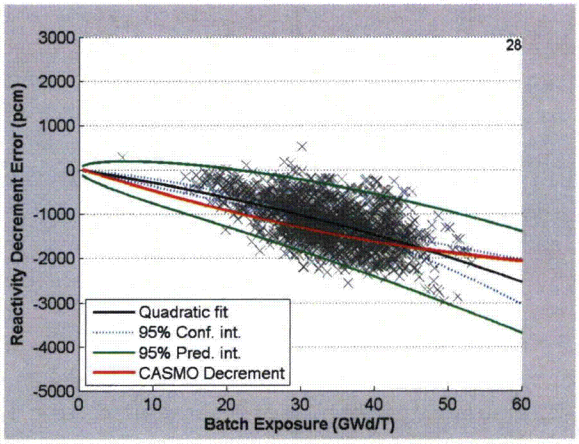

Figure 7-25
Error in Decrement – No-LFP – Quadratic

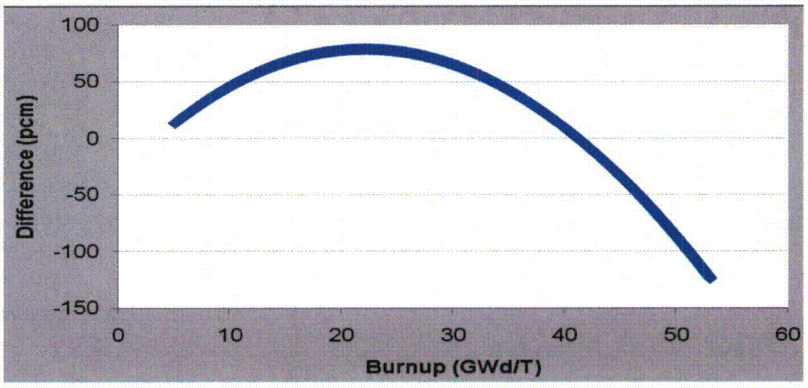

Figure 7-26
Measured vs. Known CASMO-4 (No-LFP) Reactivity Decrement Change

To provide another data point, we have also repeated all of the analysis using CASMO-5 to examine the measured errors in the ENDF-B/VII library reactivity decrement and those results are plotted in Figure 7-27.

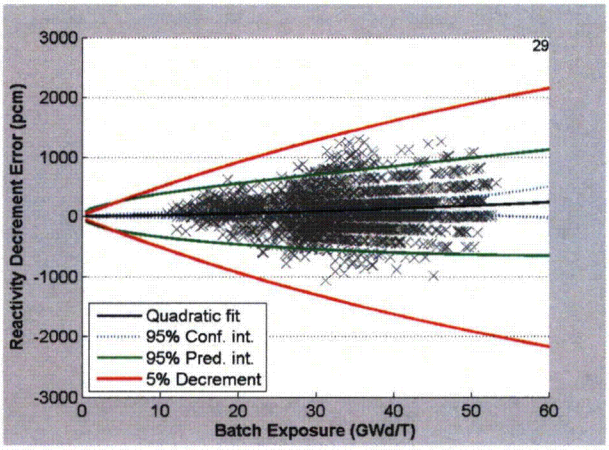

Figure 7-27
CASMO-5 Decrement Error – Quadratic Regression

CASMO-5 decrement errors have a slightly different shape than the CASMO-4 errors (see Figure 7-23), but the differences are much smaller than the estimated uncertainty of the regression fits.

Table 7-1 displays the measured CASMO-4 and CASMO-5 biases in HFP reactivity decrement and uncertainty as a function of sub-batch burnup.

Table 7-1
Measured CASMO-4 Reactivity Decrement Bias (change needed to match measurement)

Burnup (GWd/T)	10.0	20.0	30.0	40.0	50.0	60.0
CASMO-4 Bias (pcm)	81	140	178	196	192	167
CASMO-5 Bias (pcm)	19	46	81	125	177	238
Uncertainty (pcm)	250	250	250	250	250	250

7.7 Boron and Cycle Burnup Sensitivities

Plots of CASMO-4 HFP reactivity decrement errors vs. core boron concentration and cycle burnup are displayed in Figures 7-28 and 7-29, and these data show that reactivity decrement errors are relatively constant at +200 pcm, with a small dependence on core boron concentration. Reactivity decrement errors have a trend of increasing from near zero bias at BOC to approximately +200 pcm at MOC and EOC. Both trends are smaller in magnitude than the assigned uncertainty in measured HFP reactivity decrements (250 pcm).

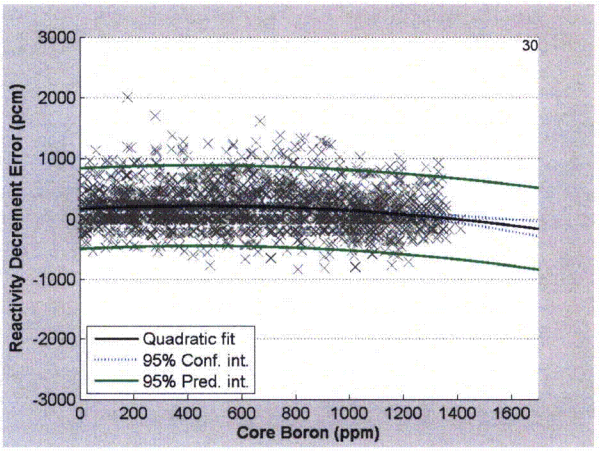

Figure 7-28
CASMO-4 Bias in Reactivity Decrement vs. Core Boron

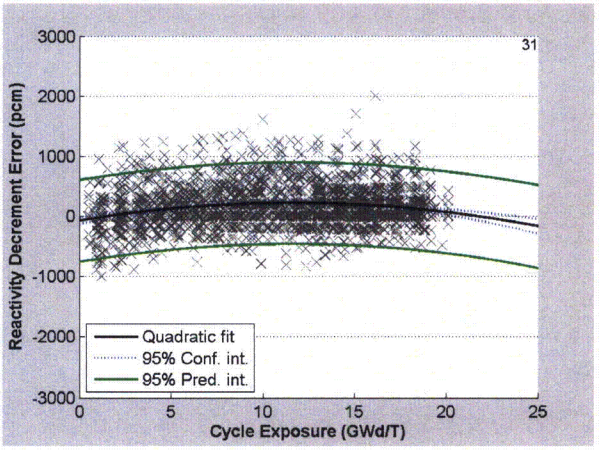

Figure 7-29
CASMO-4 Bias in Reactivity Decrement vs. Cycle Burnup

Another cross check of the accuracy of the decrement biases deduced from flux map data is to compare the BOC to EOC trends from the flux map data with the mean changes in measured boron bias from BOC to EOC. Such a comparison is presented in Table 7-2 for each of the four Duke Energy Plants - assuming a core-average burnup of 10 GWd/T at BOC and 30 GWd/T at EOC and a conversion from boron error to pcm using an assumed value of 9.0 pcm/ppm. These data shows that the mean flux map reactivity decrements agree within 113 pcm of the measured boron bias changes for each of the four reactors.

The difference between the mean BOC-to-EOC decrements bias changes from the boron data for the McGuire Units (+216 pcm) and the Catawba Units (+108 pcm) of +108 pcm also agrees well with the +82 pcm change derived from flux map data for the McGuire Units (+140 pcm) and Catawba Units (+58 pcm).

Thus, even small reactor-to-reactor differences are well-predicted from flux map data – giving further evidence that the regression fits provide accurate burnup dependences for HFP decrement biases.

The composite BOC to EOC change from the quadratic fit to measured flux map decrement biases vs. cycle exposure, displayed in Figure 7-29, of +205 pcm (-74 pcm BOC to 131 pcm at 18 GWd/T) is also consistent with the measured BOC to EOC boron bias changes.

Table 7-2
Measured CASMO-4 BOC to EOC Reactivity Decrements

Unit	Reactor Boron Bias (pcm @ 9 pcm/ppm)			Flux Map Decrement Bias (pcm)		
	BOC (ppm)	EOC (ppm)	BOC-EOC (pcm)	10 GWd/T	30 GWd/T	30-10 GWd/T
McGuire 1	-4	-30	234	107	228	121
McGuire 2	-10	-32	198	49	210	161
Catawba 1	13	5	72	96	161	65
Catawba 2	30	14	144	66	118	52
		Mean	167		Mean	100

All differences between measured boron reactivity decrement changes and measured flux map decrement data are well within the conservatively-assigned uncertainty of 250 pcm for HFP reactivity decrements, as summarized in Table 7-1.

Section 8: Measured Cold Reactivity Bias and Uncertainty

The SIMULATE-3 flux map analysis procedure described in Section 6 allowed quantification of the bias and uncertainty in CASMO reactivity decrements at hot full power (HFP) conditions. However, for spent fuel and cask criticality analyses, biases and uncertainties are needed at cold conditions.

8.1 Overview

The biases and uncertainties at HFP include errors associated with both the assembly isotopics and cross-section data uncertainties. At cold conditions (before cooling) the isotopics do not change, but there are additional uncertainties from the altered conditions. Two such sources of added uncertainty arise because of: 1) imprecise knowledge of exact physical properties (e.g., fuel temperature, coolant temperature, boron concentration) during fuel irradiation and 2) spectrum-induced reactivity changes from HFP to cold conditions from cross-section data uncertainties.

8.2 Fuel Temperature Uncertainties

At SFP or cask conditions, coolant temperature, fuel temperature and boron concentrations are all well known. At HFP conditions coolant temperatures and boron concentrations are well known, and they do not depend in any direct way on sub-batch burnups. However, fuel temperatures are not as easy to compute accurately. Fuel conductivity decreases about 50% at high burnup, and pellet swelling and gap conductance changes cause fuel temperatures to change with pellet burnup. The net effect is that there is an added uncertainty in measured reactivity decrements because of imperfect knowledge of HFP fuel temperatures.

This situation is easiest to understand by assuming that one has a lattice code that computes HFP sub-batch reactivities with zero bias – for all burnups. If there are any errors in HFP fuel temperatures, the corresponding reactivity bias must be cancelled out by other biases in the lattice code reactivities at HFP conditions. Consequently, there are uncertainties in measured HFP reactivity decrements that arise from imperfect knowledge of fuel temperatures at operating reactor conditions. In addition, even though SFP temperatures might be known exactly, the history (e.g., depletion) effects of fuel temperature errors also contribute additional uncertainties in lattice code reactivities at cold conditions.

There is no easy way to quantify precisely the fuel temperature reactivity decrement uncertainty change from HFP to cold conditions. The INTERPIN-4 plot of fuel temperature vs. burnup displayed in Figure 8-1 shows that predicted fuel temperatures decrease by about 50K as the pellet swells, the clad creeps down, and as the pellet/clad gap closes. At high burnup, the decrease in fuel conductivity overwhelms the gap conductance changes, and fuel temperatures increase significantly.

One way to conservatively treat uncertainties in fuel temperatures on HFP and cold reactivities is to treat the entire reactivity effect as additional uncertainties. By taking the highest and lowest fuel temperatures that occur anywhere in the nominal INTERPIN-4 predictions (4.75% enriched Westinghouse RFA fuel) and performing CASMO-5 calculations with these fixed temperatures, one obtains the table of reactivity differences presented in Table 8-1. These results show that at hot conditions, the instantaneous decrease in reactivity for the higher fuel temperature is partially compensated at high burnup by the production of additional plutonium, with the cumulative effect being almost zero at 55 GWd/T. However, in the branch cases to cold conditions, the higher HFP fuel temperature leads to a monotonic increase in lattice reactivity. These results show that the maximum difference reactivities are -150 pcm at HFP conditions and +206 pcm at cold conditions. Since the shape of fuel temperature variation with depletion cannot be known exactly, we use these reactivity changes to estimate the magnitude of reactivity uncertainties – not the shape of the uncertainties versus depletion. **To be conservative, we statistically combine the maximum computed changes in HFP reactivity and cold reactivity and treat this as a 2-sigma burnup decrement uncertainty of 255 pcm arising from HFP fuel temperature uncertainties – independent of sub-batch burnup.**

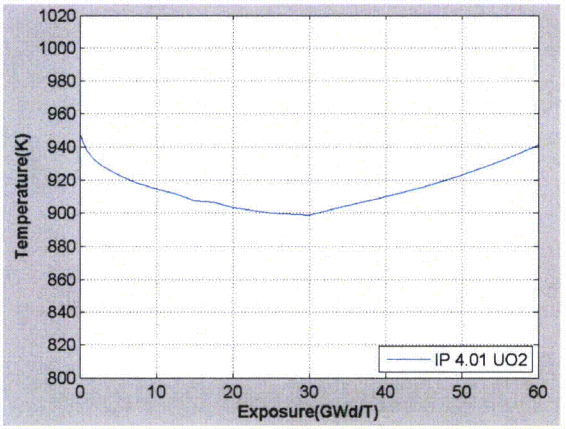

Figure 8-1
Typical INTERPIN-4 Fuel Temperature Change With Burnup

Table 8-1
Fuel Temperature Effect on Hot and Cold Lattice Reactivity

Burnup (GWd/T)	Hot Depletion (HFP)			Branch to Cold (Bor=0, Xen=0, 293K)		
	k-infinity (946K)	k-infinity (897K)	Difference 946K-897K	k-infinity (946K)	k-infinity (897K)	Difference 946K-897K
0.0	1.07712	1.07848	-0.00136	1.15285	1.15285	+0.00000
10.0	1.13346	1.13492	-0.00146	1.20192	1.20189	+0.00003
20.0	1.13467	1.13617	-0.00150	1.21248	1.21229	+0.00019
30.0	1.08533	1.08650	-0.00117	1.16481	1.16421	+0.00060
40.0	1.02515	1.02586	-0.00071	1.09975	1.09866	+0.00109
50.0	0.96862	0.96887	-0.00025	1.03605	1.03445	+0.00160
60.0	0.91905	0.91888	+0.00017	0.97875	0.97669	+0.00206

8.3 Cold Uncertainty Change From Cross-Section Uncertainties

The TSUNAMI-3D sequence in ORNL's SCALE 6 code system20 can be used in conjunction with CASMO to characterize uncertainties in hot to cold reactivity changes due to cross-section uncertainty at various burnup points. The goal of the analysis is to establish the multiplication factor uncertainty between various fuel assemblies at different conditions in a quantifiable manner and to obtain a bound on the hot-to-cold reactivity uncertainty over the various assembly types and burnups – attributed to cross-section data uncertainties.

The TSUNAMI analysis sequences are capable of estimating the impact of cross-section uncertainties in a critical system's multiplication factor k by propagating uncertainties through the use of sensitivity coefficients and first-order perturbation theory. The sensitivity coefficients represent a change in the system's response due to a change in the input parameters. In particular, TSUNAMI approach uses explicit $(S_{k,\Sigma x,g})$ and implicit $(S_{\Sigma x,g,\omega_i})$ sensitivity coefficients, which are defined in the following manner.

$$S_{k,\Sigma x,g} = \frac{\Sigma_{x,g}}{k}\frac{\partial k}{\partial \Sigma_{x,g}}$$

$$S_{\Sigma x,g,\omega_i} = \frac{\omega_i}{\Sigma_{x,g}}\frac{\partial \Sigma_{x,g}}{\partial \omega_i},$$

where $\Sigma_{x,g}$ is the macroscopic cross-section for reaction x and group g, and ω_i is the nuclear data component of some isotope i. The implicit sensitivity coefficient is propagated to k or explicit sensitivity through the use of the chain rule for derivatives. The sensitivity coefficients are summed so that they account for the fact that changes in one cross section may affect another cross section via self-shielding perturbations. Finally, the response uncertainty is obtained by summing all the contributions to the system response from the uncertainties through the sensitivity coefficients and covariance data.

In addition to computing uncertainties in the multiplication factor, the SCALE 6 code system is capable of computing a correlation coefficient, which is representative of the similarity (in terms of uncertainty) between two critical systems. The computation of the correlation coefficient is performed by the TSUNAMI-IP sequence in SCALE 6, which uses the sensitivity data generated by TSUNAMI, along with nuclear covariance data to assess the similarity between the two systems.

8.4 TSUNAMI Uncertainty Analysis

CASMO-5 was used to perform the lattice depletion and branch calculations for a variety of fuel assemblies. CASMO-5 was employed, rather than CASMO-4, because its library includes all nuclides needed to avoid the use of lumped fission products, and data is more consistent with SCALE 6. In order to obtain the burnup-dependent isotopic compositions in each fuel and burnable rod for the TSUNAMI-3D calculation, a script was developed which used the CASMO-5 lattice geometry, temperature, and region-wise isotopic composition to generate suitable SCALE 6 input files. This process was applied to all lattice types and branch conditions for selected burnup points.

A 17 x 17 Westinghouse RFA fuel assembly with 5% enrichment, 104 IFBA, and 20 WABA was selected as a base case. A case matrix was constructed for different enrichments (3.5 % and 4.25 %), number of burnable absorbers (128 IFBA, 24 WABA), and fuel pin radius (smaller than nominal) for a total of five lattice cases. All five lattice cases were depleted with CASMO-5 to 60 GWd/T and "branched" from HFP to six other conditions (HFP No Xenon, Hot Zero Power, Cold 1000 ppm boron, Cold no boron, Cold no boron with 100-hour decay, and simplified rack geometry) at eight burnup points (0.0, 0.5, 10, 20, 30, 40, 50, and 60 GWd/T).

Since the covariance library in SCALE-6 is in multi-group format, the TSUNAMI-3D sequence uses the unresolved (BONAMIST) and resolved resonance self-shielding modules (NITAWLST or CENTRMST) to produce problem-specific multi-group cross-section and sensitivity libraries for the multi-group transport calculation. Cross-sections in each fuel pin region (with unique isotopic number densities) were self-shielded in the TSUNAMI calculation. In order to reduce the run-time, the NITAWLST module was used to perform the resolved resonance self-shielding calculation which necessitated the use of the 238-group ENDF/B-V library. Forward and adjoint multi-group transport calculations in TSUNAMI-3D are performed by the KENO multi-group Monte Carlo code. Finally, the TSUNAMI-3D KENO-VI sequence was chosen to take advantage of the ¼ assembly geometry symmetry. Once forward and adjoint transport computations were completed, the SAMS module was used to generate problem-specific uncertainty data and sensitivity library to be used for post-processing. This library is read by TSUNAMI-IP to generate correlation coefficients. The specific versions of SCALE-6 that were used in this analysis were:

- tsunami-3d_k6 6.0.34 p07_jan_2009

- bonamist6.0.21 p09_jan_2009
- nitawlst6.0.16p30_dec_2008
- kenovi6.0.24p07_jan_2009
- sams66.0.29p07_jan_2009
- tsunami-ip6.0.13p30_dec_2008

8.5 TSUNAMI Analysis Results

TSUNAMI can compute cross-section uncertainties for lattice multiplication factors as a function of various lattices, conditions, and burnups. The uncertainty results for the base lattice at HFP and cold conditions as a function of burnup are shown in Table 8-2.

Table 8-2
Multiplication Factor Uncertainty (2-sigma) as Function of Burnup

Burnup (GWd/T)	0.5	10.	20.	30.	40.	50.	60.
k-infinity Hot	1.02068	1.08597	1.08298	1.03600	0.97772	0.92176	0.87200
Uncertainty (pcm)	1034	1104	1211	1265	1295	1311	1323
k-infinity Cold	1.16103	1.23979	1.25419	1.21057	1.14557	1.07995	1.01883
Uncertainty (pcm)	1015	1087	1209	1281	1326	1361	1388

The hot-to-cold reactivity uncertainties can be obtained from the data shown above and the correlation coefficient obtained from evaluation of the covariance matrix between the two states. The results from this analysis are shown in Table 8-3. The propagation of uncertainties as independent variables (without correlation) is also shown to illustrate the importance of the correlation between hot-to-cold conditions on the uncertainty.

Table 8-3
HFP to Cold Reactivity Uncertainty (2-sigma) as Function of Burnup

Burnup (GWd/T)	0	0.5	10.	20.	30.	40.	50.	60.
Uncertainty (pcm)	347	427	459	508	527	530	521	509
Uncertainty (pcm)*	1479	1476	1580	1748	1840	1893	1926	1949
* Propagation of uncertainty such that the covariance (k-hot, k-cold)=0								

The inclusion of the correlation reduces the uncertainty by about a factor of four. The two states are expected to be highly correlated due to the fact that there is no burnup difference, and isotopic compositions remain the same.

For any lattice and depletion point, the similarity between different physical conditions can be quantified by the use of the correlation coefficient. A correlation coefficient of unity indicates perfect similarity (identical systems) while a correlation of zero indicates negligible similarity. In this analysis, the correlation factor shows the similarity between different states and lattice types at a fixed burnup step.

A summary of the correlation coefficients is shown in Table 8-4 for the five lattice types between nominal (HFP) and branch conditions. The first row in each lattice type is unity because HFP is the base case. **All lattices show a very high degree of similarity between HFP and various cold conditions, at all burnup points** – even though xenon, fuel temperature, coolant temperature, boron concentration, and local rack conditions change dramatically. (For the rack case, a simplified uniform rack has been assumed with a pitch of 22.5 cm, a 0.1 cm thick stainless steel can, a 0.0625 cm thick borated aluminum poison sheet having a width of 19 cm, and a ^{10}B areal density of 0.006 gm/cm^2.)

A second comparison between different lattice types was performed at HFP, cold (no boron, 100-hour decay), and cold rack conditions, and results are presented in Tables 8-5 and 8-6. In Table 8-5, all correlation coefficients are computed relative to the base case at zero burnup. It can be seen that the similarity changes significantly with burnup as the isotopics of the fuel change from fresh uranium to the higher actinides and fission products. Table 8-6 displays the correlation coefficients for the same cases measured relative to the base case at each burnup state. These results indicate **an extremely high degree of similarity exists between all lattice types – at each burnup point**. This is important for this project, as biases in reactivity decrement as a function of burnup are derived directly from reactor measurements, and only the uncertainty of going from HFP reactor conditions to cold spent fuel pool/cask conditions is needed from the TSUNAMI analysis.

Finally, the quantities of direct interest in this study, reactivity and reactivity uncertainty between HFP and cold (no boron, 100-hour decay) are displayed in Table 8-7, for all lattice types. The maximum 2-sigma reactivity uncertainty (due to cross-section data uncertainties) over all lattice types and burnup points is 555 pcm. Table 8-8 displays the corresponding reactivity and reactivity uncertainty between HFP and cold simplified SFP rack conditions. The uncertainties displayed in Table 8-8 are uniformly lower than those in Table 8-7, indicating that the cross-section data uncertainties are less important in the SFP absorbing rack geometry. This is a reflection of the fact that the hardening of the spectrum caused by the SFP rack actually makes the spectrum closer to the lattice spectrum at HFP conditions than to the lattice spectrum at cold conditions. Consequently, the **impacts of cross section uncertainties on the reactivity changes from HFP-to-cold conditions are very similar in operating reactor conditions and cold rack geometry.**

Table 8-4
Correlation Coefficients, c_k, Between Reactor Conditions by Lattice and Burnup

		Burnup (GWd/T)							
		0.0	**0.5**	**10.0**	**20.0**	**30.0**	**40.0**	**50.0**	**60.0**
Base	HFP	1	1	1	1	1	1	1	1
	HFP No Xe	1	0.9843	0.9817	0.9831	0.9854	0.9878	0.9898	0.9914
	HZP	0.9992	0.9992	0.9992	0.9995	0.9994	0.9994	0.9995	0.9995
	Cold 1000 ppm	0.9807	0.9609	0.9608	0.9646	0.9678	0.9702	0.9723	0.9734
	Cold 0 ppm	0.9694	0.9506	0.9514	0.9560	0.9592	0.9611	0.9634	0.9640
	Decay 100 hr	0.9705	0.9512	0.9519	0.9558	0.9591	0.9613	0.9633	0.9643
	SNF Rack	0.9717	0.9543	0.9510	0.9543	0.9582	0.9605	0.9623	0.9641
128 IFBA 24 WABA	HFP	1	1	1	1	1	1	1	1
	HFP No Xe	1	0.9863	0.9829	0.9835	0.9856	0.9879	0.9899	0.9914
	HZP	0.9993	0.9993	0.9992	0.9993	0.9994	0.9994	0.9995	0.9994
	Cold 1000 ppm	0.9799	0.9638	0.9616	0.9648	0.9677	0.9703	0.9724	0.9734
	Cold 0 ppm	0.9708	0.9526	0.9525	0.9558	0.9587	0.9617	0.9638	0.9643
	Decay 100 hr	0.9702	0.9548	0.9531	0.9559	0.9585	0.9614	0.9634	0.9641
	SNF Rack	0.9725	0.9559	0.9518	0.9547	0.9572	0.9611	0.9630	0.9638
3.5 % Enrichment	HFP	1	1	1	1	1	1	1	1
	HFP No Xe	1	0.9851	0.9828	0.9853	0.9884	0.9907	0.9923	0.9934
	HZP	0.9994	0.9992	0.9993	0.9984	0.9996	0.9995	0.9994	0.9995
	Cold 1000 ppm	0.9799	0.9617	0.9637	0.9675	0.9714	0.9726	0.9738	0.9744
	Cold 0 ppm	0.9670	0.9482	0.9521	0.9569	0.9603	0.9622	0.9631	0.9641
	Decay 100 hr	0.9669	0.9482	0.9526	0.9566	0.9608	0.9622	0.9632	0.9639
	SNF Rack	0.9734	0.9565	0.9538	0.9572	0.9612	0.9630	0.9641	0.9649

		Burnup (GWd/T)							
		0.0	0.5	10.0	20.0	30.0	40.0	50.0	60.0
4.25% Enrichment	HFP	1	1	1	1	1	1	1	1
	HFP No Xe	1	0.9842	0.9818	0.9838	0.9867	0.9891	0.9910	0.9924
	HZP	0.9994	0.9993	0.9995	0.9995	0.9995	0.9995	0.9995	0.9995
	Cold 1000 ppm	0.9808	0.9617	0.9618	0.9659	0.9698	0.9718	0.9734	0.9740
	Cold 0 ppm	0.9700	0.9504	0.9512	0.9558	0.9598	0.9625	0.9636	0.9641
	Decay 100 hr	0.9696	0.9490	0.9524	0.9565	0.9602	0.9622	0.9636	0.9639
	SNF Rack	0.9730	0.9547	0.9517	0.9560	0.9596	0.9624	0.9640	0.9645
Small Pin Radius	HFP	1	1	1	1	1	1	1	1
	HFP No Xe	1	0.9816	0.9781	0.9797	0.9827	0.9857	0.9882	0.9904
	HZP	0.9992	0.9992	0.9994	0.9995	0.9995	0.9996	0.9996	0.9996
	Cold 1000 ppm	0.9814	0.9608	0.9589	0.9618	0.9652	0.9690	0.9712	0.9728
	Cold 0 ppm	0.9709	0.9498	0.9488	0.9521	0.9556	0.9591	0.9616	0.9628
	Decay 100 hr	0.9709	0.9510	0.9497	0.9530	0.9555	0.9596	0.9614	0.9630
	SNF Rack	0.9743	0.9536	0.9486	0.9513	0.9548	0.9590	0.9615	0.9632

Table 8-5
Correlation Coefficients, c_k, Between Lattice Types (Relative to 0 GWd/T)

		Burnup (GWd/T)							
		0.0	0.5	10.0	20.0	30.0	40.0	50.0	60.0
HFP	Base	1	0.9837	0.8321	0.6849	0.5867	0.5149	0.4567	0.4100
	128 I 24 W	0.9989	0.9838	0.8292	0.6827	0.5869	0.5147	0.4571	0.4115
	3.5 % Enrich.	0.9927	0.9754	0.7323	0.5779	0.4879	0.4265	0.3817	0.3490
	4.25 % Enrich.	0.9985	0.9812	0.7886	0.6346	0.5390	0.4705	0.4176	0.3777
	Small Fuel Rad.	0.9976	0.9797	0.8280	0.6804	0.5827	0.5062	0.4461	0.3964
Cold 0 ppm Decay 100 hr	Base	1	0.9991	0.8569	0.7016	0.5857	0.4936	0.4177	0.3554
	128 I 24 W	0.9988	0.9977	0.8509	0.6959	0.5823	0.4916	0.4168	0.3556
	3.5 % Enrich.	0.9941	0.9920	0.7562	0.5798	0.4648	0.3805	0.3186	0.2738
	4.25 % Enrich.	0.9988	0.9974	0.8149	0.6468	0.5293	0.4386	0.3675	0.3123
	Small Fuel Rad.	0.9979	0.9976	0.8661	0.7172	0.6015	0.5070	0.4266	0.3594
SNF Rack Geometry	Base	1	0.9992	0.8505	0.6890	0.5716	0.4792	0.4032	0.3422
	128 I 24 W	0.9988	0.9981	0.8446	0.6836	0.5675	0.4780	0.4034	0.3424
	3.5 % Enrich.	0.9940	0.9920	0.7466	0.5643	0.4488	0.3650	0.3037	0.2599
	4.25 % Enrich.	0.9988	0.9975	0.8065	0.6326	0.5138	0.4241	0.3534	0.2989
	Small Fuel Rad.	0.9984	0.9976	0.8582	0.7022	0.5854	0.4906	0.4112	0.3444

Table 8-6
Correlation Coefficients, c_k, Between Lattice Types (By Individual Burnup State)

		Burnup (GWd/T)							
		0.0	**0.5**	**10.0**	**20.0**	**30.0**	**40.0**	**50.0**	**60.0**
HFP	Base	1	1	1	1	1	1	1	1
	128 I 24 W	0.9989	0.9990	0.9998	0.9999	0.9999	1	1	1
	3.5 % Enrich.	0.9927	0.9931	0.9831	0.9870	0.9898	0.9919	0.9939	0.9958
	4.25 % Enrich.	0.9985	0.9984	0.9963	0.9969	0.9976	0.9980	0.9984	0.9988
	Small Fuel Rad.	0.9976	0.9975	0.9971	0.9977	0.9983	0.9979	0.9981	0.9982
Cold 0 ppm Decay 100 hr	Base	1	1	1	1	1	1	1	1
	128 I 24 W	0.9988	0.9986	0.9997	0.9999	1	1	1	1
	3.5 % Enrich.	0.9941	0.9939	0.9818	0.9836	0.9860	0.9885	0.9912	0.9937
	4.25 % Enrich.	0.9988	0.9987	0.9962	0.9963	0.9968	0.9972	0.9977	0.9983
	Small Fuel Rad.	0.9979	0.9982	0.9978	0.9981	0.9982	0.9984	0.9984	0.9985
SNF Rack Geometry	Base	1	1	1	1	1	1	1	1
	128 I 24 W	0.9988	0.9992	0.9997	0.9999	1	1	1	1
	3.5 % Enrich.	0.9940	0.9941	0.9817	0.9835	0.9860	0.9884	0.9910	0.9936
	4.25 % Enrich.	0.9988	0.9988	0.9961	0.9963	0.9968	0.9972	0.9977	0.9982
	Small Fuel Rad.	0.9984	0.9980	0.9977	0.9979	0.9982	0.9983	0.9986	0.9985

Table 8-7
HFP to Cold Uncertainty Matrix (2-sigma) at Cold Conditions

		Burnup (GWd/T)							
		0.0	0.5	10.0	20.0	30.0	40.0	50.0	60.0
Base	Reactivity (pcm)	9867	11843	11425	12605	13919	14986	15891	16527
	Uncertainty	347	427	459	508	527	530	521	509
128 IFBA 24 WABA	Reactivity (pcm)	9977	11927	11367	12556	13916	15009	15888	16612
	Uncertainty	337	403	450	508	533	531	521	512
3.50 % Enrichment	Reactivity (pcm)	12703	14810	13078	14402	15525	16266	16734	17034
	Uncertainty	365	437	498	555	550	537	518	500
4.25 % Enrichment	Reactivity (pcm)	11069	13112	12209	13469	14747	15699	16415	16931
	Uncertainty	350	434	473	529	540	534	520	508
Small Fuel Radius	Reactivity (pcm)	10205	12262	11602	12658	13981	14991	15849	16473
	Uncertainty	322	402	442	497	524	518	509	492

Table 8-8
HFP to Cold Uncertainty Matrix (2-sigma) in Rack Geometry

		Burnup (GWd/T)							
		0.0	**0.5**	**10.0**	**20.0**	**30.0**	**40.0**	**50.0**	**60.0**
Base	Reactivity (pcm)	-10145	-8018	-6291	-4658	-4002	-4097	-4601	-5344
	Uncertainty	222	287	324	353	358	356	349	339
128 IFBA 24 WABA	Reactivity (pcm)	-10405	-8323	-6684	-4858	-4094	-4130	-4626	-5347
	Uncertainty	212	274	317	352	364	354	346	341
3.50 % Enrichment	Reactivity (pcm)	-12437	-9905	-7382	-5715	-5839	-6687	-7688	-8688
	Uncertainty	204	266	330	364	357	349	343	337
4.25 % Enrichment	Reactivity (pcm)	-11101	-8772	-6740	-5028	-4684	-5123	-5916	-6873
	Uncertainty	211	279	327	357	359	350	342	337
Small Fuel Radius	Reactivity (pcm)	-10594	-8366	-6705	-5185	-4676	-5046	-5851	-7075
	Uncertainty	201	274	315	348	356	345	336	327

8.6 HFP to Cold Reactivity Decrement Uncertainty

Since the uncertainty changes in Table 8-8 may be dependent on the actual rack design, it is conservative to use the uncertainties computed directly at cold conditions - without taking any credit for reduction in uncertainty that would arise in SFP or cask geometry. Taking the largest HFP to cold uncertainty change from any lattice in Table 8-7 and assuming it applies to all fuel lattices; one obtains the conservative burnup dependent uncertainties displayed in Table 8-9.

Table 8-9
HFP to Cold Uncertainty (2-sigma) vs. Burnup

Burnup (GWd/T)	0.0	10.0	20.0	30.0	40.0	50.0	60.0
Uncertainty (pcm)	365	498	555	550	537	521	512

However, the uncertainty for fresh fuel in cold SFP or cask conditions will actually be determined for specific applications through evaluation of a large set of cold criticals, and there is no reason to include reactivity uncertainty due to fresh fuel cross-section uncertainties. Consequently, statistically subtracting the smallest fresh fuel uncertainty (322 pcm) from the other uncertainties in Table 8-9, one obtains the hot-to-cold reactivity uncertainties (due to cross-section uncertainties) as a function of fuel depletion, as displayed in Table 8-10.

Table 8-10
HFP to Cold Additional Uncertainty (2-sigma) vs. Burnup

Burnup (GWd/T)	10.0	20.0	30.0	40.0	50.0	60.0
Uncertainty (pcm)	380	452	446	430	410	398

8.7 Cold Reactivity Decrement Bias and Uncertainty

Assuming that the HFP-to-cold uncertainty changes are equally applicable to CASMO-4, CASMO-5, and SCALE 6 data, one can statistically combine the HFP 2-sigma uncertainty, fuel temperature 2-sigma uncertainty, and HFP to cold 2-sigma uncertainty to obtain a total uncertainty. Appending this data to the bias data of Table 7-1 one obtains the measured CASMO cold reactivity decrement biases and uncertainties, as displayed in Table 8-11.

Table 8-11
Measured Cold Reactivity Decrement Bias and Uncertainty

Burnup (GWd/T)	10.0	20.0	30.0	40.0	50.0	60.0
CASMO-4 Bias (pcm)	81	140	178	196	192	167
CASMO-5 Bias (pcm)	19	46	81	125	177	238
95% Uncertainty (pcm)	521	576	571	560	544	534
95% Uncertainty (pcm)*	594	643	639	627	614	605
* assuming 150% of nominal HFP fuel temperature to cold uncertainty (255 pcm x 1.5)						

Comparing the uncertainty bounds with those of the Kopp and prediction intervals of the cold reactivity decrement errors regressions from Section 6 (repeated here as Figures 8-2 and 8-3), one observes that the estimated **cold uncertainties at 50 GWd/T are significantly smaller than the spread in HFP prediction intervals and less than one-third the spread of the Kopp bounds.**

Figures 8-4 and 8-5 display CASMO-4 and CASMO-5 regression fits obtained without use of the post-minimization screening criteria on the reaction rate r.m.s. sensitivity and cycle burnup described in Section 6. These fits have about 50% more data points than the screened fits, but the regressions are within about 30 pcm of the screened fits from 0.0 to 50.0 GWd/T. Consequently, one can conclude that the post-minimization screening has not impacted the regression results – within the uncertainty estimates.

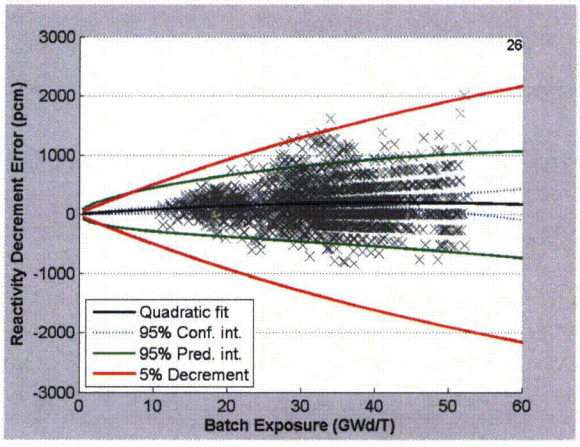

Figure 8-2
CASMO-4 Reactivity Error – Filtered

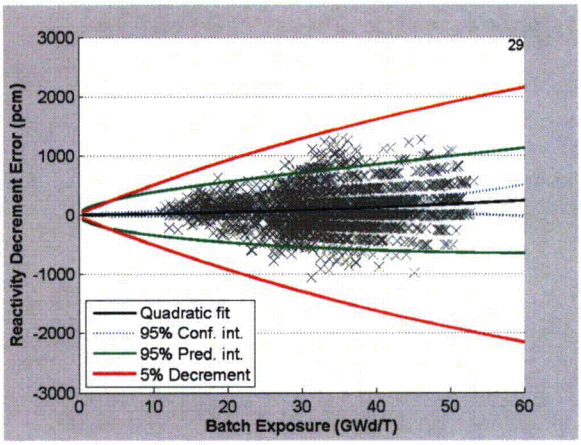

Figure 8-3
CASMO-5 Reactivity Error – Filtered

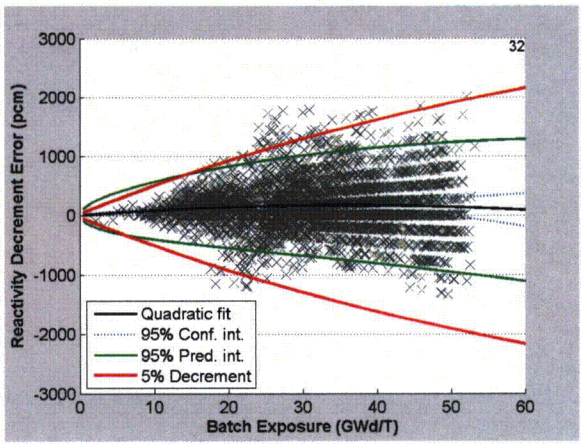

Figure 8-4
CASMO-4 Reactivity Error – No Filters

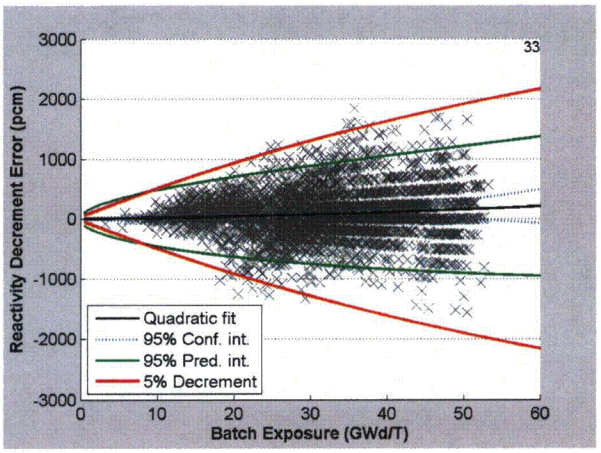

Figure 8-5
CASMO-5 Reactivity Error – No Filters

Section 9: Experimental Reactivity Decrement Benchmarks

9.1 Experimental Benchmark Methodology

The analysis presented in Section 7 has quantified the measured CASMO reactivity burnup decrement errors and has further demonstrated that these errors are essentially independent of sub-batch enrichment, boron concentrations, etc. Consequently, if one assumes the CASMO biases in reactivity decrement are independent of fuel type (within the stated uncertainties), one can construct an experimental benchmark for HFP reactivity decrement by adding CASMO biases to CASMO computed reactivity decrements. **In such a benchmark, the net effect is that lattice physics depletion uncertainties, including nuclide concentration and reactivity uncertainties, are experimentally determined.**

Since nuclide inventories between HFP and cold (no cooling) conditions are identical, the only difference between HFP and cold arise from changes in fuel and coolant temperatures. The TSUNAMI analysis presented in Section 8 has demonstrated high similarity between all fuel types at HFP and cold conditions and has quantified the uncertainty changes from HFP-to-cold conditions. Thus, one obtains an experimental benchmark for cold reactivity decrement by adding the additional uncertainties that arise from HFP to cold conditions. Table 8-11 contains the CASMO bias and uncertainty data used to construct such experimental burnup reactivity decrement benchmarks.

9.2 Experimental Benchmark Specification

Eleven cases have been selected for experimental benchmarks, based on the Westinghouse RFA assembly. CASMO calculations have been performed for each case in Table 9-1, covering a range of:

- enrichments
- burnable absorber loadings
- boron concentrations
- fuel and coolant temperatures
- decay times

Table 9-1
Benchmark Lattice Cases

1	3.25% Enrichment
2	5.00% Enrichment
3	4.25% Enrichment
4	off-nominal pin diameter depletion
5	20 WABA depletion
6	104 IFBA depletion
7	104 IFBA plus 20 WABA depletion
8	high boron depletion = 1500 ppm
9	branch to hot rack (150°F coolant/fuel) = 338.7K
10	branch to high rack boron = 1500 ppm
11	high power depletion (power, coolant/fuel temp)

Case 3 with 4.25% enrichment and no burnable absorbers was chosen as the base case from which the lattice parameters were perturbed. For each case, the following calculations were performed:

- CASMO was depleted to 60 GWd/T at the specified power density, temperatures, and boron concentrations.
- Cold cooling cases to 100 hours, 1 year, 5 years, and 15 years were performed for each branch case.
- Branch cases to cold were performed as restarts from the cooling cases at burnups of 10, 20, 30, 40, 50, and 60 GWd/T.

Since the anticipated application of these experimental benchmarks is for analysts to measure biases for their SFP or cask analysis tools (usually Monte Carlo), small simplifications of the standard CASMO HFP depletion models were made to make subsequent analysis easier:

- Thermal expansion of materials is ignored (cold dimensions are used)
- Spacer grids are not modeled
- Water in guide tubes is modeled at the same temperature as the coolant
- Buckling search to critical is not used (since this is difficult for Monte Carlo methods)

None of these effects are important for the purposes of the experimental benchmark – it is only important that there be consistency between the CASMO models and the models used with the SFP or cask tools.

The detailed descriptions of the eleven cases are contained in Appendix B.

9.3 Experimental Reactivity Decrement Tables

The k-infinity from each computed CASMO-5 cold case was used to construct reactivity decrement tables, to which the CASMO-5 experimental biases (from Table 8-11) were added to obtain cold experimental reactivity decrements and uncertainties – displayed in the tables of Appendix C.

9.4 End –Users Application of Experimental Reactivity Decrements

User's applications of experimental reactivity decrements for each case (or those deemed relevant by the end-user) are anticipated to follow these steps:

1. Lattice depletions are performed with the user's lattice depletion tool to 60 GWd/T at the precise physical conditions specified in the Benchmarks.
2. Decay calculations for each cooling interval of interest (e.g., 0, 100-hour, 5-years, and 15-years) are performed with the user's lattice depletion tool from each depletion branch (10, 20, 30, 40, 50, 60 GWd/T) of Step 1.
3. Fuel number densities at each depletion/cooling branch from Step 2 are transferred to the user's criticality model (often Monte Carlo) of the lattice, and cold k-infinities are computed for each combination of lattice/burnup/cooling interval and lattice conditions.

   (Note: SFP/cask criticality analysis may make modeling approximations which involve averaging of fuel pin number densities. In such cases, the averaging must also be performed at this Step of the Benchmark analysis.)
4. Step 3 k-infinities are used to construct reactivity decrement tables as a function of lattice type, burnup, and cooling interval (analogous to those in Appendix C).
5. Step 4 reactivity decrement tables are differenced from the experimental reactivity decrement tables of Appendix C to construct biases for the user's methodology/tools as a function of lattice type, burnup, and cooling interval.
6. Reactivity decrement uncertainties are applied (Appendix C Table C-1) for each reactivity decrement of Step 5."
7. Biases from Step 5 and the uncertainties from Step 6 are combined with biases and uncertainties arising from other portions of the SFP/cask criticality analysis.

   (Note: Users have the flexibility to choose different approaches to combining biases and uncertainties. For example: a user might choose to be conservative and apply the largest observed reactivity decrement bias to all cases; independent of lattice type, burnup, cooling interval, or lattice conditions.)

9.5 Sensitivity of Experimental Burnup Reactivity Decrements

The measured reactivity burnup decrements presented in Appendix C are based on measured CASMO-5 biases. However one could have used any lattice code/library to infer reactivity decrements, and measured reactivity decrements should fall within the measurement uncertainties.

When CASMO-4 is used to compute measured reactivity decrements, the difference in burnup decrements relative to those inferred with CASMO-5, are displayed in Table 9-2. It can be seen that the largest differences are less than 2% – which occurs at 60 GWd/T.

Table 9-2
Percent Difference in Reactivity Decrement (C4 - C5) No Cooling

Case	Sub-batch burnup (GWd/T)					
	10	20	30	40	50	60
1	-1.03	-0.42	0.18	0.69	1.13	1.38
2	-1.66	-1.04	-0.65	-0.21	0.29	0.80
3	-1.46	-0.83	-0.41	0.09	0.63	1.09
4	-1.53	-1.02	-0.54	-0.05	0.52	1.01
5	-0.79	-0.60	-0.37	0.10	0.58	1.04
6	-0.33	-0.43	-0.29	0.05	0.47	0.88
7	-0.32	-0.23	-0.17	0.12	0.52	0.89
8	-1.40	-0.72	-0.29	0.22	0.73	1.16
9	-1.63	-1.02	-0.55	-0.05	0.49	0.95
10	-1.11	-0.45	0.05	0.63	1.23	1.78
11	-0.88	-0.36	0.07	0.51	1.03	1.46

When reactivity decrements are inferred using CASMO-4 with the no lumped fission product library, the reactivity decrement differences relative to CASMO-4 are displayed in Table 9-3. It can be seen that even though CASMO-4 computed reactivities are as much as 2000 pcm different, the measured reactivity decrements differences are less than 1.7%. This provides substantial evidence that measured reactivity decrements are insensitive to the choice of lattice code/library.

Table 9-3
Percent Difference in Reactivity Decrement (No-LFP - C4) No Cooling

Case	Sub-batch burnup (GWd/T)					
	10	20	30	40	50	60
1	0.99	0.94	0.68	0.38	0.06	-0.22
2	0.78	0.82	0.77	0.62	0.39	0.15
3	0.87	0.89	0.76	0.54	0.27	0.00
4	0.75	0.73	0.62	0.38	0.12	-0.19
5	0.43	0.76	0.76	0.57	0.32	0.06
6	0.48	0.79	0.76	0.54	0.27	0.00
7	0.22	0.67	0.76	0.57	0.34	0.06
8	0.81	0.86	0.74	0.55	0.30	0.04
9	0.92	0.89	0.79	0.57	0.29	0.00
10	0.11	-0.15	-0.44	-0.85	-1.24	-1.66
11	0.83	0.80	0.70	0.47	0.23	-0.06

After 15 years of cooling, the measured reactivity decrement differences between CASMO-4 and CASMO-5 are displayed in Table 9-4. The largest differences are about 4% at a burnup of 10.0 GWd/T, and this difference is approximately 500 pcm - within the quoted measurement uncertainty. For larger burnups, where the reactivity decrements increase, the percentage differences become much smaller. The increase in reactivity decrement with cooling is particularly sensitive to cross-section data for $^{241}Pu/^{241}Am$ (14-year half-life, beta decay) and $^{155}Eu/^{155}Gd$ (4.7-year half-life, beta decay).

Table 9-4
Percent Difference in Reactivity Decrement (C4 - C5) 15-Year Cooling

Case	Sub-batch burnup (GWd/T)					
	10	20	30	40	50	60
1	-3.28	-1.93	-1.17	-0.60	-0.17	0.02
2	-4.43	-2.84	-2.24	-1.66	-1.10	-0.56
3	-4.01	-2.61	-1.88	-1.28	-0.70	-0.22
4	-4.24	-2.82	-2.10	-1.45	-0.83	-0.33
5	-2.05	-2.05	-1.72	-1.22	-0.71	-0.24
6	-1.60	-1.90	-1.64	-1.24	-0.81	-0.39
7	-1.14	-1.40	-1.42	-1.11	-0.70	-0.34
8	-3.85	-2.37	-1.69	-1.14	-0.58	-0.15
9	-4.13	-2.64	-1.94	-1.30	-0.73	-0.25
10	-3.60	-1.99	-1.22	-0.49	0.15	0.67
11	-3.68	-2.17	-1.50	-0.90	-0.33	0.11

These results support the observation that measured reactivity decrements are not sensitive to the choice of lattice code/library.

Section 10: Summary of Conclusions

10.1 General Conclusions

The flux map analysis methods developed and demonstrated in this report are capable of providing experimental determination of fuel reactivity burnup decrement biases and uncertainties. The large amount of flux map data utilized in the 44 cycles of Duke Energy reactor analysis provided sufficient experimental sub-batch reactivity estimates (approximately 2500 points) such that resulting uncertainties in measured HFP sub-batch reactivity decrement errors are less than 250 pcm for burnups up to 55 GWd/T.

TSUNAMI analysis demonstrated such a high degree of correlation between PWR fuel assemblies that nuclear data uncertainties are nearly independent of assembly design and enrichment. TSUNAMI analysis has demonstrated that extremely high correlation of reactivities between hot-to-cold conditions results in additional uncertainties for extending HFP reactivity decrement measurements to cold conditions of less than 450 pcm over the range of burnups from 0 to 60 GWd/T.

10.2 CASMO-Specific Conclusions

Reactivity decrement biases computed with CASMO showed no enrichment dependence (within statistical uncertainties) over the range of 3.5 to 5.0% ^{235} U enrichment.

Results demonstrate that the Kopp Memo 5% reactivity decrement uncertainty assumption, often applied in Spent Fuel Pool criticality analysis, is both valid and conservative for cold SFP reactivities computed with CASMO-4 or CASMO-5 codes.

Results provide a basis for supporting a far smaller reactivity burnup decrement uncertainty for CASMO-4 and CASMO-5 than the 5% criteria suggested in the Kopp Memo, as displayed in the biases and uncertainties of Table 10-1.

Table 10-1
CASMO Measured Cold Reactivity Decrement Bias and 2σ Uncertainty (delta-k in pcm)

Burnup (GWd/T)	10.0	20.0	30.0	40.0	50.0	60.0
CASMO-4 Bias (pcm)	81	140	178	196	192	167
CASMO-5 Bias (pcm)	19	46	81	125	177	238
95% Uncertainty (pcm)	521	576	571	560	544	534

10.3 Range of Fuel Applications

The results presented in this report are, strictly speaking, applicable only to those fuel types included in the analysis, namely: 1) 3.5 – 5.0% enrichment, 2) Westinghouse RFA fuel with IFBA and WABAs, and 3) AREVA MarkBW fuel with LBP pins. For other fuel types, additional analysis may be needed to demonstrate that results of this study are applicability to those fuel types.

10.4 Related Conclusions

Reactivity decrement biases derived from flux map data have also been shown to be similar to those derived from the change in biases of reactor soluble boron concentrations from beginning of cycle (BOC) to end of cycle (EOC). This conclusion is based on the close agreement between changes in reactor boron biases and sub-batch reactivity decrement biases computed from flux map data with the CASMO and SIMULATE-3 tools. These results add credibility to the more general assertion that changes in boron biases for other code systems should also be reliable indicators of fuel sub-batch reactivity decrement biases.

10.5 Experimental Benchmarks

The experimental biases derived for the CASMO-5 lattice physics code have been used to develop a series of experimental benchmarks that can be used to quantify reactivity decrement biases and uncertainties for other code systems used in lattice depletion and SFP/cask criticality analysis.

Specification of eleven experimental lattice benchmarks, covering a range of enrichments, burnable absorber loading, boron concentration, and lattice types have been documented in this report.

Interested parties can use these experimental benchmarks and their specific analysis tools to generate reactivity decrement biases and uncertainties that are unique to those tools.

Section 11: References

1. L. Kopp, NRC memorandum from L. Kopp to T. Collins, "Guidance on the Regulatory Requirements for Criticality Analysis of Fuel Storage at Light-Water Reactor Power Plants," dated August 19, 1998 (ADAMS Accession No. ML003728001).
2. J. L. Eller, Letter, "Reference: Fuel, Core, and Operational Data to Support Core Physics Benchmark Analyses," DPC-1553.05.00.0222, Rev 0, March (2011).
3. D. Hagrman, et al., "INTERPIN-4 Model Improvements and Verification," SSP-07/445 Rev 0, Studsvik Scandpower, Inc. (2007).
4. D. Knott, et al., "CASMO-4 Methodology Manual," STUDSVIK/SOA-95/02, Studsvik of America, Inc. (1995).
5. J. Rhodes, et al., "CASMO-5 Development and Applications," PHYSOR-2006, Vancouver, BC, Canada. September 10-14, (2006).
6. T. Bahadir, et al., "CMSLINK User's Manual," STUDSVIK/SOA-97/04, Studsvik of America, Inc. (1997).
7. J. Cronin, et al., "SIMULATE-3 Methodology Manual," STUDSVIK/SOA-95/18, Studsvik of America, Inc. (1995).
8. R. MacFarlane, D. W. Muir, "NJOY99 -Code System for Producing Pointwise and Multigroup Neutron and Photon Cross Sections from ENDF/B Data," Los Alamos National Laboratory, RSIC PSR-480, (2000).
9. R. Lawrence, "Progress in Nodal Methods for the Solutions of the Neutron Diffusion and Transport Equations," Prog. Nucl. Energy, Vol. 17, No. 3, Pergamon Press, (1986).
10. K. Smith, et al., "QPANDA: An Advanced Nodal Method for LWR Analysis," Trans. Am. Nucl. Soc., Vol. 50, p 532, San Francisco, CA, (1985).
11. P. Esser and K. Smith, "A Semi-Analytic Two-group Nodal Model for SIMULATE-3," Trans. Am. Nucl. Soc., Vol. 68, p 220, San Diego, CA, (1993).
12. K. Smith, "Assembly Homogenization Techniques for Light Water Reactor Analysis," Prog. Nucl. Energy, Vol. 17, No. 3, Pergamon Press, (1986).

13. K. Smith and K. Rempe, "Mixed-Oxide and BWR Pin Power Reconstruction in SIMULATE-3," PHYSOR 90, Vol. 2, p. VIII-11, Marseille, France, (1990).

14. K. Rempe, et al., "SIMULATE-3 Pin Power Reconstruction: Methodology and Benchmarking," Proc. International Reactor Physics Conference, Vol. III, p. 19, Jackson, WY, (1988).

15. K. Smith, "MOX Analysis Methods in SIMULATE-3," Trans. Am. Nucl. Soc., Vol. 76, p 181, Orlando FL, (1997).

16. K. Smith and P. Esser, Nodal Transport Model for SIMULATE," Proc. Spring Mtg., Kyoto, Japan, A49, Atomic Energy Society of Japan, (1993).

17. K. Smith, "Practical and Efficient Iterative Method for LWR Fuel Assembly Homogenization," Trans. Am. Nucl. Soc., Vol. 71, p 238, Washington, DC, (1994).

18. K. Smith, "Topical Report on Studsvik's Core Management System (CMS)," SSP-09/477-C, Rev 0, Studsvik Scandpower, Inc. (2010).

19. Mathworks, "MATLAB 7 Data Analysis", Version 7.11.0 (R2010b),The Mathworks, Inc. (2010).

20. M. L. Williams, B. T. Rearden, "SCALE-6 Sensitivity/Uncertainty Methods and Covariance Data," IDOC 11583.

21. C. Vitanza, "Overview of the OECD- Halden Reactor Project," *Nuclear Engineering and Design*, Vol., 207, p 207-221, July (2001).

Appendix A: Studsvik CMS Analysis Codes

The Studsvik Core Management System (CMS) is routinely used to perform the neutronic and thermal-hydraulic analysis needed for design, optimization, and safety analysis of nuclear reactor cores. While the CMS suite of codes is capable of performing steady-state and transient (dynamic) analysis of reactor cores, the methods described in this document are restricted to the CMS codes needed to perform steady-state and pseudo steady-state core analysis.

A.1 Code System Overview

The CMS code system consists of five separate codes which are used as a package to perform reactor core analysis. The five codes are:

- **INTERPIN-4**[3] for analyzing the 1-D fuel temperatures for an individual fuel pin, as a function of:
- Fuel pin design (e.g., enrichment, gas pressurization, etc.)
- Linear heat loading
- Fuel burnup
- **CASMO-4**[4] or **CASMO-5**[5] for analyzing the 2-D neutronic behavior of an individual fuel assembly, as a function of:
- Lattice design (e.g., pin enrichment layout, burnable absorber design, etc.)
- Local conditions (e.g., fuel temperature, coolant density, boron content, etc.)
- Fuel burnup
- Control rod insertion
- **CMSLINK**[6] for generating a library of tabularized CASMO-4 data for a collection of fuel assemblies and reflector types, as a function of:
- Fuel burnup
- Thermal hydraulic conditions
- Control rod insertion
- Fuel history effects
- **SIMULATE-3**[7] for analyzing the detailed 3-D reactor core neutronic and thermal-hydraulic behavior over the reactor core lifetime, as a function of:
- Reactor power

- Coolant flow rate and inlet temperature
- Fuel burnup
- Control bank insertion

INTERPIN-4 and CMSLINK are often considered as auxiliary codes in the CMS suite, and they are described in this document only to the extent required to understand their interaction with CASMO and SIMULATE-3. On the other hand, CASMO and SIMULATE-3 are very large (many hundreds of thousands of lines of FORTRAN) codes which perform the bulk of the physics modeling in CMS.

This section details some of the more important physics models and methods which are important for understanding how CASMO and SIMULATE-3 are used for this project.

A.2 INTERPIN-4

CASMO and SIMULATE-3 need fuel temperature data as part of their respective physical models. CASMO requires best-estimate average fuel pin temperature for each lattice type, and this temperature is typically assigned uniformly to all fuel pins in the lattice. Since the CASMO case matrix includes lattice calculations (both branches and depletions) to off-nominal fuel temperatures, downstream SIMULATE-3 results are not very sensitive to the nominal CASMO fuel temperatures. SIMULATE-3 results, however, are sensitive to the input fuel temperature tables – which provide the relationship between linear power density and the average fuel pin temperature. INTERPIN-4 is used to generate steady-state fuel temperature data that is provided to SIMULATE-3. INTERPIN-4 solves the 1-D radial heat conduction problem for an axial nodalized fuel pin, and temperatures are dependent on the physical models used to close the system of equations.

A.3 INTERPIN-4 Thermal Conductivities

The cladding thermal conductivity in INTERPIN-4 is from MATPRO:

$$k_{clad} = 7.51 + 2.09\times10^{-2}T - 1.45\times10^{-5}T^2 + 7.67\times10^{-9}T^3 \quad (W/m/K)$$

This oxide fuel conductivity model is taken from a recent NFI correlation that is plotted in Figure A-1 for UO_2 fuel at 4 different burnups. It can be seen that the conductivity degradation from fresh to 60 GWd/T burnup is between 40 and 60 percent, and this degradation has a very significant effect on fuel temperatures as a function of burnup.

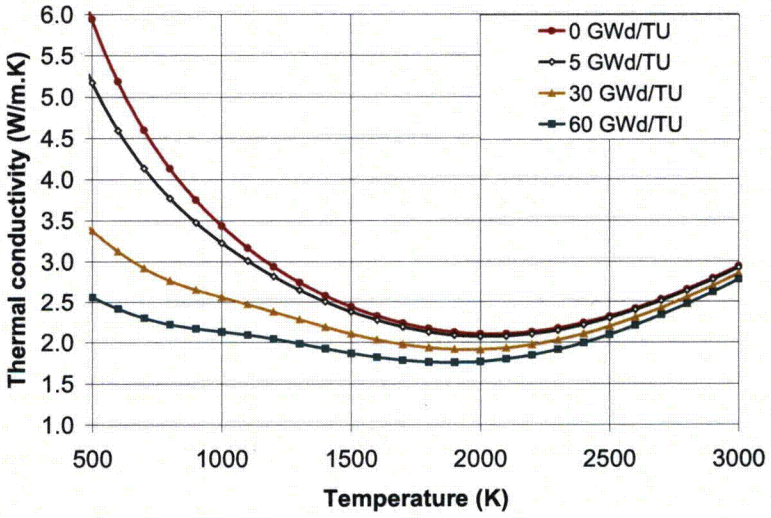

Figure A-1
UO_2 Conductivity as a Function of Burnup and Temperature

A.4 INTERPIN-4 Solid Pellet Swelling and Gap Conductance

As fuel pellets are irradiated, solid pellet swelling occurs because of the production of embedded gaseous fission products. This pellet swelling is modeled in INTERPIN-4 as a simple function of fuel burnup, E, in GWd/T

$$\left(\Delta V / V\right)_{fuel} = 0.7 \times 10^{-3}\ E$$

The fuel/clad gap conductance is modeled in INTERPIN-4 with two principal terms: a gaseous conductance term and a solid contact conductance term. The benchmark parameters of the Kjaerheim-Roldstad gaseous gap conductance sub-model (that accounts for the effect of fuel pellet surface and clad inner surface roughness) and the minimum residual gap of the Ross Stoute solid contact conductance model have both been calibrated to match measured centerline temperatures from pin irradiations in the Halden Reactor Project[21].

A.5 INTERPIN-4 Fuel Temperature Edits for SIMULATE-3

When INTERPIN-4 is used to generate SIMULATE-3 fuel temperature data, several calculations are automatically performed at different power levels, and results (similar to those of Figure A-2) are used to derive functional fits of the difference between average fuel temperature and the bulk coolant temperature. These data tables are then used directly in SIMULATE-3, and the lifetime-averaged fuel temperature is used as input to CASMO.

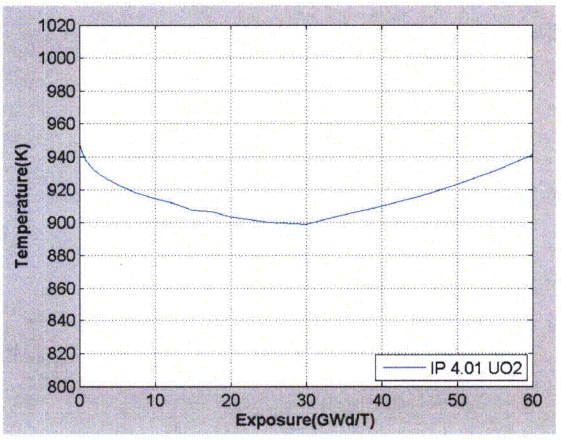

Figure A-2
Typical INTERPIN-4 Fuel Temperature Change With Burnup

A.6 CASMO-4 Lattice Physics Code

CASMO-4 is a two-dimensional transport theory lattice physics code used to analyze PWR and BWR fuel assemblies. CASMO-4 computes multi-group, multi-dimensional neutron flux distributions by solving the neutron transport eigenvalue problem. The resulting neutron flux solutions are used to compute coupled nuclide depletion, gamma production, and gamma transport within a fuel assembly. CASMO-4 can model fuel assemblies containing collections of cylindrical fuel rods, cylindrical burnable absorber rods, cluster control rods, and in-core instruments. CASMO-4's two-dimensional heterogeneous geometrical capabilities permit modeling of both single-assembly and Cartesian collections of assemblies. CASMO-4 is used to generate assembly neutronic data for the SIMULATE-3 nodal reactor analysis code. A flow diagram of a typical CASMO-4 calculation is displayed in Figure A-3.

A.7 CASMO-4 Cross Section Library

The CASMO-4 multi-group neutronic data library (N-Library) is the production neutronic data library used with CASMO-4, and it has been generated with the NJOY[8] data processing code that converts basic evaluated neutronic data (e.g., ENDF/B, JEF, etc.) from its continuous-energy form into multi-group neutronic data tables – as a function of material temperature and background cross sections. The CASMO-4 neutronic data library employs 70 neutron energy groups to cover the range from 0.0 to 10.0 MeV, consisting of 14 groups in the fast range (from 9.118 keV to 10.0 MeV), 13 groups in the resonance range (4.0 eV to 9.118 keV), and 43 groups in the thermal range (0.0 to 4.0 eV – with clustered groups around the 0.3 eV ^{239}Pu and 1.0 eV ^{240}Pu resonances).

The N-Library contains absorption, fission, nu-fission, transport, and scattering cross sections for 108 nuclides and materials, including; 18 important heavy metal isotopes (^{234}U to ^{246}Cm), 30 explicit and 2 lumped fission products

(1 saturating and 1 non-saturating), 5 common LWR moderators, numerous LWR structural materials, and many common LWR burnable absorber isotopes. In addition to cross-section data, the library contains fission neutron emission spectra, fission product yields, and delayed neutron yields for all fissionable isotopes and decay constants for all radioactive isotopes. The starting point for the N-library was data produced in 1985 with NJOY from the ENDF/B-IV evaluated nuclear data files. When additional isotopes were added to the initial library or when deficiencies with ENDF/B-IV data were discovered, more recently-evaluated data was used to generate additional/replacement data.

As a result, the N-library contains data from JEF-1 for:

- Am-241 to Am-243
- Cm-242 to Cm-246
- Co-59, Ag-107, Ag-109, Cd-113, In-115
- Natural Hf, Hf-176 to Hf-180
- Pu-239 to Pu-242

from JEF-2.1 for:

- Er-162 to Er-171
- Tm-169 to Tm-171
- Gd-154 to Gd-158
- U-236

and from ENDF-B/VI, release 4 for:

- Mg, Zr, Nb, Mo, Sn
- Eu-154 and Eu-155

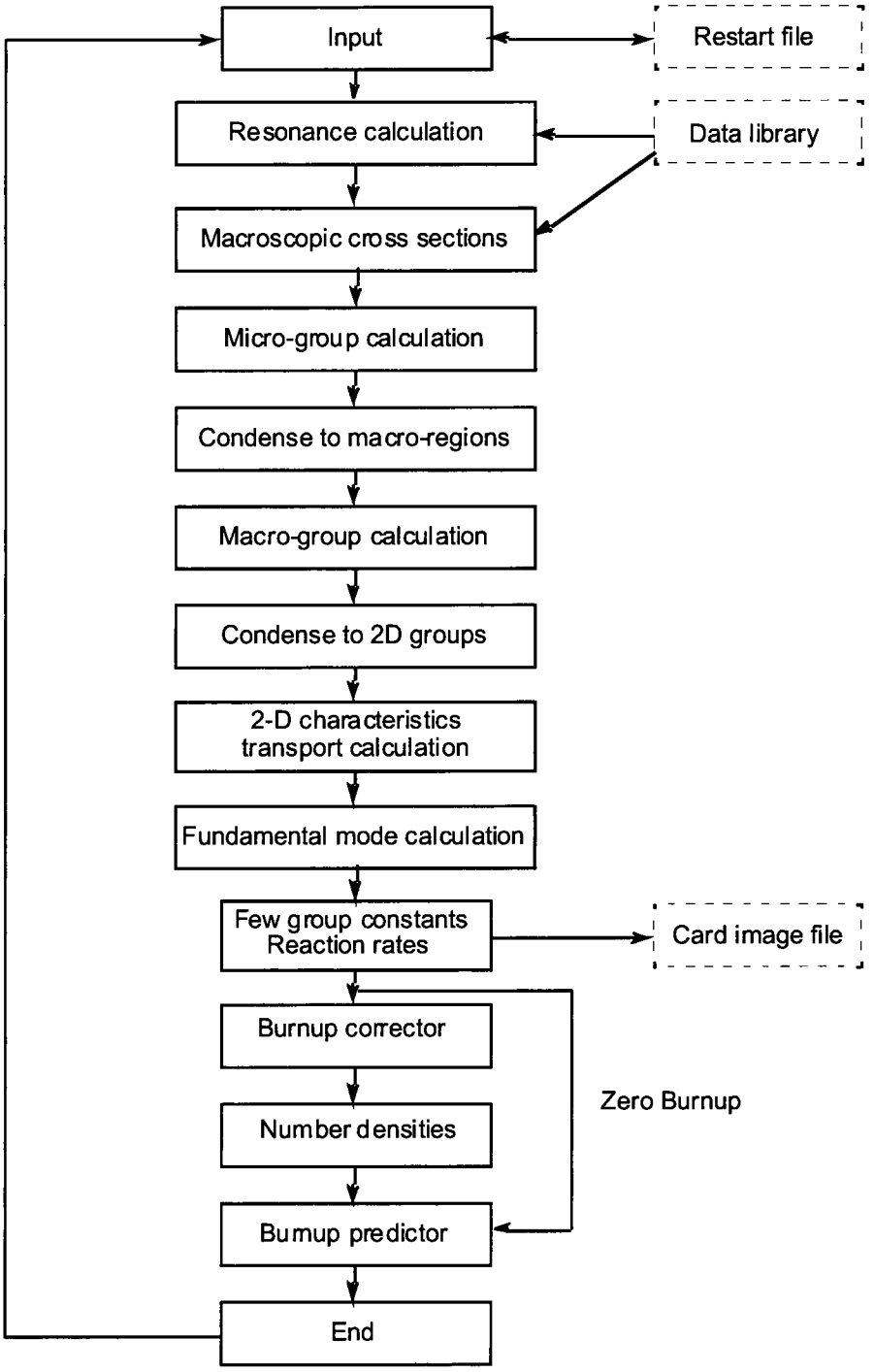

Figure A-3
Computational Flow Diagram of CASMO-4

A.8 CASMO-4 Isotopic Depletion Model

Once assembly flux distributions are known, reaction rates for each depletable nuclide are constructed so that the fuel depletion calculation can be performed. CASMO-4 makes the linearized chain approximation to decouple the depletion equations. The only approximation required in the linearized chain model is that "backward" transition rates (e.g., *n2n*, and alpha decay) in the middle of depletion chains be assumed constant over each time step.

When CASMO-4 detects the presence of gadolinia burnable absorbers in a lattice it automatically reduces burnup steps to 0.5 GWd/T until the gadolinia absorption is negligible, and then it reverts to large default depletion steps.

At each depletion step, CASMO-4 assumes that the power remains constant with depletion (rather than assuming that the flux remains constant). This is particularly important for accurate depletion, since the flux level and the average energy yield per fission change during a burnup step. The assumption necessitates a simple iterative calculation of the flux normalization so that the computed power at each depletion step remains constant.

A.9 CASMO-5 Lattice Physics Code

CASMO-5 is a significantly upgraded version from CASMO-4. The principal differences from CASMO-4 are:

- The "N" nuclear data library was replace with an ENDF/B-VII library
- The number of isotopes and materials in the library was increased from 108 to ~400
- The use of lumped fission products was eliminated
- The library group structure was changed from 70 to 586 energy groups
- Resonance models were upgraded to improve the two-term rational approximation
- The number of energy groups in the 2D transport (MOC) was increased from 8 to 19
- The ray spacing in the transport solver was reduced to 0.05 cm in all energy groups
- The polar angle quadrature was changed from Gauss-Legendre to the optimal T-Y
- The nuclide burnup model was changed from linearized chains to a partial matrix exponential

A.10 CASMO Baffle/Reflector Models

PWR baffle and reflector data needed for SIMULATE-3 are generated directly with CASMO. CASMO builds a 2-D transport model in which homogenous baffle and homogeneous reflector regions are appended to the side of the fuel

assembly, as depicted in Figure A-4. This 2-D transport problem is solved with reflecting boundary conditions on three sides and a vacuum boundary condition on the outer reflector surface. CASMO provides direct edits of the baffle/reflector cross sections and homogenization data that are used by SIMULATE-3 for its nodal model of PWR cores. Similar models are also built for the top and bottom reflectors based on the users' specifications of the 1-D material representations above and below the fueled portion of the core.

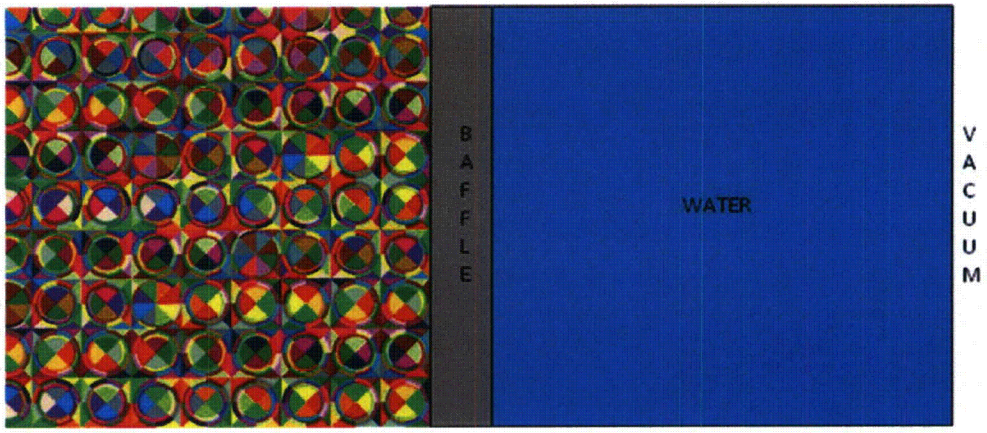

Figure A-4
CASMO Baffle/Reflector Geometry

A.11 CMSLINK – CASMO-to-SIMULATE Linking Code

CMSLINK is a utility processing code used in CMS to gather and format all CASMO data needed in SIMULATE-3. CMSLINK reads the CASMO data files, evaluates the depletion and branch cases that are available, determines the most appropriate multi-dimensional table representation, and creates a binary data library that can be read by SIMULATE-3.

A.12 CMSLINK Multi-dimensional Data Tabulation

CMSLINK creates 1-D, 2-D and 3-D data tables for each of the assembly-averaged CASMO neutronic data, as a function of burnup (EXP), moderator temperature history (HTMO), boron history (HBOR), fuel temperature history (HTFU), moderator temperature (density, TMO), shut down cooling (SDC), boron concentration (BOR), control rod presence (CRD), and fuel temperature (TFU). For PWR lattices, the data tables and their secondary and tertiary dependencies consist are:

- Base 2-D table vs. (EXP, HTMO)
- Delta HBOR, 2-D table vs. (EXP, HBOR)
- Delta HTFU, 2-D table vs. (EXP, HTFU)
- Delta TMO, 2-D table vs. (EXP, TMO)
- Delta SDC, 2-D table vs. (EXP, SDC)

- Delta BOR,3-D table vs. (EXP, BOR, TMO)
- Delta CRD,3-D table vs. (EXP, CRD, TMO)
- Delta TFU,3-D table vs. (EXP, TFU, TMO)

Since pin power reconstruction and detector reaction rate data are very large (e.g., pin power form functions), a simplified data representation is used for this data. For PWR lattices, the data tables consist of:

- Base 1-D table vs. (EXP)
- Delta TMO,1-D table vs. (EXP)
- Delta CRD,2-D table vs. (EXP,CRD)
- Delta HBOR,1-D table vs. (EXP)
- Delta SDC,1-D table vs. (EXP)
- Delta BOR,1-D table vs. (EXP)
- Delta TFU,1-D table vs. (EXP)

CMSLINK creates a binary library containing data, for each CASMO lattice type, including the complete description of independent variables, table structure, and table values for every data table. In addition, QA file trail data (code version numbers, neutron library version numbers, executable creation dates, executing computers and run dates) are added to the library to provide a traceable data trail into SIMULATE-3.

A.13 SIMULATE-3 Nodal Code Overview

SIMULATE-3[9-18] is the three-dimensional advanced nodal diffusion code used in the CMS system for analyzing the pseudo steady-state behavior of PWR and BWR cores. SIMULATE-3 is a coupled nodal neutronics/thermal-hydraulic code capable of performing fuel depletion needed to model the reactor core throughout its lifetime. The flow of a typical SIMULATE-3 computational sequence is depicted in the Figure A-5. It can be seen from this figure that for each depletion step, SIMULATE-3 performs a nested iteration to synchronize thermal-hydraulic conditions, nuclear data, neutronics power distributions, and fuel assembly depletion. When all nonlinear fields are converged, SIMULATE-3 then performs pin power reconstruction to recover individual pin power distributions and detector reaction rates. The details of each of the major modules in SIMULATE-3 are described in the following sections of this report.

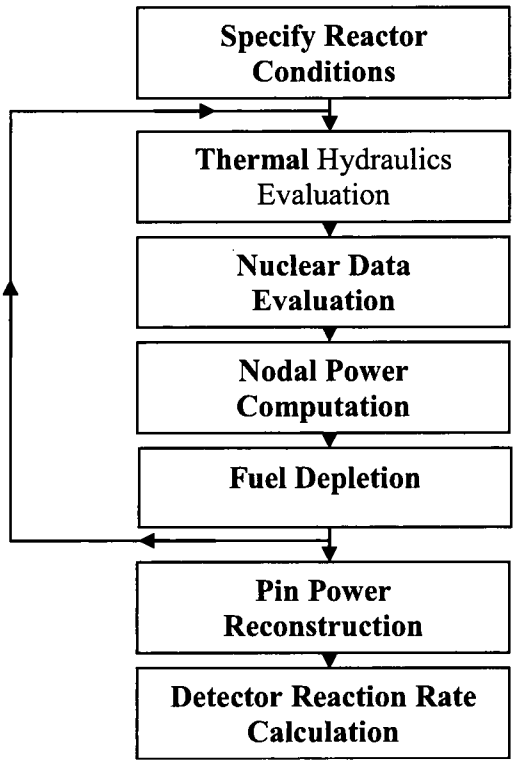

Figure A-5
SIMULATE-3 Flowchart

A.14 SIMULATE-3 PWR Thermal Hydraulics Model

The SIMULATE-3 PWR thermal hydraulics uses one characteristic hydraulic channel per fuel assembly (or four when using 4 node per assembly neutronics model) with the assumption of no radial cross-flow between assemblies. The axial nodalization of the thermal hydraulics is identical to that used in the neutronics, with 24 or more nodes in typical applications. Since SIMULATE-3 is a steady-state (not dynamic) code, these assumptions result in a thermal-hydraulic model that is basically a heat balance – with the following additional assumptions:

- Assembly inlet flows are uniform (or distributed with a user-specified distribution)
- Assembly inlet temperatures are uniform (or distributed with a user-specified distribution)
- All fluid properties are evaluated at the primary system pressure (default is 2250 psi)
- Direct energy deposition in coolant (neutron slowing down, gamma deposition, etc.) is a fixed fraction of the total power generated in a node (default is 2.5%)

Given these assumptions, the coolant enthalpy is computed by marching up each channel and adding the energy produced in each node to the enthalpy, and the coolant density is evaluated from the enthalpy using water properties from the ASME steam tables.

In SIMULATE-3, the node-averaged fuel temperature for node n is computed from the node-averaged coolant temperature, a tabulated function of linear power density of each node, P_n, and a constant quadratic term having the form:

$$TFU_n = TMO_n + TFU_m(EXP, P)P_n + TFU_m^q P_n^2$$

The linear tables are constructed for each fuel type, m, and are constructed as a function of nodal fuel burnup and power density, while the quadratic term is constant for each fuel type. The linear term is a user-input table for SIMULATE-3, and within the CMS suite of codes, INTERPIN-4 is used to generate the fuel temperature data tables.

The neutronic feedback in SIMULATE-3 is based on node-averaged conditions (the rod-by-rod variation in temperatures is ignored), and consequently node-averaged coolant density and fuel temperature are the only thermal-hydraulic parameters needed for steady-state SIMULATE-3 PWR calculations.

A.15 SIMULATE-3 Nuclear Data Interpolation

Once the thermal-hydraulic conditions are known (at each neutronic/hydraulic iteration), nuclear data is evaluated for each node of the core model. Values for all instantaneous library parameters (BOR, DEN, TFU, SDC, and CRD) and each historical parameter (EXP, HTMO, HBOR, and HTFU) are constructed for each node. Linear interpolations in the 2-D and 3-D CMSLINK data tables are then performed to evaluate the required node-by-node parameters.

These data provide the non-linear link between the thermal hydraulics, fuel depletion, and neutronics models of SIMULATE, and multiple iterations are required to obtain a converged solution of core conditions.

A.16 SIMULATE-3 Two-group Nodal Diffusion Model

Once the thermal-hydraulic conditions and cross sections are known for each node of the core model, a three-dimensional diffusion model for the core can be constructed, using standard notation, as

$$-\nabla \cdot D_g(r)\nabla\Phi_g(r) + \Sigma_{t,g}(r)\Phi_g(r) = \sum_{g'=1}^{2}\left[\frac{\chi_g}{k_{eff}}\nu\Sigma_{f,g'}(r) + \Sigma_{gg'}(r)\right]\Phi_{g'}(r)$$

Integrating this equation over the volume of each node in the core model, one obtains the nodal neutron balance equation

$$\sum_{s=1}^{6}\left[\frac{J_g^{m,s}}{h_s}\right]+\bar{\Sigma}_{t,g}^{m}\bar{\Phi}_g^{m}=\sum_{g'=1}^{2}\left[\frac{\chi_g}{k_{eff}}\overline{\nu\Sigma}_{f,g'}^{m}+\bar{\Sigma}_{gg'}^{m}\right]\bar{\Phi}_{g'}^{m},$$

where

$J_g^{m,s} \equiv$ average net neutron current on surface, s, of node m

$\bar{\Phi}_g^{m} \equiv \frac{1}{V^m}\int\Phi_g(r)dV$ is the average scalar neutron flux in node m

$\bar{\Sigma}_{x,g}^{m} \equiv \frac{1}{\bar{\Phi}_g^{m}V^m}\int\Sigma_{x,g}^{m}(r)\,\Phi_g(r)dV$

and $V^m \equiv$ volume of node m

The nodal balance equation simply expresses the fact that the net neutron production in node m equals the rate at which neutrons leak out of the six surfaces of node m. The nodal balance equation cannot be solved without additional relationships that relate the surface-averaged net currents to the node-averaged scalar fluxes. SIMULATE-3 uses the well known transverse-integration method to derive these required coupling relationships. For instance, by integrating the nodal diffusion equation over the y and z directions, one obtains a 1-D coupling expression as a function of x

$$-\tilde{D}_g^{m}(x)\frac{d^2}{dx^2}\tilde{\Phi}_g^{m}(x)+\tilde{\Sigma}_{t,g}^{m}(x)\tilde{\Phi}_g^{m}(x)=\sum_{g'=1}^{2}\left[\frac{\chi_g}{k_{eff}}\nu\tilde{\Sigma}_{f,g'}^{m}(x)+\tilde{\Sigma}_{gg'}^{m}(x)\right]\tilde{\Phi}_{g'}^{m}(x)+L_g^{m,x}(x)$$

where the transverse leakage for direction x in node m has been defined as

$$-L_g^{m,x}(x)\equiv\frac{1}{h_y h_z}\iint\tilde{D}_g^{m}(x)\left[\frac{d^2}{dy^2}+\frac{d^2}{dz^2}\right]\Phi_g(r)\,dy\,dz$$

This transverse leakage expression is a rigorous expression for the x-dependence of the flux in node m. If one makes the assumption that the diffusion coefficient is independent of position within node m, an expression that relates the shape of the x-directed net current in node m to the transverse-integrated scalar flux can be written as

$$J_g^{m,x}(x) = -\tilde{D}_g^m \frac{d}{dx}\tilde{\Phi}_g^m(x)$$

The principal assumption in the transverse-integrated nodal methods is that the x-shape of the transverse leakage in node m can be represented accurately by a quadratic fit (preserving the node-averaged net leakages) to the average transverse leakage in three neighboring nodes m-1, m, and m+1. This approach permits one to construct 1-D coupling equations for each of the x, y, and z directions, and the transverse leakage terms depend only on the face-averaged net currents – which become known as the nodal balance equations are iteratively solved.

In order to fully close this system of equations, one must specify how the transverse-integrated fluxes are to be represented. SIMULATE-3 has two different approximations for the transverse-integrated flux shapes for direction u within each node:

$$\tilde{\Phi}_g^m(u) = \bar{\Phi}_g^m + \phi_g^{1,m}u + \phi_g^{2,m}(3u^2 - \frac{1}{4}) + \phi_g^{3,m}(u^3 - \frac{u}{4}) + \phi_g^{4,m}(u^4 - \frac{3u^2}{10} + \frac{1}{80})$$

or

$$\tilde{\Phi}_g^m(u) = \bar{\Phi}_g^m + \phi_g^{1,m}u + \phi_g^{2,m}(3u^2 - \frac{1}{4}) + \phi_g^{3,m}(u^3 - \frac{u}{4}) + \phi_g^{4,m}(u^4 - \frac{3u^2}{10} + \frac{1}{80})$$
$$+ \phi_g^{c,m}\left[\cosh(\kappa_g u) - \frac{2}{\kappa_g}\sinh(\kappa_g u)\right] + \phi_g^{s,m}\left[\sinh(\kappa_g u)\right]$$

where

$$\kappa_g = \sqrt{\tilde{\Sigma}_g^m / \tilde{D}_g^m}$$

For analysis of UO_2 cores, SIMULATE-3 uses the polynomial expansion to represent the scalar flux shapes for both the fast and thermal groups. When cores containing MOX fuel assemblies are detected in SIMULATE-3, the thermal flux expansions are automatically changed to use the transcendental functions so that more accurate flux shapes are obtained at the interfaces between UO_2 and MOX assemblies.

A.17 SIMULATE-3 Macroscopic Depletion Model

SIMULATE-3 performs fuel depletion throughout the life of the reactor core. Explicit nuclide concentrations for ^{135}I, ^{135}Xe, ^{149}Pm and ^{149}Sm are tracked directly in SIMULATE-3 by solving the nuclide depletion chains and using CASMO generated data for: 1) fission yields, 2) capture cross sections, and 3) decay constants. All other isotopes are treated indirectly in SIMULATE-3 with a macroscopic depletion model. In SIMULATE-3's macroscopic depletion model, CASMO data has been tabulated as a function of fuel burnup (EXP). Consequently, SIMULATE-3 needs only compute the fuel burnup – all other isotopic depletion effects are treated indirectly by interpolating in the CMSLINK data tables to the appropriate burnup point.

Actual fuel isotopic concentrations depend on the local conditions that the fuel assembly experiences during its lifetime. In order to approximate these "history effects", SIMULATE-3 treats water density, fuel temperature, and boron concentration as history variables. For instance, nodes at the top of the core have been depleted with less coolant density that those nodes at the bottom of the core. The resulting harder spectrum leads to production of more plutonium (per GWd/T) at the top of the core.

SIMULATE-3 models this dependence on water density history by interpolating in the CMSLINK data tables with the historical density of coolant and interpolates in the CMSLINK history data tables. Each node in the core experiences a time-varying fuel temperature, coolant density, and boron, and consequently, historical variables must be integrated in time to yield appropriate history values. In SIMULATE-3 a weighted history model is used to accumulate the history variables. As an example, when the burnup, in node m, advances from E^m to $E^m + \Delta E^m$ the boron history in node m is accumulated as

$$HBOR^m(E^m + \Delta E^m) \equiv \frac{HBOR^m(E^m) + w \cdot BOR^m(E^m)\Delta E^m}{E^m + w \cdot \Delta E^m}$$

This weighted history formulation is motivated by the fact that when conditions change significantly, the most recent history tends to "burn in" more quickly than would be modeled by unity history weighting. The weighting parameter, w, is computed for each fuel type and history variable from the build-up rates in the CMSLINK library data. Typically the history weighting parameter is in the range of 2.0 to 2.5. This history treatment allows SIMULATE-3 to model depletion effect more accurately than if only fuel burnup was used.

SIMULATE-3 also treats the burnup shape within each core node. Homogenized cross-section terms are represented as functions of position in the radial direction. If the spatial shape of the cross section is known, it directly impacts the algebraic relationship for the nodal coupling parameters. The intra-nodal spatial shape of burnup in SIMULATE-3 is modeled by tracking the node surface-averaged burnups as well as the node-averaged burnup. A quadratic polynomial shape for the burnup is constructed for each direction using the two

surface-averaged burnups for that direction and the node-averaged burnup. The quadratic burnup shape is then transformed into a quadratic cross-section shape and these shapes are used when solving for nodal coupling parameters. Treatment of the spatial variation of burnup within each node improves the accuracy of computed reactor core flux and power distributions.

A.18 SIMULATE-3 Detector Reaction Rate Computation

The SIMULATE-3 nodal method provides transverse-integrated flux shapes in each of the three directions. The nodal flux at each radial corner points of the assembly are evaluated by constructing a 2-D distribution from the x- and y-directed transverse-integrated fluxes and evaluating these distributions at each of the 4 corners as:

$$\tilde{\Phi}_g^{cp} = \left. \frac{\tilde{\Phi}_g^m(x) \cdot \tilde{\Phi}_g^m(y)}{\bar{\Phi}_g^m} \right|_{cp}$$

Since each of the four nodes that meet at a corner can be used to approximate the corner point flux, one can combine the four homogeneous flux estimates, together with the four CASMO corner point form functions (analogous to the surface discontinuity factors) to obtain a single estimate for the corner point flux:

$$\Phi_g^{cp} = \frac{\tilde{\Phi}_{g,i,j}^{cp}\left[\frac{\Phi_g^{cp,CASMO}}{\bar{\Phi}_g^{CASMO}}\right]_1 + \tilde{\Phi}_{g,i+1,j}^{cp}\left[\frac{\Phi_g^{cp,CASMO}}{\bar{\Phi}_g^{CASMO}}\right]_2 + \tilde{\Phi}_{g,i,j+1}^{cp}\left[\frac{\Phi_g^{cp,CASMO}}{\bar{\Phi}_g^{CASMO}}\right]_3 + \tilde{\Phi}_{g,i+1,j+1}^{cp}\left[\frac{\Phi_g^{cp,CASMO}}{\bar{\Phi}_g^{CASMO}}\right]_4}{4}$$

Detector reaction rates for movable in-core detectors are computed directly in SIMULATE-3 from the two-group fluxes at the detector location (the heterogeneous corner point fluxes). The reaction rates for isotope i and interaction type α are computed using detector cross sections from the CMSLINK library and reconstructed fluxes as:

$$RR_\alpha^i = \Phi_1^{CP}\sigma_{\alpha 1}^i + \Phi_2^{CP}\sigma_{\alpha 2}^i$$

Appendix B: Reactivity Benchmark Specifications

Eleven experimental benchmarks, based on simplifications of publically-available data for the Westinghouse RFA and OFA assemblies, are described here. They cover a range of

- enrichments
- burnable absorber ladings
- boron concentrations
- fuel and coolant temperatures
- decay times

For each case in Table B-1, a complete geometrical and material description follows, and the experimental reactivity decrement tables are presented in Appendix C.

The non-proprietary data sources for the benchmark cases are:

- RFA-like lattice and pin dimensions: TVA Watts Bar FSAR Amendment 98
  (pbadupws.nrc.gov/docs/ML1013/ML101370696.pdf)
- OFA-like lattice/pin dimensions: **NUREG/CR-6761(ORNL/TM-2000/373)**
  (www.nrc.gov/reading-rm/doc-collections/nuregs/.../cr6761/cr6761.pdf)
- WABA pin dimensions: **NUREG/CR-6761(ORNL/TM-2000/373)**
  (www.nrc.gov/reading-rm/doc-collections/nuregs/.../cr6761/cr6761.pdf)
- IFBA and WABA burnable absorber loading patterns: ORNL/TM-1999/255
  (www-rsicc.ornl.gov/FMDP/TM1999_255.pdf)
- IFBA ^{10}B boron loading: Westinghouse products and services online flysheet
  (www.westinghousenuclear.com/products_&_services/.../NF-FE-0009.pdf)
- WABA boron loading: ORNL/TM-13170/V3
  (www.ornl.gov/~webworks/cppr/y2001/rpt/97530.pdf)
- IFBA modeling thickness and inert materials density: "Dissolution, Reactor, and Environmental Behavior of ZrO_2-MgO Inert Fuel Matrix Neutronic Evaluation of MgO-ZrO_2 Inert Fuels," Department of Nuclear Engineering,

Ben-Gurion University of the Negev, Beer-Sheva, Israel, February 2005 (http://aaa.nevada.edu/paper/trp19_03.pdf)

Note that all lattices are depleted with a power density of 104.5 W/cc (38.1 W/gm heavy metal) – except for case 11 which is depleted at 156.75 W/cc (150% of nominal power density).

Table B-1
Benchmark Lattice Cases

1	3.25% Enrichment
2	5.00% Enrichment
3	4.25% Enrichment
4	off-nominal pin diameter depletion
5	20 WABA depletion
6	104 IFBA depletion
7	104 IFBA plus 20 WABA depletion
8	high boron depletion = 1500 ppm
9	branch to hot rack (150°F coolant/fuel) = 338.7K
10	branch to high rack boron = 1500 ppm
11	high power depletion (power, coolant/fuel temp)

B.1 Nominal Fuel Assembly

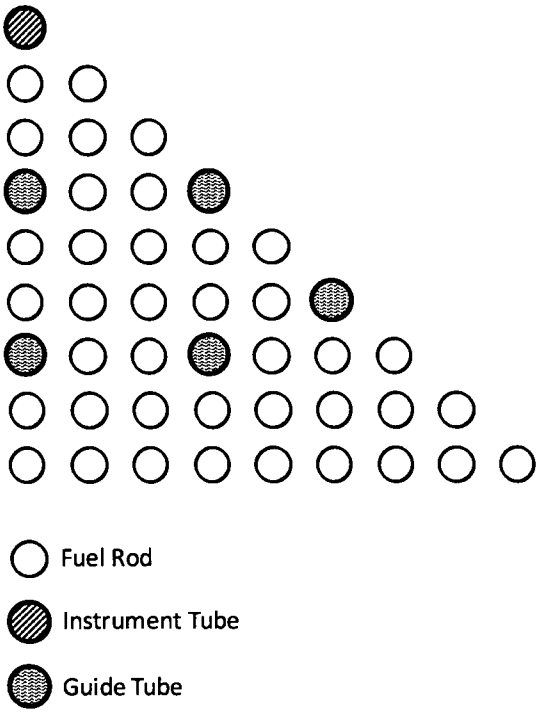

Physical Description

Number of pins along side	17
Pin pitch	1.2598 cm
Inter-assembly spacing	21.5036 cm
Fuel pellet OR	0.4096 cm
Clad IR	0.4180 cm
Clad OR	0.4750 cm
Guide/instrument tube IR	0.5610 cm
Guide/instrument tube OR	0.6120 cm

Structural Material Description

Material (Zr-4)Density	6.55 (g/cm3)
Temp., unheated	580K
Temp., heated	$0.12*T_{fuel}+0.88*T_{coolant}$
Nuclide	**Number Density**
Zr-4	4.32444E+22

Coolant Description, Depletion (Nominal)

Boron Concentration	900 ppm
Temperature	580 K
Nuclide	**Number Density**
H	4.75756E+22
O	2.37894E+22
B	3.56773E+19

Coolant Description, Cold

Boron Concentration	0 ppm
Temperature	293 K
Nuclide	**Number Density**
H	6.67431E+22
O	3.33738E+22

B.2 CASE 1: 3.25% Enriched - No Burnable Absorbers

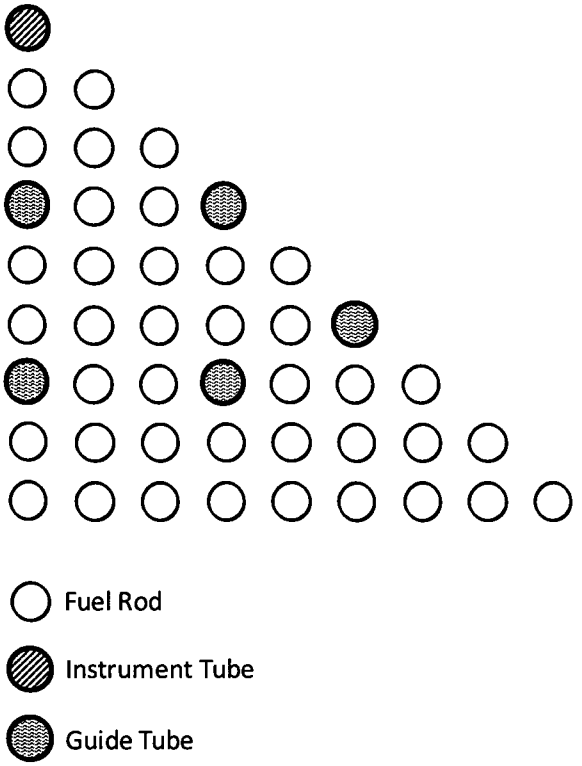

Fuel Material Description	
Material Density	10.340 (g/cm3)
Fuel Temperature	900 K
Nuclide	**Number Density**
U-235	7.59010E+20
U-234	6.09917E+18
U-238	2.23037E+22
O	4.61377E+22

B.3 CASE 2: 5.00% Enriched - No Burnable Absorbers

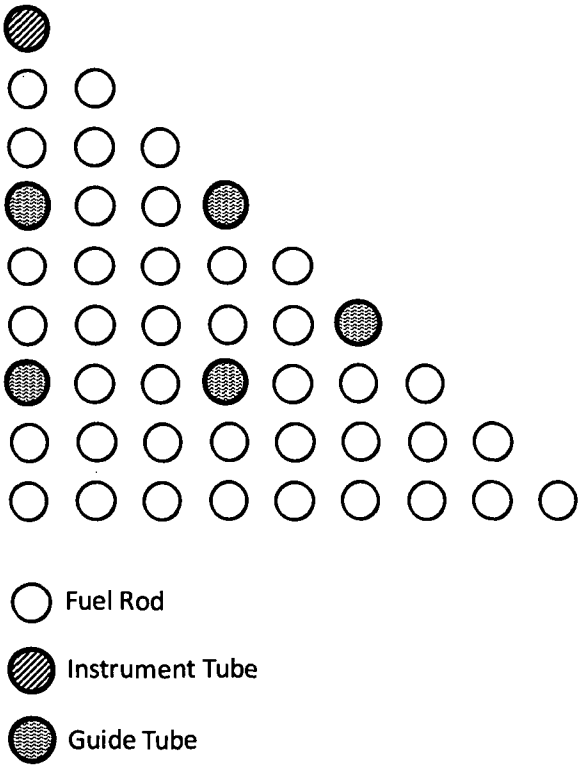

Fuel Rod

Instrument Tube

Guide Tube

Fuel Material Description

Material Density	10.340 (g/cm3)
Fuel Temperature	900 K
Nuclide	**Number Density**
U-235	1.16768E+21
U-234	9.38308E+18
U-238	2.18964E+22
O	4.61469E+22

B.4 CASE 3: 4.25% Enriched - No Burnable Absorbers

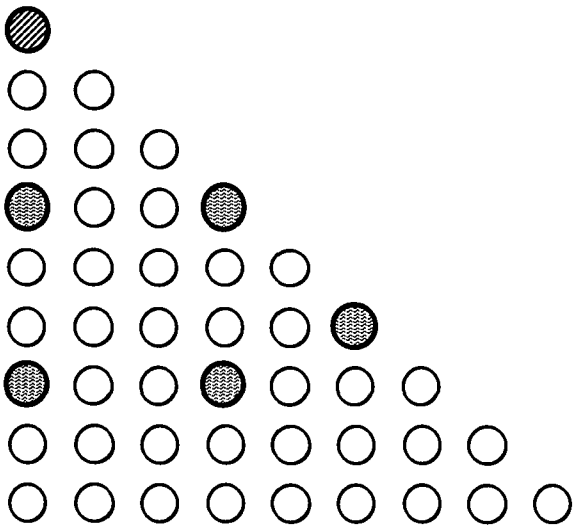

Fuel Rod

Instrument Tube

Guide Tube

Fuel Material Description

Material Density	10.340 (g/cm3)
Fuel Temperature	900 K
Nuclide	**Number Density**
U-235	9.92536E+20
U-234	7.97571E+18
U-238	2.20709E+22
O	4.61429E+22

B.5 CASE 4: Small Fuel Pin

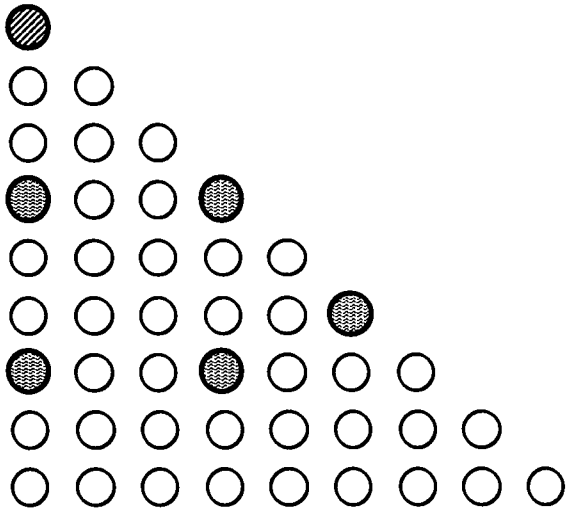

Fuel Rod

Instrument Tube

Guide Tube

Physical Description

Number of pins along side	17
Pin pitch	1.2598 cm
Inter-assembly spacing	21.5036 cm
Fuel pellet OR	0.3922 cm
Clad IR	0.4000 cm
Clad OR	0.4572 cm
Guide/instrument tube IR	0.5610 cm
Guide/instrument tube OR	0.6120 cm

Structural Material Description

Material (Zr-4)Density	6.55 (g/cm3)
Temp., unheated	580K
Temp., heated	$0.12*T_{fuel}+0.88*T_{coolant}$
Nuclide	**Number Density**
Zr-4	4.32444E+22

Fuel Material Description

Material Density	10.340 (g/cm3)
Fuel Temperature	900 K
Nuclide	**Number Density**
U-235	9.92536E+20
U-234	7.97571E+18
U-238	2.20709E+22
O	4.61429E+22

B.6 CASE 5: Lumped Burnable Poison (WABA) Pins

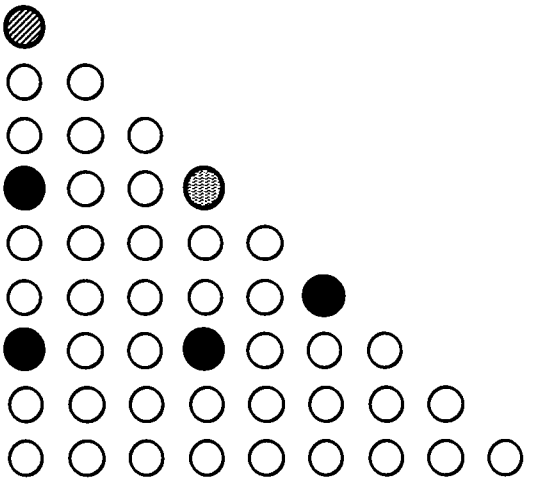

Fuel Rod

Instrument Tube

Guide Tube

LBP

Fuel Material Description

Material Density	10.340 (g/cm3)
Fuel Temperature	900 K
Nuclide	**Number Density**
U-235	9.92536E+20
U-234	7.97571E+18
U-238	2.20709E+22
O	4.61429E+22

Lumped Burnable Poison (WABA)

Annular clad IR	0.2860 cm
Annular clad OR	0.3390 cm
Active region IR	0.3530 cm
Active region OR	0.4040 cm
Inner clad IR	0.4180 cm
Inner clad OR	0.4840 cm
Outer clad IR	0.5610 cm
Outer clad OR	0.6120 cm

Active Region

Material Density	3.65 (g/cm3)
Boron Loading	6.03 mg/cm B-10
Nuclide	**Number Density**
C	1.40923E+21
O	6.23784E+22
Al	4.15904E+22
B-10	2.99030E+21

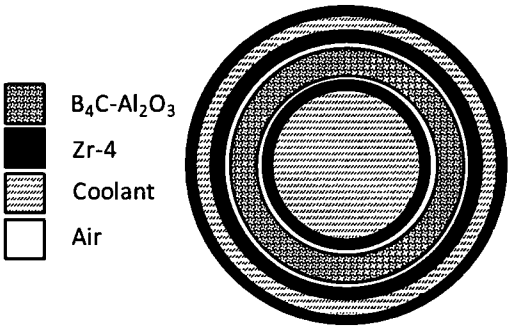

B.7 CASE 6: 104 Integral Fuel Burnable Absorbers (IFBA) Pins

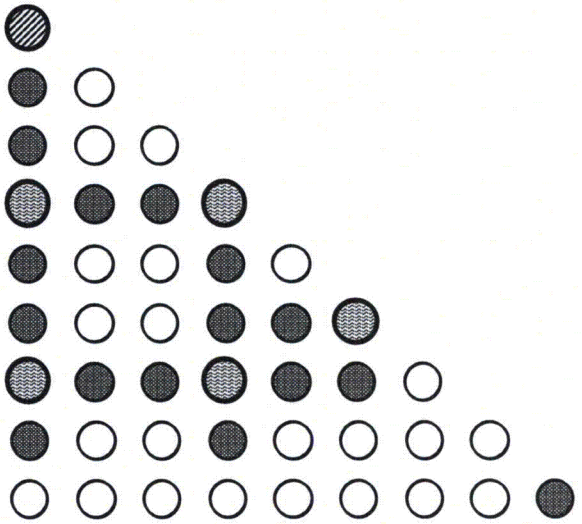

Fuel Rod

Instrument Tube

Guide Tube

IFBA Rod

Fuel Material Description	
Material Density	10.340 (g/cm3)
Fuel Temperature	900 K
IFBA Description	
Material Density	6.100 (g/cm3)
Coating Density	0.925 mg/cm B-10
Coating Thickness	0.01 mm
Nuclide	**Number Density**
U-235	9.92536E+20
U-234	7.97571E+18
U-238	2.20709E+22
O	4.61429E+22
Zr-4	3.22187E+22
B-10	2.15913E+22

B.8 CASE 7: 104 IFBA and 20 WABA Pins

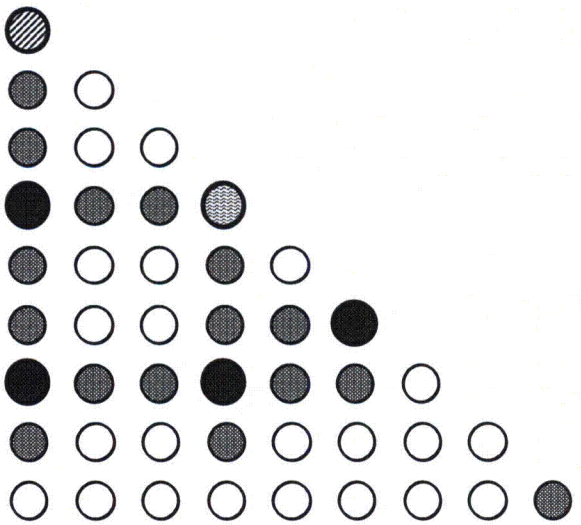

Fuel Rod

Instrument Tube

Guide Tube

IFBA Rod

LBP

Fuel Material Description

Material Density	10.340 (g/cm3)
Fuel Temperature	900 K

IFBA Description

Material Density	6.100 (g/cm3)
Coating Density	0.925 mg/cm B-10
Coating Thickness	0.01 mm
Nuclide	**Number Density**
U-235	9.92536E+20
U-234	7.97571E+18
U-238	2.20709E+22
O	4.61429E+22
Zr-4	3.22187E+22
B-10	2.15913E+22

Lumped Burnable Poison (WABA)

Material Density	3.65 (g/cm3)
Boron Loading	6.03 mg/cm B-10
Nuclide	**Number Density**
C	1.40923E+21
O	6.23784E+22
Al	4.15904E+22
B-10	2.99030E+21

B.9 CASE 8: High Boron Depletion

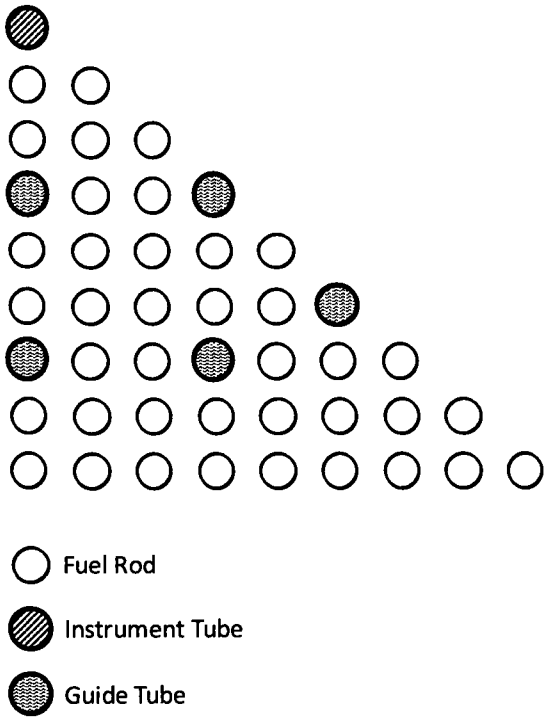

Fuel Material Description

Material Density	10.340 (g/cm3)
Fuel Temperature	900 K
Nuclide	**Number Density**
U-235	9.92536E+20
U-234	7.97571E+18
U-238	2.20709E+22
O	4.61429E+22

Coolant Description, Depletion

Boron Concentration	1500 ppm
Temperature	580 K
Nuclide	**Number Density**
H	4.75756E+22
O	2.37894E+22
B	5.94621E+19

B.10 CASE 9: Nominal Case Branch to Hot Rack Fuel and Coolant Conditions

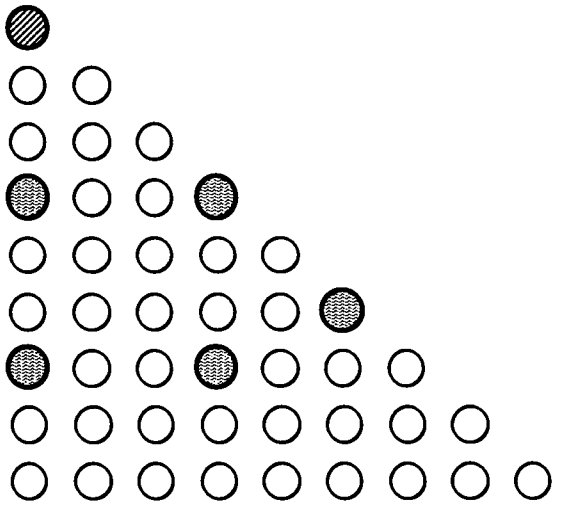

Fuel Rod

Instrument Tube

Guide Tube

Fuel Material Description

Material Density	10.340 (g/cm3)
Fuel Temperature	900 K
Nuclide	**Number Density**
U-235	9.92536E+20
U-234	7.97571E+18
U-238	2.20709E+22
O	4.61429E+22

Coolant Description, Cold

Boron Concentration	0 ppm
Temperature	338.7 K
Nuclide	**Number Density**
H	6.55262E+22
O	3.27653E+22

B.11 CASE 10: Nominal Case Branch to High Rack Boron

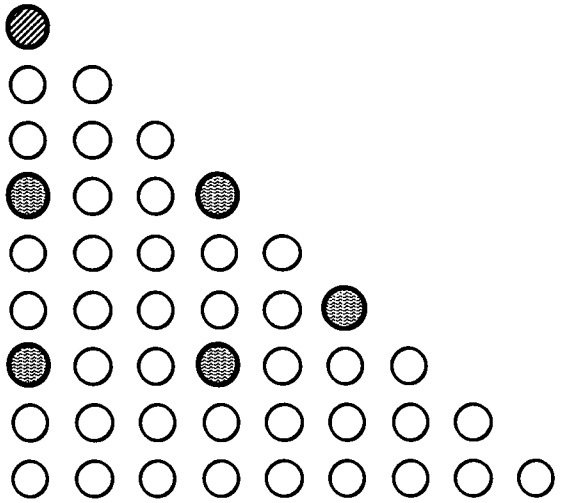

Fuel Rod

Instrument Tube

Guide Tube

Fuel Material Description

Material Density	10.340 (g/cm3)
Fuel Temperature	900 K
Nuclide	**Number Density**
U-235	9.92536E+20
U-234	7.97571E+18
U-238	2.20709E+22
O	4.61429E+22

Coolant Description, Cold

Boron Concentration	1500 ppm
Temperature	293 K
Nuclide	**Number Density**
H	6.67431E+22
O	3.33738E+22
B	8.34184E+19

B.12 CASE 11: High Power (150% of Nominal) Depletion

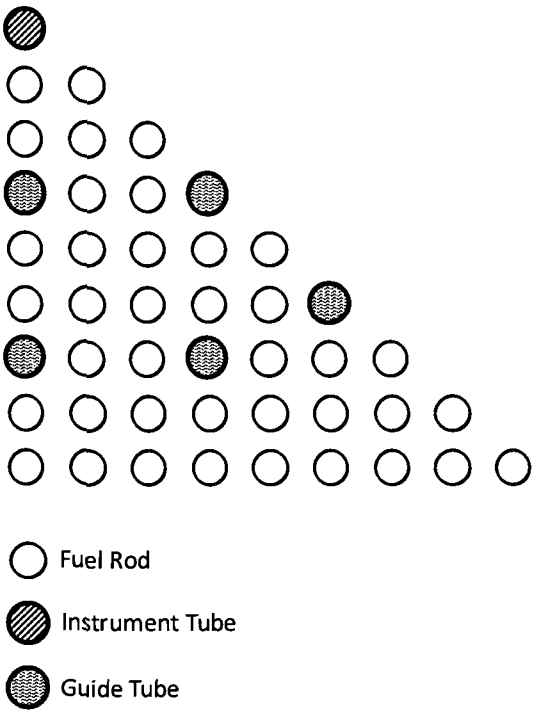

Fuel Material Description

Material Density	10.340 (g/cm3)
Fuel Temperature	1072.5 K
Nuclide	**Number Density**
U-235	9.92536E+20
U-234	7.97571E+18
U-238	2.20709E+22
O	4.61429E+22

Coolant Description, Depletion

Boron Concentration	900 ppm
Temperature	592.5 K
Nuclide	**Number Density**
H	4.55525E+22
O	2.27778E+22
B	3.41601E+19

Appendix C: Experimental Reactivity Decrements

Tables of experimental reactivity decrements for the 11 cases of Appendix B are presented in the following set of tables. The four sets represent cooling intervals of 0 hours, 100 hours, 5 years, and 15 years.

The definition of cold reactivity decrement as a function of lattice burnup, B, is defined as: $k_{inf}(B) - k_{ref}$, where k_{ref} is taken as $k_{inf}(B=0)$ for lattices without burnable absorbers. **Thus, $k_{inf}(B)$ for cases 5, 6, and 7 is computed with burnable absorbers still in the lattice,** while k_{ref} is taken from case 3 without burnable absorbers. This definition is used so that high-burnup reactivity decrement does not depend directly on the initial burnable absorber loading. While this definition is different from that commonly used in rack criticality analysis, it is more consistent with reactor data used to generate the measured decrement biases – which do include burnable absorbers. Since k_{ref} does not include burnable absorbers, the reported reactivity decrements include the combined reactivity change of both fuel and burnable absorbers. At high burnup, the reactivity of the burnable absorber approaches zero, and the reactivity decrement is dominated by the change in reactivity of the fuel.

Given that the changes in reactivity decrement uncertainties with burnup are so small (driven in large part by the choice of using of the maximum observed HFP and fuel temperature uncertainties at any burnup), it is convenient to simply fix the uncertainties on cold reactivity decrement to the maximum values in Table 8-11 – that is, 576 pcm for nominal power density and 643 pcm for 150% power density condition. The assigned uncertainties are independent of fuel burnup and are displayed for each of the eleven Benchmark Cases in Table C-1.

The entire contents of this report are taken directly from a proprietary Studsvik report bearing the same title (report number, **SSP-11/409-C Rev. 0)** for which all work has been performed under the approved Studsvik QA Programs. If subsequent applications of data contained in this report require quality assurance, the proprietary QA version of this report can be obtained directly from Studsvik Scandpower, Inc.

Table C-1
Reactivity Decrement Uncertainty

Case	delta-k
1	0.00576
2	0.00576
3	0.00576
4	0.00576
5	0.00576
6	0.00576
7	0.00576
8	0.00576
9	0.00576
10	0.00576
11	0.00643

Note that the WABA burnable absorbers are not removed in these calculations.

C.1 Burnup Reactivity Decrements: Cold, No Cooling

Table C-2
Measured Reactivity Decrement – No Cooling

Case	Sub-batch Burnup (GWd/T)					
	10	20	30	40	50	60
1	-0.1779	-0.2754	-03589	-04302	-04873	-0.5300
2	-0.1606	-0.2457	-0.3218	-0.3931	-0.4597	-0.5200
3	-0.1683	-0.2589	-0.3393	-0.4130	-0.4788	-0.5347
4	-0.1677	-0.2615	-0.3480	-0.4300	-0.5050	-0.5690
5	-0.2462	-0.2757	-0.3400	-0.4091	-0.4719	-0.5255
6	-0.2165	-0.2643	-0.3371	-0.4100	-0.4762	-0.5328
7	-0.2911	-0.2834	-0.3383	-0.4061	-0.4691	-0.5233
8	-0.1684	-0.2569	-0.3343	-0.4044	-0.4665	-0.5191
9	-0.1698	-0.2602	-0.3398	-0.4125	-0.4772	-0.5320
10	-0.1289	-0.2082	-0.2803	-0.3466	-0.4053	-0.4543
11	-0.1750	-0.2631	-0.3392	-0.4078	-0.4682	-0.5194

C.2 Burnup Reactivity Decrements: Cold, 100-hour Cooling

Table C-3
Measured Reactivity Decrement – 100-Hour Cooling

Case	Sub-batch Burnup (GWd/T)					
	10	20	30	40	50	60
1	-0.1329	-0.2339	-0.3211	-0.3956	-0.4554	-0.5002
2	-0.1146	-0.2021	-0.2806	-0.3545	-0.4238	-0.4867
3	-0.1223	-0.2157	-0.2990	-0.3758	-0.4445	-0.5029
4	-0.1207	-0.2176	-0.3075	-0.3931	-0.4715	-0.5385
5	-0.2045	-0.2335	-0.2998	-0.3717	-0.4372	-0.4932
6	-0.1736	-0.2215	-0.2968	-0.3726	-0.4418	-0.5009
7	-0.2524	-0.2418	-0.2981	-0.3686	-0.4343	-0.4910
8	-0.1216	-0.2129	-0.2932	-0.3662	-0.4310	-0.4860
9	-0.1237	-0.2171	-0.2998	-0.3756	-0.4432	-0.5005
10	-0.0967	-0.1784	-0.2530	-0.3217	-0.3826	-0.4335
11	-0.1235	-0.2149	-0.2945	-0.3664	-0.4299	-0.4838

C.3 Burnup Reactivity Decrements: Cold, 5-Year Cooling

Table C-4
Measured Reactivity Decrement – 5-Year Cooling

Case	Sub-batch Burnup (GWd/T)					
	10	20	30	40	50	60
1	-0.1370	-0.2471	-0.3447	-0.4284	-0.4951	-0.5445
2	-0.1163	-0.2086	-0.2943	-0.3761	-0.4529	-0.5222
3	-0.1247	-0.2245	-0.3164	-0.4018	-0.4781	-0.5425
4	-0.1232	-0.2263	-0.3250	-0.4197	-0.5063	-0.5797
5	-0.2069	-0.2424	-0.3171	-0.3974	-0.4703	-0.5321
6	-0.1760	-0.2304	-0.3140	-0.3984	-0.4751	-0.5403
7	-0.2547	-0.2507	-0.3154	-0.3941	-0.4672	-0.5296
8	-0.1241	-0.2218	-0.3106	-0.3922	-0.4645	-0.5254
9	-0.1261	-0.2257	-0.3168	-0.4009	-0.4759	-0.5390
10	-0.0986	-0.1858	-0.2675	-0.3430	-0.4096	-0.4647
11	-0.1268	-0.2245	-0.3125	-0.3928	-0.4636	-0.5232

C.4 Burnup Reactivity Decrements: Cold, 15-Year Cooling

Table C-5
Measured Reactivity Decrement – 15-Year Cooling

Case	Sub-batch Burnup (GWd/T)					
	10	20	30	40	50	60
1	-0.1422	-0.2655	-0.3768	-0.4720	-0.5471	-0.6021
2	-0.1184	-0.2184	-0.3140	-0.4058	-0.4918	-0.5690
3	-0.1277	-0.2372	-0.3405	-0.4369	-0.5226	-0.5942
4	-0.1260	-0.2385	-0.3488	-0.4551	-0.5516	-0.6325
5	-0.2102	-0.2555	-0.3415	-0.4325	-0.5145	-0.5833
6	-0.1792	-0.2432	-0.3382	-0.4334	-0.5194	-0.5917
7	-0.2581	-0.2639	-0.3398	-0.4291	-0.5111	-0.5806
8	-0.1273	-0.2348	-0.3351	-0.4276	-0.5092	-0.5773
9	-0.1291	-0.2384	-0.3408	-0.4357	-0.5198	-0.5900
10	-0.1014	-0.1971	-0.2885	-0.3729	-0.4468	-0.5074
11	-0.1300	-0.2377	-0.3373	-0.4284	-0.5084	-0.5752

The Electric Power Research Institute Inc., (EPRI, www.epri.com) conducts research and development relating to the generation, delivery and use of electricity for the benefit of the public. An independent, nonprofit organization, EPRI brings together its scientists and engineers as well as experts from academia and industry to help address challenges in electricity, including reliability, efficiency, health, safety and the environment. EPRI also provides technology, policy and economic analyses to drive long-range research and development planning, and supports research in emerging technologies. EPRI's members represent more than 90 percent of the electricity generated and delivered in the United States, and international participation extends to 40 countries. EPRI's principal offices and laboratories are located in Palo Alto, Calif.; Charlotte, N.C.; Knoxville, Tenn.; and Lenox, Mass.

Together...Shaping the Future of Electricity

Program:
Nuclear Power

1022909

Electric Power Research Institute
3420 Hillview Avenue, Palo Alto, California 94304-1338 • PO Box 10412, Palo Alto, California 94303-0813 USA
800.313.3774 • 650.855.2121 • askepri@epri.com • www.epri.com